2021

Deterministic and statistical methods for inverse problems with partial data

Yanfang Liu
Michigan Technological University, yanfangl@mtu.edu

DETERMINISTIC AND STATISTICAL METHODS FOR INVERSE PROBLEMS WITH PARTIAL DATA

By

Yanfang Liu

A DISSERTATION

Submitted in partial fulfillment of the requirements for the degree of

DOCTOR OF PHILOSOPHY

In Mathematical Sciences

MICHIGAN TECHNOLOGICAL UNIVERSITY

2021

This dissertation has been approved in partial fulfillment of the requirements for the Degree of DOCTOR OF PHILOSOPHY in Mathematical Sciences.

Department of Mathematical Sciences

Dissertation Advisor:	*Dr. Jiguang Sun*
Committee Member:	*Dr. Fan Dai*
Committee Member:	*Dr. Jingfeng Jiang*
Committee Member:	*Dr. Yang Yang*
Department Chair:	*Dr. Jiguang Sun*

Contents

List of Figures

List of Tables

Preface

This dissertation is submitted for the degree of Doctor of Philosophy at Michigan Technological University. Several chapters in this dissertation are the result of collaborative work under the supervision of Dr. Jiguang Sun[1], and have been published in or submitted to referred journals.

- Chapter 2: *Quality-Bayesian Approach to Inverse Acoustic Source Problems with Partial Data*. SIAM J. Sci. Comput. 43 (2021), no. 2, A1062–A1080.
- Chapter 3: *A deterministic-statistical approach to reconstruct moving sources using sparse partial data*. Inverse Problems 37 (2021), no. 6, Paper No. 065005, 18 pp.
- Chapter 4: *An inverse medium problem using Stekloff eigenvalues and a Bayesian approach*. Inverse Problems 35 (2019), no. 9, 094004, 20 pp.
- Chapter 5: *Bayesian inversion for an inverse spectral problem of transmission eigenvalues*. In revision, Research in the Mathematical Sciences.

[1]Department of Mathematical Sciences at Michigan Technological University

Acknowledgments

First, I would like to express my gratitude to my advisor, Dr. Jiguang Sun for the patience, guidance, encouragement and support starting in 2015. He always talked to me gently and patiently even if I made mistakes. Dr. Sun serves not only as an academic advisor but also a mentor to my personality. I cannot ask for a better advisor.

Besides my advisor, I would like to thank the rest of my thesis committee members: Dr. Yang Yang, Dr. Fan Dai, Dr. Jingfeng Jiang for their engagement and insightful comments. In particular, Dr. Yang Yang's kindness and lectures benefit me greatly. I would also like to thank many faculty members in the department, especially Ann Humes and Philip Kendall as teaching mentors.

In addition, I want to give a special thank to my family for their continued support. My parents, my siblings, and my niece have always supported me.

I would like to thank my friends at MTU, Dr. Ruihao Huang, Dr. Sulin Wang, Dr. Xiaoyu Liang, Dr. Zhongyuan Hu, Xuewei Cao, Jacob Blazejewski, for the help and happiness you gave me.

Abstract

Inverse problems with partial data have many applications in science and engineering. They are more challenging than the complete data cases since the lack of data increases ill-posedness and nonlinearity. The use of only deterministic or statistical methods might not provide satisfactory results. We propose to combine the deterministic and statistical methods to treat such inverse problems. The thesis is organized as follows.

In Chapter 1, we briefly introduce the inverse problems and their applications. The classical deterministic methods and Bayesian inversion are discussed. The chapter is concluded with a summary of contributions.

Chapter 2 considers the reconstruction of the unknown acoustic sources using partial data. First, we extend the direct sampling method to approximate the source locations. Second, the inverse problem is formulated as a statistical inference problem using the Bayes' formula. The source locations obtained in the first step are coded in the priors. Then a Metropolis-Hastings algorithm is used to explore the posterior density.

In Chapter 3, a two-step deterministic-statistical approach is proposed to recover the trajectories of moving sources using partial measured data. In the first step, an approximate direct sampling method is developed to obtain the locations of the sources at different times. Such information is coded in the priors, which is critical for the success of the Bayesian method in the second step. The combined approach inherits the merits of the deterministic method and Bayesian inversion as demonstrated by the numerical examples.

Chapter 4 studies the reconstruction of Stekloff eigenvalues and the index of refraction of an inhomogeneous medium from Cauchy data. The inverse spectrum problem of Stekloff eigenvalues is investigated by the reciprocity gap method. Then a Bayesian approach is proposed to estimate the index of refraction using a few reconstructed

eigenvalues.

In Chapter 5, we consider the inverse spectral problem to determine the material properties given a few transmission eigenvalues. The lack of theoretical results motivates us to propose a Bayesian approach to formulate a statistical inference problem. The MCMC algorithm is used to explore the posterior density. Due to the non-uniqueness nature of the problem, we adopt the local conditional means (LCM) to characterize the posterior density function.

Chapter 1

Introduction

This chapter presents a brief introduction of the inverse problems, the applications, deterministic methods, and Bayesian methods. The main contributions of the dissertation are summarized at the end of the chapter.

1.1 Inverse problems

Inverse problems have been a particular interesting field in mathematical research. They have numerous applications such as the atmospheric sciences, geophysics, materials sciences, image processing, signal processing, oceanography, hydrology, and traffic flow control.

In 1976, Keller [64] gave a definition of inverse problems:

> *We call two problems inverses of one another if the formulation of each involves all or part of the solution of the other. Often, for historical reasons, one of the two problems has been studied extensively for some time, while the other is newer and not so well understood. In such cases, the former problem is called the direct problem, while the latter is called the inverse problem.*

In general, a problem is called a direct problem if all the necessary parameters

are provided and one needs to predict the measurements given the relation between the parameters and measurements. In contrast, the process to decide the unknown parameters given measurements is often considered as an inverse problem. Usually the direct problem has been thoroughly studied and there are many results available. On the other hand side, the inverse problem was investigated at a later time with less results. Furthermore, in many cases, the inverse problem is more challenging due to the fact that it is inherently nonlinear and ill-posed. In particular, the inverse problems studied in this thesis are severely ill-posed since only partial data are available.

In mathematical physics, according to Hadamard [45], a problem is said to be well-posed if

1. there exists a solution to the problem (existence),

2. there is at most one solution to the problem (uniqueness),

3. the solution depends continuously on the data (stability).

A precise definition of well-posedness is as follows.

Definition 1.1.0.1. *(Chapter 4.1 in [30]) Let $A : U \subset X \to V \subset Y$ be an operator from a subset U of a normed space X into a subset V of a normed space Y. The equation*

$$A(\varphi) = f$$

is called well-posed or properly posed if $A : U \to V$ is bijective and the inverse operator $A^{-1} : V \to U$ is continuous. Otherwise the equation is ill-posed or improperly posed.

For a long time, researchers mainly concentrate on the study of well-posed problems that have unique solutions and depend continuously on the given data. Ill-posed problems connected with partial differential equations in mathematical physics were only viewed as purely academic interest. This situation changed dramatically due to the wide applications of inverse problems in real life, the improvement of computation

capabilities, as well as the development of new methods for ill-posed problems. Nowadays, the inverse problem is an active area in mathematics, sciences, and engineering, equally important as the direct problem.

1.2 Deterministic Methods

Traditionally the inverse problems were treated using deterministic methods. Most deterministic methods can be classified as the iterative methods [98, 58, 43, 49, 5, 36, 61] and the direct methods [25, 27, 66, 67, 24, 7, 68, 55, 72, 97].

One can formulate an inverse problem as an optimization problem for a cost function and the minimizer is the solution to the inverse problem. To compute the minimizer, iterative methods such as the Newton type methods [98, 58, 43, 49] and gradient descent methods [5, 36, 61] are applied. Due to the facts that in each step one needs to solve a direct problem and that the convergence may be slow, iterative methods are usually computationally expensive. In addition, to ensure convergence, iterative techniques need a good initial guess, which is often difficult to obtain. Nevertheless, successful iterative methods can provide detail and accurate information of the unknowns.

Direct methods usually build some indicator functions according to the properties of the associated partial differential equations. Using indicator functions over the sampling domain, one can obtain qualitative information of the unknowns such as the location and size of a target. Furthermore, the implementation of the direct methods is simple in general. A drawback of direct methods is that they require substantial amount of measurement data. When only partial data are available, their performance deteriorates quickly. Well-known direct methods include the linear sampling method, the factorization method, the reciprocity gap method, the extended sampling method, the direct sampling method, the orthogonality sampling method, etc. [25, 27, 24, 7, 66, 67, 23, 68, 91, 95, 57, 86, 88].

Due to the ill-posedness of the inverse problems, regularization techniques are also often used. The basic idea of regularization methods is to construct a stable approximate solution of an ill-posed problem. Consider the ill-posed linear equations of the first kind

$$A\varphi = y, \tag{1.2.1}$$

where $A : X \to Y$ is a compact operator. The following theorem guarantees the existence of a unique solution for a popular regularization method - Tikhonov regularization [106, 30].

Theorem 1.2.1. *Let $A : X \to Y$ be a compact linear operator and let $\gamma > 0$. Then for each $y \in Y$ there exist a unique $\varphi_\gamma \in X$ such that*

$$||A\varphi_\gamma - y||^2 + \gamma\|\varphi_\gamma\|^2 = \inf_{\varphi \in X} \left\{||A\varphi - y||^2 + \gamma\|\varphi\|^2\right\}. \tag{1.2.2}$$

The parameter γ is called the regularization parameter. The minimizer φ_γ is given by the unique solution of $\gamma\varphi_\gamma + A^*A\varphi_\gamma = A^*y$ and depends continuously on y.

1.3 Bayesian method

In recent year, statistical methods have received more attention for inverse problems [63, 99, 10, 38, 110, 62]. Statistical inversion theory reformulates inverse problems as problems of statistical inference by means of Bayesian statistics. In the Bayesian framework, all the parameters are modeled as random variables. The randomness, which describes the observer's uncertainty concerning their values, is expressed in the distribution of the variables. The solution to the inverse problem in the statistical inversion perspective is the probability distribution that provides a probabilistic description of the interest unknowns when all information available has been included in the model.

1.3.1 Bayes' formula

Consider the inverse problem of getting information about $x \in X$ from the measurement $y \in Y$. The model which relates these two quantities x and y may be inaccurate and contain parameters that are not well known to us. In practice the measurement y always contains noises. The statistical problem can be written as

$$y = f(x, e), \tag{1.3.3}$$

where $f : X \times Y \to Y$ is the model function, and $e \in Y$ encapsulates the poorly known parameters as well as the measurement noise. We refer to the directly observable random variable y as the measurement, the non-observable random variable x that is of primary interest as the unknown, and the variable e that is neither observable nor of primary interest as parameters or noises.

In the Bayesian statistical theory, the prior information can be coded into the prior density π_{pr} which expresses what we know about the unknown before performing the measurement of y. The conditional distribution of the measurement y given x is referred to as the likelihood, denoted by $\pi(y|x)$. It expresses the likelihood of different measurement outcomes given x. The conditional distribution $\pi(x|y_{\text{observed}})$ which describes what we know about x given the realized observation $y = y_{\text{observed}}$ is called the posterior distribution of x.

Given $y = y_{\text{observed}}$, the goal of the Bayesian inverse problem is to seek statistical information of x by exploring the conditional probability distribution $\pi(x|y_{\text{observed}})$. The following theorem describes the relationship between the prior, likelihood and the posterior distribution.

Theorem 1.3.1. *(Theorem 3.1 in [63]) Assume that the random variable $x \in X$ has a known prior probability density $\pi_{pr}(x)$ and the data consist of the observed value $y_{observed}$ of an observable random variable $y \in Y$ such that $\pi(y_{observed}) > 0$. Then the posterior probability distribution of x, given the data $y_{observed}$, is*

$$\pi_{post}(x) = \pi(x|y_{observed}) = \frac{\pi_{pr}(x)\pi(y_{observed}|x)}{\pi(y_{observed})}. \tag{1.3.4}$$

For simplicity, we shall write $y = y_{\text{observed}}$. The observed value of y is used in the evaluation of the posterior distribution. The joint probability density of x and y is denoted by $\pi(x, y)$. Then the marginal density of y in (1.3.4) is

$$\pi(y) = \int_X \pi(x, y)dx = \int_X \pi_{\text{pr}}(x)\pi(y|x)dx, \tag{1.3.5}$$

which is a normalization constant.

1.3.2 Estimators

As discussed above, the solution to the Bayesian inverse problem is defined to be the posterior probability densities of the unknown parameters. To characterize the posterior density functions, one can calculate different point estimates, such as maximum a posteriori (MAP) and conditional mean (CM).

Definition 1.3.1.1. *Given the posterior probability density $\pi(x|y)$ of the unknown $x \in X$, the maximum a posteriori estimate (MAP) x_{MAP} is*

$$x_{MAP} = arg\max_{x \in X} \pi(x|y).$$

Definition 1.3.1.2. *The conditional mean (CM) of the unknown x conditioned on y is defined as*

$$x_{CM} = E\{x|y\} = \int_X x\pi(x|x)\mathrm{d}x,$$

provided that the integral converges.

However, for the problem which has non-unique solution, point estimators mentioned above might not carry sufficient/correct information of the unknowns. Hence we also use the local estimators introduced in [103] when necessary.

Definition 1.3.1.3. *(LMAP) We call x^* a local MAP, denoted by x_{LMAP}, if*

$$\pi(x^*|y) \geqslant \epsilon \max_{x \in X} \pi(x|y) \quad \text{and} \quad x^* = arg \max_{x \in N(x^*)} \pi(x|y)$$

for some constant $\epsilon \in (0, 1)$ and $N(x^*)$ a neighborhood of x^*.

Definition 1.3.1.4. *(LCM) The local conditional mean x_{LCM} is define as*

$$x_{LCM} = \int_S x\pi(x|y)\mathrm{d}x,$$

where S is a subset of X.

1.3.3 Likelihood function

In the statistical inversion it is important to construct the likelihood function. The likelihood function contains the forward model used in classical inversion techniques as well as information about the noise, other measurement, and modelling uncertainties.

Most often, the noise is assumed to be additive and mutually independent of the unknown x. Then the statistical model (1.3.3) is of the form

$$y = f(x) + e,$$

where $x \in X$, $y, e \in Y$,and x and e are mutually independent. Denote the probability distribution of the noise e is $\pi_{\text{noise}}(e)$. Under the assumption of the mutual independence of x and e, we can derive that

$$\pi(y|x) = \pi_{\text{noise}}(y - f(x)).$$

Hence, from Bayes' formula (1.3.4), one can obtain

$$\pi(x|y) \propto \pi_{\text{pr}}(x)\ \pi_{\text{noise}}(y - f(x)),$$

where $\propto$ means proportional to.

Denote by $\mathcal{N}$ the normal distribution. We assume that the noise e follows a Gaussian distribution, i.e., $\pi_{\text{noise}}(e) = \mathcal{N}(0, \Gamma_{\text{noise}})$, where $\Gamma_{\text{noise}} \in Y \times Y$ is positive definite. Let $P(x; y) = \frac{1}{2}(y - f(x))^\top \Gamma_{\text{noise}}^{-1}(y - f(x))$. Assume that the posterior measure μ with density $\pi_{\text{post}}(x)$ is absolutely continuous with respect to the prior measure μ_0 with density $\pi_{\text{pr}}(x)$. Using (1.3.4) and (1.3.5), we can relate μ with μ_0 by

$$\frac{\mathrm{d}\mu}{\mathrm{d}\mu_0}(x) = \frac{1}{Z(y)} \exp\left(-P(x; y)\right), \tag{1.3.6}$$

where $Z(y) = \int_X \exp(-P(x;y))\mathrm{d}\mu_0(x)$ is the normalization constant. The formula (1.3.6) is understood as the Radon-Nikodym derivative of the posterior probability measure μ with respect to the prior measure μ_0.

1.3.4 Markov chain Monte Carlo methods

One effective way to explore the posterior probability distribution is the Markov chain Monte Carlo (MCMC) techniques. The basic idea of MCMC methods is to design a Markov chain $\{x_n\}_{n=1}^{\infty}$ that is drawn from the posterior measure μ in (1.3.6). The MCMC methods are systematic ways of generating samplings from the distribution we want to explore and contain significant innovation in the design of methods. In this section, we will introduce one common procedure of the MCMC methods known as the Metroplis-Hasting (M-H) algorithm.

In the M-H algorithm, the aim is to construct a transition kernel $q(x,u)$ such that the proposed move u from the current state of Markov chain x is distributed as $q(x,u)$. We define acceptance ration $\alpha(x,u)$

$$\alpha(x,u) = \min\left\{1, \frac{\pi_{\text{post}}(u)q(u,x)}{\pi_{\text{post}}(x)q(x,u)}\right\}$$

and a random variable $\gamma(x,u)$, which is independent of the probability space underlying the transition kernel q, with the property that

$$\gamma(x,u) = \begin{cases} 1 & \text{with probability } \alpha(x,u), \\ 0 & \text{otherwise.} \end{cases}$$

In particular, in the M-H algorithm, the transition kernel q satisfies the detailed balance equation, which is given by

$$\pi_{\text{post}}(u)\alpha(u,x)q(u,x) = \pi_{\text{post}}(x)\alpha(x,u)q(x,u).$$

When a point $x_n \in X$ is given, we can postulate that the kernel q either propose a move to $u \in X$ with probability $\gamma(x_n,u)$ or it proposes no move away from x_n with

probability $1-\gamma(x_n,u)$, i.e.

$$x_{n+1}=\gamma(x_n,u)u+(1-\gamma(x_n,u))x_n \text{ with } u\sim q(x_n,u). \tag{1.3.7}$$

The following theorem states that the empirical distribution of the Markov chain generated by the M-H algorithm converges weakly to that of the measure μ.

Theorem 1.3.2. *Given μ in* (1.3.6)*, the Markovian sequence $\{x_n\}_{n=1}^{\infty}$ defined by* (1.3.7) *is invariant for μ: if $x_1\sim\mu$, then $x_n\sim\mu$ for all $n\geqslant 1$. Furthermore, if the resulting Markov chain is ergodic then, for any continuous bounded function $g:X\to\mathbb{R}$,*

$$\lim_{N\to\infty}\frac{1}{N}\sum_{n=1}^{N}g(x_n)=\int_X g(x)\mu(\mathrm{d}x)$$

almost certainly.

Instead of a solution of the unknown as the deterministic method, the statistical method, by formulating the inverse problem as a statistical inference, provides the probability distribution of the unknown which may contain more information. In most cases, the posterior distribution cannot be obtained analytically. Computational tools such as MCMC methods are applied to explore π_{post}. The choice of prior allows us to include useful information of the unknown. However, the prior may be subjective and lead to unreliable inference of the unknown. Motivated by the facts that i) the direct methods are simple to implement and can produce qualitative information of the unknown; ii) only partial measurement is available; iii) informative prior distribution can significantly reduce the computation cost of the MCMC methods, we propose to integrate the information obtained in the direct methods into the prior distribution of Bayesian method for the inverse problems with partial data.

1.4 Main Contributions

Inverse problems with partial data are challenging. In many cases, the use of a single method cannot provide satisfactory results. In this thesis, we propose to combine the

deterministic and statistical methods to treat several inverse problems. In particular, the deterministic methods are used to obtain qualitative information of the unknowns such as the approximate location and size of the target. This information is built in the priors for the statistical methods to obtain quantitative information, e.g., the shape of the target. The proposed approach has been applied to recover 1) the location and magnitude of static sources, 2) the trajectories of moving sources, 3) the material property using Stekloff eigenvalues, and 4) the index of refraction using transmission eigenvalues.

Chapter 2

Quality-Bayesian Approach to Inverse Acoustic Source Problems with Partial Data [1]

2.1 Introduction

In this chapter, we consider the inverse problem to reconstruct the locations and intensities of the acoustic sources from partial near-field or far-field data. This problem has importance in various applications such as biomedical imaging and the identification of pollution sources [56, 35]. We refer the readers to [56, 2, 84, 3] and the references therein for various methods proposed in literature.

Recently, a new quality-Bayesian approach, which combines a qualitative method and the Bayesian inference, is proposed for the inverse scattering problem [80]. The approach has two steps. First, qualitative information of the obstacle such as the size and location is obtained using the extended sampling method (ESM) [84, 86]. Second, the inverse problem is formulated as a statistical inference problem using the

[1] This chapter has been published as an article in SIAM Journal on Scientific Computing. https://doi.org/10.1137/20M132345X

Bayes' formula [63, 99]. Then a Markov chain Monte Carlo (MCMC) algorithm is used to explore the posterior density of the parameters for the unknown obstacle. The information obtained in the first step is coded in the priors. The method provides satisfactory results using partial data.

In this chapter, we extend the methodology in [80] to the inverse acoustic source problem with partial data (see Fig. 2.1). In the first step, a direct sampling method (DSM) is employed to approximate the locations of the sources. The DSM is a non-iterative method to reconstruct the unknown scatterers [96, 57]. Recently, the DSM was used in [1, 115] to reconstruct the locations of multiple multipolar sources from single-frequency Cauchy data. For multi-frequency data, we construct new indicator functions for the inverse source problems. Similar to those in [88, 3, 115], the indicator decays as the sampling point moves away from the source (see, e.g., [88]). The DSM has some attractive features: (i) it is easy to implement and computationally cheap; (ii) the algorithm does not need any a priori information of the sources; and (iii) the method can provide reliable location estimations of the unknown sources; (iv) the method is robust for the noise data. These features make the DSM a good candidate to obtain some qualitative information of the sources.

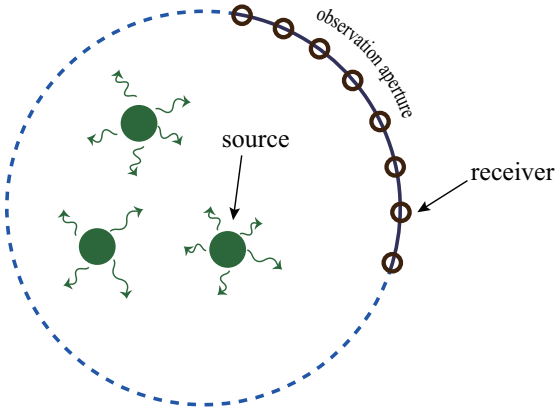

Figure 2.1: Inverse source problem with partial near-field data.

In the second step, for the details of the source, we resort to the Bayesian inversion.

In Bayesian statistics, the parameters of the model are viewed as random variables. The number and locations of the sources obtained in the first step are coded in the priors. By using the Bayes' formula, a posterior distribution of the unknown parameters is obtained. The well-posedness is proved and a Metropolis-Hastings (MH) MCMC algorithm is used to explore the posterior density. Consequently, statistical estimates for the unknown parameters can be obtained. We refer the readers to [63, 99] for the Bayesian inversion and [10, 13, 80, 83] for the applications. The current chapter and [80] share the basic idea of using a combined deterministic-statistical approach for the inverse problems with partial data. However, there are several major differences. Firstly, the physical models are different. The study in [80] considers the inverse scattering problem using partial data due to a single frequency. This chapter treats the inverse source problem using multi-frequency partial data. Secondly, the deterministic method used in [80] is the ESM, which can only treat a single target. In this chapter, the DSM is extended to treat multiple targets, which is clearly an advantage. Thirdly, in the sampling stage, due to the nature of the problem under consideration, the computation of the forward problem is simpler. Thus the speed of the inversion in the current chapter is much faster than that in [80].

Inverse problems with partial measurements arise in many applications of practical importance. In contrast to the cases of full measurements, they are more challenging since the reconstructions usually deteriorate when the data become less. This chapter proposes an effective combined deterministic-statistical approach. The contributions include: 1) an effective DSM for partial data to approximate locations of multiple acoustic sources; 2) an MCMC algorithm to reconstruct the details of the sources based on the information obtained by the DSM; 3) an analysis of the indicator functions; and 4) the well-posedness of the posterior density distribution. The DSM and MCMC are based on the same physical model and use the same set of partial data. The merits of both methods are inherited by the proposed approach as demonstrated by the numerical examples. The rest of chapter is organized as follows. In

Section 2.2, we present the direct and inverse source problems under investigation. In Section 2.3, we develop a DSM to obtain the approximate locations of the unknown sources. In Section 2.4, the Bayesian method is employed to reconstruct the details of the sources. In Section 2.5, numerical examples are presented to show the effectiveness of the quality-Bayesian approach using complete and partial data. Finally, in Section 2.6, we draw some conclusions.

2.2 Direct and Inverse Source Problems

Let $F \in L^2(\mathbb{R}^2)$ denote sources with $\operatorname{supp} F \subset V$, where V is a bounded domain in $\mathbb{R}^2$. The time-harmonic acoustic wave $u \in H^1_{loc}(\mathbb{R}^2)$ radiated by F satisfies

$$\Delta u + k^2 u = F \quad \text{in } \mathbb{R}^2, \tag{2.2.1a}$$

$$\lim_{r\to\infty} \sqrt{r}\left(\frac{\partial u}{\partial r} - iku\right) = 0, \quad r = |x|, \tag{2.2.1b}$$

where k is the wavenumber, (2.2.1a) is the Helmholtz equation and (2.2.1b) is the Sommerfeld radiation condition. Recall that the fundamental solution to the Helmholtz equation is given by

$$\Phi_k(x,y) = \frac{i}{4} H_0^{(1)}(k|x-y|),$$

where $H_0^{(1)}$ is the Hankel function of the zeroth order and the first kind. It is well-known that $\Phi_k(x,y)$ satisfies [30]

$$(\Delta + k^2)\Phi_k(x,y) = -\delta(x-y), \tag{2.2.2}$$

where δ is the Dirac distribution. The solution u to (2.2.1) has the asymptotic expansion

$$u(x,k) = \frac{e^{i\frac{\pi}{4}}}{\sqrt{8k\pi}} \frac{e^{ikr}}{\sqrt{r}} \left\{ u^\infty(\hat{x},k) + \mathcal{O}\left(\frac{1}{r}\right)\right\} \quad \text{as } r \to \infty,$$

where $\hat{x} = x/|x| \in \mathbb{S}$, $\mathbb{S} := \{|\hat{x}| = 1 : \hat{x} \in \mathbb{R}^2\}$. The function $u^\infty(\hat{x},k)$, $\hat{x} \in \mathbb{S}$, is the far-field pattern of $u(x,k)$. The solution u to (2.2.1) and u^∞ can be written as [30]

$$u(x,k) = \int_V \Phi_k(x,y) F(y) dy, \tag{2.2.3}$$

$$u^\infty(\hat{x},k)=\int_V \Phi_k^\infty(\hat{x},y)F(y)dy, \tag{2.2.4}$$

where

$$\Phi_k^\infty(\hat{x},y)=\exp\left(-ik\hat{x}\cdot y\right) \tag{2.2.5}$$

is the far-field pattern of $\Phi_k(x,y)$.

The inverse source problem (ISP) of interest is to determine F from one of the following data sets (see Fig. 2.1):

i) $\{u(x,k): x\in\Gamma,\ k\in[k_m,k_M]\}$,

ii) $\{u^\infty(\hat{x},k): \hat{x}\in S\subset\mathbb{S},\ k\in[k_m,k_M]\}$,

where Γ is a measurement curve outside V, and $k_m<k_M$ are two fixed wavenumbers. By complete data, we mean that Γ is a simple closed curve with V inside, or $S=\mathbb{S}$. Otherwise, the measured data is partial.

In this chapter, we consider two F's for (2.2.1). The first one is the combination of monopole and dipole sources (see, e.g.,[115])

$$F_j(x)=(\lambda_j+\xi_j\cdot\nabla)\delta(x-z_j),\quad j=1,\dots,J, \tag{2.2.6}$$

where J is the number of sources, z_j's represent the source locations, λ_j's and ξ_j's are the scalar and vector intensities such that $|\lambda_j|+|\xi_j|>0$ and $\lambda_j\xi_j=0$. The second one is the union of

$$F_j(x)=\lambda_j\exp(-\xi_j|x-z_j|^2),\quad j=1,\dots,J, \tag{2.2.7}$$

where λ_j's and ξ_j's are the scalar intensities. For simplicity, we write

$$F(x;z,\boldsymbol{\lambda},\boldsymbol{\xi})=\sum_{j=1}^{J}F_j(x;z_j,\lambda_j,\xi_j),\quad \operatorname{supp}F_j(x;z_j,\lambda_j,\xi_j)\subset V_j, \tag{2.2.8}$$

where $\boldsymbol{\lambda}=(\lambda_1,\dots,\lambda_J)$, $\boldsymbol{\xi}=(\xi_1,\dots,\xi_J)$, and $V_j\subset V$.

A source with an extended support cannot be uniquely determined from measurement data at a fixed frequency [33]. Multiple frequency data guarantee the uniqueness and improve the reconstructions [35, 8]. In fact, the reconstruction by the DSM with single frequency partial data can be useless (see Section 2.5.1).

2.3 Direct Sampling Method

Given the measured far-field or near-field data, we propose a direct sampling method (DSM) to reconstruct the number and locations of the sources. The method only involves numerical integrations and is robust for noisy partial data, making the DSM a fast algorithm to obtain some qualitative information. The DSM proposed in [57] is to reconstruct point-like scatterers using the near-field data of all directions due to a single incident plane wave. In this section, we extend it to treat the inverse acoustic source problem by introducing new indicator functions such that it can process 1) both near-field and far-field data; 2) data of a few observation directions; and 3) multi-frequency data. Another advantage of the DSM is that it can reconstruct the locations of multiple targets, while the ESM in [80] can only reconstruct a single target.

Let D be the sampling domain such that $V \subset D$ and n be the unit outward normal to ∂D. Denote by $\mathcal{A} := \{k_i\}_{i=1}^N \subset [k_m, k_M]$ a finite set of discrete wavenumbers. We define two functions

$$I(z_p) = \sum_{k_i \in \mathcal{A}} \int_\Gamma u(x, k_i) \bar{\Phi}_{k_i}(x, z_p) ds(x), \quad z_p \in D, \tag{2.3.9}$$

and

$$I^\infty(z_p) = \sum_{k_i \in \mathcal{A}} \int_{\mathbb{S}} u^\infty(\hat{x}, k_i) \bar{\Phi}^\infty_{k_i}(\hat{x}, z_p) ds(\hat{x}), \quad z_p \in D, \tag{2.3.10}$$

where $\bar{\Phi}_{k_i}(x, z_p)$ and $\bar{\Phi}^\infty_{k_i}(\hat{x}, z_p)$ are the conjugates of $\Phi_{k_i}(x, z_p)$ and $\Phi^\infty_{k_i}(\hat{x}, z_p)$, respectively.

2.3.1 Near-field Indicator

For near-field data, inserting (2.2.3) into (2.3.9) and changing the order of integration, we have that

$$\begin{aligned} I(z_p) &= \sum_{k_i \in \mathcal{A}} \int_\Gamma \int_V \Phi_{k_i}(x,y) F(y) dy \bar{\Phi}_{k_i}(x,z_p) ds(x) \\ &= \sum_{k_i \in \mathcal{A}} \int_V \int_\Gamma \Phi_{k_i}(x,y) \bar{\Phi}_{k_i}(x,z_p) ds(x) F(y) dy. \end{aligned} \tag{2.3.11}$$

From (2.2.2), for $\Phi_{k_i}(x,y)$ and $\bar{\Phi}_{k_i}(x,z_p)$, it holds that

$$\int_D (\Delta \Phi_{k_i}(x,y) + k^2 \Phi_{k_i}(x,y)) \bar{\Phi}_{k_i}(x,z_p) dx = -\bar{\Phi}_{k_i}(y,z_p), \tag{2.3.12}$$

$$\int_D (\Delta \bar{\Phi}_{k_i}(x,z_p) + k^2 \bar{\Phi}_{k_i}(x,z_p)) \Phi_{k_i}(x,y) dx = -\Phi_{k_i}(y,z_p). \tag{2.3.13}$$

Using (2.3.12), (2.3.13), the Green's formula and the Sommerfeld radiation condition, we derive

$$\begin{aligned} \Phi_{k_i}(y,z_p) - \bar{\Phi}_{k_i}(y,z_p) &= \int_\Gamma \left\{ \frac{\partial \Phi_{k_i}(x,y)}{\partial n} \bar{\Phi}_{k_i}(x,z_p) - \frac{\partial \bar{\Phi}_{k_i}(x,z_p)}{\partial n} \Phi_{k_i}(x,y) \right\} ds(x) \\ &\approx \int_\Gamma (ik_i \Phi_{k_i}(x,y) \bar{\Phi}_{k_i}(x,z_p) + ik_i \bar{\Phi}_{k_i}(x,z_p) \Phi_{k_i}(x,y)) ds(x), \end{aligned} \tag{2.3.14}$$

which implies

$$\int_\Gamma k_i \Phi_{k_i}(x,y) \bar{\Phi}_{k_i}(x,z_p) ds(x) \approx \mathrm{Im}(\Phi_{k_i}(y,z_p)), \tag{2.3.15}$$

where $\mathrm{Im}(\cdot)$ denotes the imaginary part.

For $y \in V$ and $z_p \in D$, define the kernel function for (2.3.11)

$$H(y,z_p) = \int_\Gamma \Phi_{k_i}(x,y) \bar{\Phi}_{k_i}(x,z_p) ds(x), \quad k_i \in \mathcal{A}. \tag{2.3.16}$$

Thus,

$$H(y,z_p) \propto \frac{1}{k_i} J_0(k_i |y - z_p|), \quad k_i \in \mathcal{A}, \tag{2.3.17}$$

where J_0 is the zeroth order Bessel function and $\propto$ means "proportional to".

Due to (2.3.11) and (2.3.17), $I(z_p)$ is a superposition of the Bessel functions. From the asymptotic property of $J_0(t)$ [30], one has that

$$J_0(t) = \frac{\sin t + \cos t}{\sqrt{\pi t}} \left\{ 1 + \mathcal{O}\left(\frac{1}{t}\right) \right\}, \quad \text{as } t \to \infty, \tag{2.3.18}$$

and $I(z_p)$ decays similarly when $z_p \to \infty$.

The discussion leads to an indicator for the near-field data

$$I_{DSM}(z_p) = \frac{\left| \sum\limits_{k_i \in \mathcal{A}} \langle u(x, k_i), \Phi_{k_i}(x, z_p) \rangle_{L^2(\Gamma)} \right|}{\sum\limits_{k_i \in \mathcal{A}} \|u(x, k_i)\|_{L^2(\Gamma)} \|\Phi_{k_i}(x, z_p)\|_{L^2(\Gamma)}}, \quad \forall z_p \in D, \tag{2.3.19}$$

where the inner product $\langle \cdot, \cdot \rangle_{L^2(\Gamma)}$ is defined as

$$\langle u(x, k_i), \Phi_{k_i}(x, z_p) \rangle_{L^2(\Gamma)} = \int_\Gamma u(x, k_i) \bar{\Phi}_{k_i}(x, z_p) ds(x).$$

2.3.2 Far-field Indicator

Substituting (2.2.4) into (2.3.10), and changing the order of integration, we have that

$$\begin{aligned} I^\infty(z_p) &= \sum_{k_i \in \mathcal{A}} \int_S \int_V \Phi^\infty_{k_i}(\hat{x}, y) F(y) dy \bar{\Phi}^\infty_{k_i}(\hat{x}, z_p) ds(\hat{x}) \\ &= \sum_{k_i \in \mathcal{A}} \int_V \int_S e^{-ik_i \hat{x} \cdot y} e^{ik_i \hat{x} \cdot z_p} ds(\hat{x}) F(y) dy. \end{aligned} \tag{2.3.20}$$

For $y \in V$ and $z_p \in D$, define the kernel function

$$H^\infty(y, z_p) = \int_S e^{ik_i \hat{x} \cdot (z_p - y)} ds(\hat{x}), \quad k_i \in \mathcal{A}. \tag{2.3.21}$$

By Funk-Hecke formula [30],

$$H^\infty(y, z_p) = 2\pi J_0(k_i |y - z_p|), \quad k_i \in \mathcal{A}. \tag{2.3.22}$$

Due to (2.3.18), $I^\infty(z_p)$ is large when $z_p \in V$ and decays when $z_p \to \infty$. Consequently, we define an indicator for far-field data as

$$I^\infty_{DSM}(z_p) = \frac{\left| \sum\limits_{k_i \in \mathcal{A}} \langle u^\infty(\hat{x}, k_i), \Phi^\infty_{k_i}(\hat{x}, z_p) \rangle_{L^2(S)} \right|}{\sum\limits_{k_i \in \mathcal{A}} \|u^\infty(\hat{x}, k_i)\|_{L^2(S)} \|\Phi^\infty_{k_i}(\hat{x}, z_p)\|_{L^2(S)}}, \tag{2.3.23}$$

where

$$\langle u^\infty(\hat{x}, k_i), \Phi_{k_i}^\infty(\hat{x}, z_p)\rangle_{L^2(S)} = \int_S u^\infty(\hat{x}, k_i)\bar{\Phi}_{k_i}^\infty(\hat{x}, z_p)ds(\hat{x}).$$

The algorithm to approximate the locations of the unknown sources is as follows.

DSM for ISP

1. Collect the data $u(x, k_i)$ on Γ (or $u^\infty(\hat{x}, k_i)$ on S) for $k_i \in \mathcal{A}$.

2. Generate sampling points for D.

3. Calculate $I_{DSM}(z_p)$ (or $I_{DSM}^\infty(z_p)$) for all sampling points $z_p \in D$.

4. Find the local maximizers z^{DSM}'s of $I_{DSM}(z_p)$ (or $I_{DSM}^\infty(z_p)$).

The DSM provides the number and rough locations of the sources. Such qualitative information is integrated into the priors for the following Bayesian inversion.

2.4 Bayesian Inversion

In this section, we present the Bayesian inversion for the inverse acoustic source problem using the near-field data. The far-field case is similar. Let $\boldsymbol{\phi} = (\boldsymbol{\lambda}, \boldsymbol{\xi}, z_1, \ldots, z_J)^T$. Define the forward operator $\mathcal{K} : \mathbb{R}^N \to L^2(\Gamma)$ as follows

$$\mathcal{K}(\boldsymbol{\phi}) := \int_V \Phi_k(y, x)F(x; \boldsymbol{\phi})dx.$$

For F given by (2.2.6), $N = 5J$. For F given by (2.2.7), $N = 4J$.

The statistical model for (2.2.1) can be written as

$$Y = \mathcal{K}(\boldsymbol{\phi}) + Z,$$

where Y is the noisy measurement of $u(x, k)$ and Z is the Gaussian noise, i.e., $Z \sim \mathcal{N}(0, \gamma^2 I)$.

Denote by $\mu^Y(d\boldsymbol{\phi}) = \mathbb{P}(d\boldsymbol{\phi}|Y)$ the posterior measure and by $\mu_0(d\boldsymbol{\phi}) = \mathbb{P}(d\boldsymbol{\phi})$ the prior measure for $\boldsymbol{\phi}$. In this chapter, μ_0 is chosen to be Gaussian. Other priors, e.g.,

the level set prior, can be used as well. The analysis of these priors can be found in, e.g., [54, 34, 50]. For the inverse problem under our consideration, the Gaussian prior coding the information obtained by the DSM outperforms the Whittle-Matérn prior and the level set prior (see Section 2.5.5).

The statistical inverse problem is to find the posterior measure $\mu^Y(d\boldsymbol{\phi})$. Assume that μ^Y is absolutely continuous with respect to μ_0, i.e., $\mu^Y \ll \mu_0$. By Bayes' formula,

$$\frac{d\mu^Y}{d\mu_0}(\boldsymbol{\phi}) = \frac{1}{L(Y)} \exp\left(-G(\boldsymbol{\phi}; Y)\right), \tag{2.4.24}$$

where $\exp(-G(\boldsymbol{\phi}; Y))$ is the likelihood such that

$$G(\boldsymbol{\phi}; Y) := \frac{1}{2\gamma^2} \|Y - \mathcal{K}(\boldsymbol{\phi})\|^2_{L^2(\Gamma)}, \tag{2.4.25}$$

and

$$L(Y) := \int_{\mathbb{R}^N} \exp\left(-G(\boldsymbol{\phi}; Y)\right) d\mu_0(\boldsymbol{\phi}), \tag{2.4.26}$$

is the normalizing constant of μ^Y.

In the rest of this section, we show the well-posedness of the posterior measure following [99]. We first analyze the forward operator $\mathcal{K}$.

Lemma 2.4.1. *(Page 441 of [111]) Let $z \in \mathbb{C}$ and $Re(z) > 0$. Then the following Nicholson's formula holds*

$$J^2_\nu(z) + Y^2_\nu(z) = \frac{8}{\pi^2} \int_0^\infty K_0(2z \sinh t) \cosh(2\nu t) dt, \tag{2.4.27}$$

where

$$K_0(z) = \int_0^\infty e^{-z \cosh t} dt,$$

$J_\nu(z)$ and $Y_\nu(z)$ are the νth order Bessel function and Neumann function, respectively.

Using Nicholson's formula (2.4.27), the following property holds for $\mathcal{K}$.

Lemma 2.4.2. *There exists a constant C such that*

$$\|\mathcal{K}(\boldsymbol{\phi})\|_{L^2(\Gamma)} \leqslant C|\boldsymbol{\phi}|_\infty, \tag{2.4.28}$$

where C depends on Γ and V.

Proof. According to (2.2.3),

$$u(x,k)=\int_V \frac{i}{4}H_0^{(1)}(k|x-y|)F(y)dy. \tag{2.4.29}$$

Let

$$\tau^*=\min\{|x-y|:x\in\Gamma,y\in V\}\quad\text{and}\quad\tau=|x-y|.$$

By (2.4.27), it holds that

$$\begin{aligned}|H_\nu^{(1)}(k\tau)|^2&=J_\nu^2(k\tau)+Y_\nu^2(k\tau)\\&=\frac{8}{\pi^2}\int_0^\infty K_0(2k\tau\sinh t)\cosh(2\nu t)dt\\&\leqslant\frac{8}{\pi^2}\int_0^\infty K_0(2k\tau^*\sinh t)\cosh(2\nu t)dt\\&=|H_\nu^{(1)}(k\tau^*)|^2.\end{aligned} \tag{2.4.30}$$

Combining (2.4.29) and (2.4.30), we obtain that

$$\begin{aligned}|u(x,k)|&=\left|\int_V\frac{i}{4}H_0^{(1)}(k|x-y|)F(y)dy\right|\\&\leqslant\frac{1}{4}\int_V|H_0^{(1)}(k\tau^*)||F(y)|dy\\&\leqslant\frac{|V|}{4}|H_0^{(1)}(k\tau^*)|\|F(y)\|_\infty.\end{aligned} \tag{2.4.31}$$

Since $k\geqslant k_m$, it holds that

$$\|u(x,k)\|_{L^2(\Gamma)}\leqslant\frac{|V|}{4}|H_0^{(1)}(k_m\tau^*)|\|F(y)\|_\infty\leqslant C\frac{|V|}{4}|H_0^{(1)}(k_m\tau^*)||\boldsymbol{\phi}|_\infty. \tag{2.4.32}$$

This completes the proof. ■

Corollary 2.4.2.1. *There exists a constant C, such that*

$$\|\mathcal{K}(\boldsymbol{\phi}_1)-\mathcal{K}(\boldsymbol{\phi}_2)\|_{L^2(\Gamma)}\leqslant C|\boldsymbol{\phi}_1-\boldsymbol{\phi}_2|_\infty, \tag{2.4.33}$$

where C depends on Γ and V.

Let μ_1 and μ_2 denote two probability measures. Assume that μ_1 and μ_2 are both absolutely continuous with respect to a third measure μ.

Definition 2.4.2.1. *The Hellinger and total variation metrics between μ_1 and μ_2 are, respectively, defined as*

$$d_H(\mu_1,\mu_2)=\left(\frac{1}{2}\int\left(\sqrt{d\mu_1/d\mu}-\sqrt{d\mu_2/d\mu}\right)^2 d\mu\right)^{1/2} \tag{2.4.34}$$

and

$$d_{TV}(\mu_1,\mu_2)=\frac{1}{2}\int |d\mu_1/d\mu - d\mu_2/d\mu|\, d\mu. \tag{2.4.35}$$

Both Hellinger and total variation metrics are independent of the choice of the measure μ. If μ_1 and μ_2 are both absolutely continuous with respect to μ, then Hellinger and total variation metrics are equivalent (see, e.g., Lemma 6.36 of [99]).

Theorem 2.4.3. *Assume that μ_0 is a Borel probability measure on $\mathbb{R}^N$. Let μ^Y and $\mu^{Y'}$ be the measures defined by (2.4.24) for Y and Y', respectively. Suppose μ^Y and $\mu^{Y'}$ are both absolutely continuous with respect to μ_0. Then the Bayesian inverse problem (2.4.24) is well-posed in both Hellinger and total variational metrics, i.e., there exists a constant $M=M(r)>0$ with $\max\{|Y|,|Y'|\}<r$, such that*

$$d_H(\mu^Y,\mu^{Y'})\leqslant M\|Y-Y'\|_\infty \quad \textit{and} \quad d_{TV}(\mu^Y,\mu^{Y'})\leqslant M\|Y-Y'\|_\infty. \tag{2.4.36}$$

Proof. Define the normalizing constant

$$L(Y)=\int_{\mathbb{R}^N}\exp\left(-\frac{1}{2\gamma^2}\|Y-\mathcal{K}(\boldsymbol{\phi})\|^2_{L^2(\Gamma)}\right)d\mu_0(\boldsymbol{\phi}). \tag{2.4.37}$$

Clearly,

$$0\leqslant L(Y)\leqslant 1.$$

Now we show that $L(Y)$ is strictly positive. From Lemma 2.4.2 and (2.4.37), it follows that

$$\begin{aligned} L(Y) &\geqslant \int_{B(R)}\exp\left(-\frac{1}{\gamma^2}\left(\|Y\|^2_{L^2(\Gamma)}+\|\mathcal{K}(\boldsymbol{\phi})\|^2_{L^2(\Gamma)}\right)\right)d\mu_0(\boldsymbol{\phi}) \\ &\geqslant \int_{B(R)}\exp(-M)d\mu_0(\boldsymbol{\phi}) \\ &= \exp(-M)\mu_0(B(R)), \end{aligned} \tag{2.4.38}$$

where $B(R)$ denotes a ball with a large enough radius R.

We claim that $\mu_0(B(R)) > 0$. To see this, consider the disjoint sets $A_n := \{\boldsymbol{\phi} |\, n - 1 \leqslant \|\boldsymbol{\phi}\| < n\}$, $\forall n \in \mathbb{N}$. Then $\{A_n\}$ are measurable and $\sum_{n=1}^{\infty} \mu_0(A_n) = \mu_0(\bigcup_{n=1}^{\infty} A_n) = 1$. Consequently, there exists at least one $A_n \in \{A_n\}_{n=1}^{\infty}$ satisfying $\mu_0(A_n) \neq 0$. Combining with (2.4.38), it holds that $L(Y) > 0$.

Using the mean value theorem and Lemma 2.4.2, we have that

$$\begin{aligned} |L(Y) - L(Y')| &\leqslant \int_{\mathbb{R}^N} \exp(-G(\boldsymbol{\phi}; Y)) \, |G(\boldsymbol{\phi}; Y) - G(\boldsymbol{\phi}; Y')| \, d\mu_0(\boldsymbol{\phi}) \\ &\leqslant \int_{\mathbb{R}^N} \frac{1}{2\gamma^2} \left| \|Y - \mathcal{K}(\boldsymbol{\phi})\|_{L^2(\Gamma)}^2 - \|Y' - \mathcal{K}(\boldsymbol{\phi})\|_{L^2(\Gamma)}^2 \right| d\mu_0(\boldsymbol{\phi}) \\ &\leqslant M \|Y - Y'\|_{\infty}. \end{aligned} \tag{2.4.39}$$

By the definition of d_H, it holds that

$$\begin{aligned} & d_H^2(\mu^Y, \mu^{Y'}) \\ &= \frac{1}{2} \int_{\mathbb{R}^N} \left\{ \left(\frac{\exp(-G(\boldsymbol{\phi}; Y))}{L(Y)} \right)^{1/2} - \left(\frac{\exp(-G(\boldsymbol{\phi}; Y'))}{L(Y')} \right)^{1/2} \right\}^2 d\mu_0(\boldsymbol{\phi}) \\ &= \frac{1}{2} \int_{\mathbb{R}^N} \left\{ \left(\frac{\exp(-G(\boldsymbol{\phi}; Y))}{L(Y)} \right)^{1/2} - \left(\frac{\exp(-G(\boldsymbol{\phi}; Y'))}{L(Y)} \right)^{1/2} \right. \\ &\qquad \left. + \left(\frac{\exp(-G(\boldsymbol{\phi}; Y'))}{L(Y)} \right)^{1/2} - \left(\frac{\exp(-G(\boldsymbol{\phi}; Y'))}{L(Y')} \right)^{1/2} \right\}^2 d\mu_0(\boldsymbol{\phi}) \\ &\leqslant L(Y)^{-1} \int_{\mathbb{R}^N} \left\{ \exp\left(-\frac{1}{2} G(\boldsymbol{\phi}; Y) \right) - \exp\left(-\frac{1}{2} G(\boldsymbol{\phi}; Y') \right) \right\}^2 d\mu_0(\boldsymbol{\phi}) \\ &\qquad + \left| L(Y)^{-1/2} - L(Y')^{-1/2} \right|^2 \int_{\mathbb{R}^N} \exp\left(-G(\boldsymbol{\phi}; Y') \right) d\mu_0(\boldsymbol{\phi}). \end{aligned} \tag{2.4.40}$$

Again, using the mean value theorem and Lemma 2.4.2, we have that

$$\begin{aligned} & \int_{\mathbb{R}^N} \left\{ \exp\left(-\frac{1}{2} G(\boldsymbol{\phi}; Y) \right) - \exp\left(-\frac{1}{2} G(\boldsymbol{\phi}; Y') \right) \right\}^2 d\mu_0(\boldsymbol{\phi}) \\ &\leqslant \int_{\mathbb{R}^N} \exp(-G(\boldsymbol{\phi}; Y)) \left| \frac{1}{2} G(\boldsymbol{\phi}; Y) - \frac{1}{2} G(\boldsymbol{\phi}; Y') \right|^2 d\mu_0(\boldsymbol{\phi}) \\ &\leqslant \int_{\mathbb{R}^N} \frac{1}{16\gamma^4} \left| \|Y - \mathcal{K}(\boldsymbol{\phi})\|^2 - \|Y' - \mathcal{K}(\boldsymbol{\phi})\|^2 \right|^2 d\mu_0(\boldsymbol{\phi}) \\ &\leqslant M \|Y - Y'\|_{\infty}^2. \end{aligned} \tag{2.4.41}$$

According to the boundedness of $L(Y)$ and $L(Y')$, it holds that

$$\begin{aligned} &\left|L(Y)^{-1/2} - L(Y')^{-1/2}\right|^2 \\ &\leqslant M \max\left(L(Y)^{-3}, L(Y')^{-3}\right) |L(Y) - L(Y')|^2 \\ &\leqslant M\|Y - Y'\|_\infty^2. \end{aligned} \tag{2.4.42}$$

Combining (2.4.38)-(2.4.42) we obtain that

$$d_H(\mu^Y, \mu^{Y'}) \leqslant M\|Y - Y'\|_\infty.$$

Due to Lemma 6.36 of [99], it also holds that

$$d_{TV}(\mu^Y, \mu^{Y'}) \leqslant M\|Y - Y'\|_\infty.$$

The proof is complete. ■

The solution to the Bayesian inverse problem is the posterior distribution μ^Y. To explore μ^Y, we resort to the Markov chain Monte Carlo (MCMC) method. Based on the samples generated by the MCMC, various statistical estimates such as maximum a posteriori (MAP) and conditional mean (CM) can be obtained. In this chapter, we employ the preconditioned Crank-Nicolson (pCN) Metropolis-Hastings (MH) algorithm for the MCMC [31].

Algoritm pCN-MH:

1. Set $n \leftarrow 0$ and choose an initial value $\boldsymbol{\phi}_0$.

2. Propose a move according to

$$\begin{aligned} \tilde{\lambda}_{j,n} &= \left(1-\beta^2\right)^{1/2} \lambda_{j,n} + \beta W_n, \quad W_n \sim \mathcal{N}(0,1), \\ \tilde{\xi}_{j,n} &= \left(1-\beta^2\right)^{1/2} \xi_{j,n} + \beta W_n, \quad W_n \sim \mathcal{N}(0,1) (\text{or } \mathcal{N}(\mathbf{0}, I_{2\times 2})) \\ \tilde{z}_{j,n} &= z^{DSM} + \sqrt{\sigma} W_n, \quad W_n \sim \mathcal{N}(z_j^{DSM}, I_{2\times 2}). \end{aligned}$$

3. Compute

$$\alpha(\boldsymbol{\phi}_n, \tilde{\boldsymbol{\phi}}_n) = \min\left\{1, \exp\left(G\big(F(x;\boldsymbol{\phi}_n);Y\big) - G(F(x;\tilde{\boldsymbol{\phi}}_n);Y)\right)\right\}.$$

4. Draw $\tilde{\alpha} \sim \mathcal{U}(0,1)$. If $\alpha(\boldsymbol{\phi}_n, \tilde{\boldsymbol{\phi}}_n) \geqslant \tilde{\alpha}$, set $\boldsymbol{\phi}_{n+1} = \tilde{\boldsymbol{\phi}}_n$. Else, $\boldsymbol{\phi}_{n+1} = \boldsymbol{\phi}_n$.

5. When $n =$ MaxIt, the maximum sample size, stop.

   Otherwise, set $n \leftarrow n+1$ and go to Step 2.

2.5 Numerical Examples

We present four examples to show the performance of the proposed quality-Bayesian approach. Let $V = [-4,4] \times [-4,4]$. For point sources (2.2.6), the solution to the forward problem (2.2.1) is computed using the formula in Section 4.1 of [115]. For extended sources (2.2.7), the solution to (2.2.1) is approximated using (2.2.3) or (2.2.4) as follows. Generate a triangular mesh $\mathcal{T}$ for V with mesh size h. For $\hat{x} := (\cos\theta, \sin\theta)$, $\theta \in [0, 2\pi)$, and a fixed wavenumber k, the far-field pattern is approximated by

$$u^{\infty}(\hat{x}; k) \approx \sum_{T \in \mathcal{T}} e^{-ik\hat{x}\cdot y_T} F(y_T)|T|, \tag{2.5.43}$$

where $T \in \mathcal{T}$ is a triangle, y_T is the center of T, and $|T|$ denotes the area of T. The synthetic data are computed using a mesh with $h \approx 0.06$. Then 5% random noise is added

$$u^m(x,k) := u(x,k) + 0.05(\tilde{Z}_1 + i\tilde{Z}_2) \max|u|,$$

where $\tilde{Z}_1, \tilde{Z}_2 \sim \mathcal{N}(0,1)$. Considering the magnitude of the noise, in the sampling stage, a relatively coarse mesh is used to compute the solution to the forward problem (2.2.1), which speeds up the algorithm. All the examples are done on a MacBook Pro (2.3 GHz Quad-Core Intel Core i7, 32 GB memory). The DSM is super fast and takes less than a few seconds. The time used in the MCMC stage for 10000 samples is a few minutes.

Examples 1 and 3 use the near-field data, which are measured on a circle with radius $R = 6.5$ and centered at the origin. Examples 2 and 4 use the far-field data. Define

$$S_1 := [0, 2\pi), \quad S_2 := [0, \pi), \quad S_3 := [\pi/8, 5\pi/8).$$

The near-field data are

$$\{u(x;k_j)|x=(R\cos\theta,R\sin\theta),\theta\in S_i,i=1,2,3,j=1,\ldots,N_k\}.$$

The far-field data are

$$\{u^\infty(\hat{x};k_j)|\hat{x}=(\cos\theta,\sin\theta),\theta\in S_i,i=1,2,3,j=1,\ldots,N_k\}.$$

The aperture S_1 represents complete data and S_2, S_3 represent partial data. Equally spaced measurement angles are used: 80 for S_1, 40 for S_2 and 20 for S_3. The N_k wavenumbers in $[k_m, k_M]$ are given by

$$k_j = k_m + (j-1)(k_M - k_m)/(N_k - 1), \quad j = 1, \cdots, N_k. \tag{2.5.44}$$

The sampling domain for DSM is chosen to be the same as V and is divided into 201×201 uniformly distributed sampling points. The priors are Gaussian and the locations obtained by the DSM are the means for $z_i, i = 1, \ldots, J$. We call them DSM-Gaussian priors in the rest of this section. Numerical examples show that this prior is effective for the inverse problems under consideration.

2.5.1 Example 1

Let $F(x) = \sum_{j=1}^3 \lambda_j \delta(x - z_j)$ with

$$\{\lambda_j\}_{j=1}^3 = \{6,5,7\}, \quad \{z_j\}_{j=1}^3 = \{(2,2),(-2,2),(0,-2)\}.$$

Set $k_m = 5$, $k_M = 10$ and $N_k = 10$. In Fig. 2.2, we plot the indicator functions using data associated with S_1, S_2, S_3 by the DSM. The reconstructed locations $\{z_j^{DSM}\}_{j=1}^3$ are

$$S_1 : \{(2.00,2.00),(-2.00,2.00),(0.00,-2.00)\},$$
$$S_2 : \{(2.00,2.00),(-2.00,2.00),(0.00,-2.00)\},$$
$$S_3 : \{(2.00,2.00),(-2.00,2.00),(0.00,-2.00)\}.$$

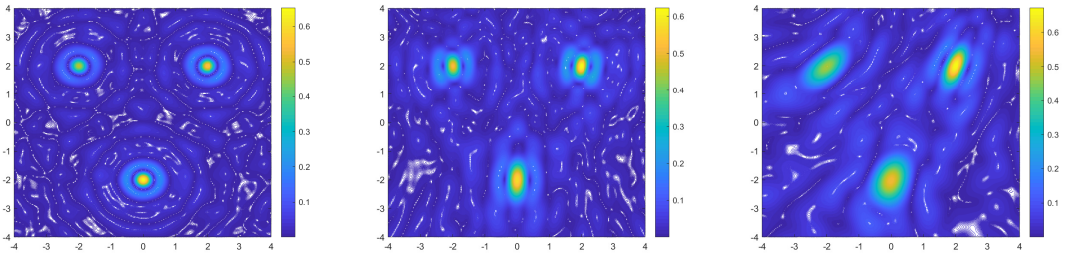

Figure 2.2: Example 1 plots of the indicators of the DSM. Left: S_1. Middle: S_2. Right: S_3.

For monopole sources, the locations are accurate even for partial data (S_2 and S_3), although the plots of the indicators in Fig. 2.2 are quite different.

In the Bayesian inversion stage, we take $\beta = 0.03$ and $\sigma = 0.0004$ in **pCN-MH**. The maximum number of samples is set to be 10000. The first 3000 samples are discarded and the conditional mean of the posterior density for each parameter is computed. The results are shown in Table 2.1, where $\cdot^\star$ represents the conditional mean. The reconstructed parameters are close to the exact ones.

j	Exact Parameters		Reconstructed parameters for S_1	
	λ_j	z_j	$\lambda_j^\star$	$z_j^\star$
1	6	(2, 2)	5.8528	(1.9980, 1.9967)
2	5	(-2, 2)	5.0681	(-2.0026, 2.0040)
3	7	(0, -2)	6.9588	(-0.0003, -1.9982)
j	Reconstructed parameters for S_2		Reconstructed parameters for S_3	
	$\lambda_j^\star$	$z_j^\star$	$\lambda_j^\star$	$z_j^\star$
1	5.9798	(2.0000, 1.9954)	6.2389	(2.0103, 1.9990)
2	5.0730	(-2.0017, 2.0087)	4.8071	(-1.9949, 1.9938)
3	6.9029	(-0.0100, -1.9934)	6.9066	(0.0259, -2.0054)

Table 2.1: Exact and reconstructed parameters for Example 1.

In Table 2.2, we show the CPU time in seconds of the proposed method. The numbers for other examples are similar and thus omitted.

Apertures	DSM algorithm	MCMC algorithm (10000 samples)	
	CPU time(s)	CPU time(s)	Average time(s)/1000 samples
S_1	4.2412	102.4620	10.2462
S_2	4.2302	101.3700	10.1370
S_3	4.1236	96.1320	9.6132

Table 2.2: The CPU time in seconds for Example 1.

As mentioned in Section 2.3, multiple frequency data are necessary to obtain meaningful reconstructions of sources, in particular, when the data are partial. In Fig. 2.3, we plot the indicator functions using single frequency data ($k = 5$) with S_1, S_2, S_3 by the DSM. It can be seen that the results are almost useless, in particular, for S_3.

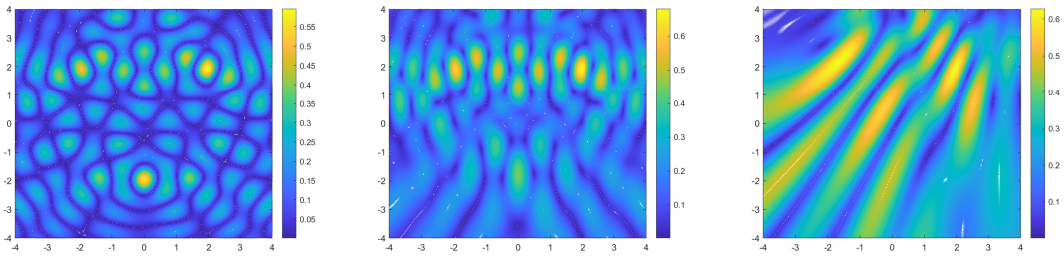

Figure 2.3: Plots of the indicators of the DSM using single frequency data ($k = 5$). Left: S_1. Middle: S_2. Right: S_3.

2.5.2 Example 2

Let $F(x) = \sum_{j=1}^{3}(\lambda_j + \xi_j \cdot \nabla)\delta(x - z_j)$ with

$$\{\lambda_j\}_{j=1}^{3} = \{0, 9, 0\},$$

$$\{\xi_j\}_{j=1}^3 = \{(\sqrt{2}, -\sqrt{2}), (0,0), (2,0)\},$$
$$\{z_j\}_{j=1}^3 = \{(2,0), (-2,2), (-2,-2)\}.$$

Again, $k_m = 5$, $k_M = 10$ and $N_k = 10$. In Fig. 2.4, we plot the indicator functions for S_1, S_2, S_3. The locations of sources $\{z_j^{DSM}\}_{j=1}^3$ reconstructed by the DSM are

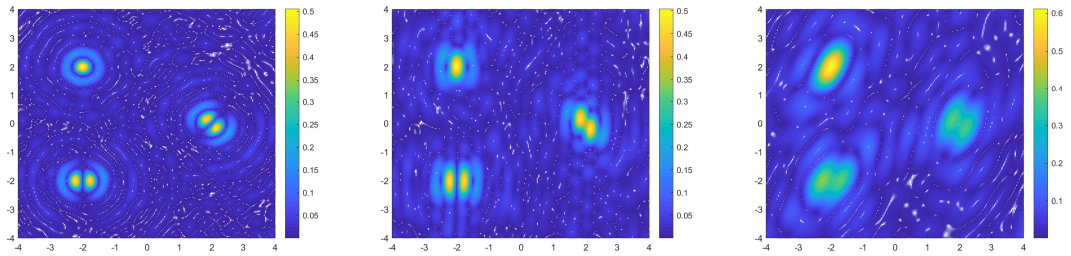

Figure 2.4: Example 2 plots the indicators of the DSM. Left: S_1. Middle: S_2. Right: S_3.

$$S_1 : \{(2.00, 0.00), (-2.00, 2.00), (-2.00, -2.00)\},$$
$$S_2 : \{(2.00, -0.02), (-2.00, 2.04), (-2.00, -2.02)\},$$
$$S_3 : \{(1.98, 0.00), (-2.00, 2.00), (-2.20, -1.94)\}.$$

For partial data, the reconstructed locations are not as accurate as the case of full data, but still satisfactory.

In the Bayesian inversion stage, we set $\beta = 0.05$ and $\sigma = 0.0004$. Then 20000 samples are drawn from the prior distribution and the first 5000 samples are discarded. The inversion results of the MCMC algorithm are shown in Table 2.3. In particular, for partial data, the reconstructed locations are improved in general.

2.5.3 Example 3

Let $F(x) = \sum_{j=1}^2 \lambda_j \exp(-\xi_j \|x - z_j\|^2)$ with

$$\{\lambda_j\}_{j=1}^2 = \{3, -4\},$$

j	Exact Parameters			Reconstructed parameters for S_1		
	λ_j	ξ_j	z_j	$\lambda_j^\star$	$\xi_j^\star$	$z_j^\star$
1	-	$(\sqrt{2}, -\sqrt{2})$	(2, 0)	-	(1.4886, -1.4727)	(1.9936, -0.0019)
2	9	-	(-2, 2)	8.9373	-	(-1.9863, 2.0037)
3	-	(2, 0)	(-2, -2)	-	(1.9696, -0.0350)	(-2.0030, -1.9970)
j	Reconstructed parameters for S_2			Reconstructed parameters for S_3		
	$\lambda_j^\star$	$\xi_j^\star$	$z_j^\star$	$\lambda_j^\star$	$\xi_j^\star$	$z_j^\star$
1	-	(1.4087, -1.4573)	(1.9948, -0.0111)	-	(1.4073, -1.1819)	(2.0037, 0.0072)
2	8.9656	-	(-2.0077, 2.0116)	7.7530	-	(-1.9899, 2.0016)
3	-	(1.7725, 0.0003)	(-2.0022, -2.0173)	-	(1.7091, 0.0544)	(-2.1487, -1.9156)

Table 2.3: Exact and reconstructed parameters for Example 2.

$$\{\xi_j\}_{j=1}^2 = \{2.5, 1\},$$
$$\{z_j\}_{j=1}^2 = \{(2,2), (-1.5, -1.5)\}.$$

Set $[k_m, k_M] = [2, 7]$ and $N_k = 10$. In Fig. 2.5, we plot the indicator functions for S_1, S_2, S_3. The reconstructed locations $\{z_j^{DSM}\}_{j=1}^2$ by the DSM are

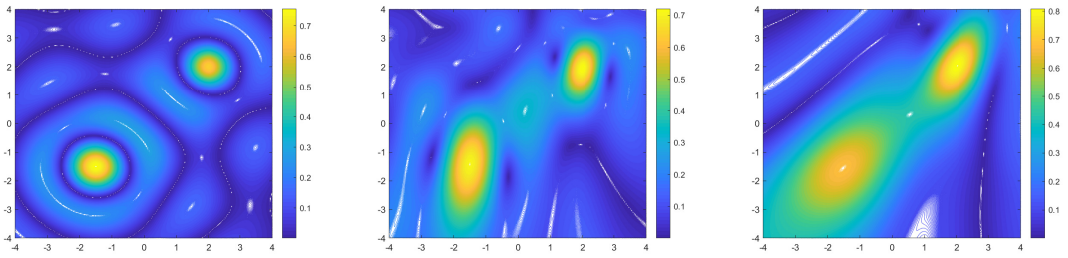

Figure 2.5: Example 3 plots of the indicators of the DSM. Left: S_1. Middle: S_2. Right: S_3.

$$S_1 : \{(2.00, 2.00), (-1.52, -1.52)\},$$
$$S_2 : \{(2.00, 1.96), (-1.52, -1.44)\},$$
$$S_3 : \{(2.04, 2.04), (-1.52, -1.56)\}.$$

The locations are satisfactory. However, the results deteriorate for partial data.

In the Bayesian inversion stage, we set $\beta = 0.03$ and $\sigma = 0.004$. 15000 samples are drawn and the first 3000 samples are discarded. The inversion results are shown in Table 2.4.

j	Exact Parameters			Reconstructed parameters for S_1		
	λ_j	ξ_j	z_j	$\lambda_j^\star$	$\xi_j^\star$	$z_j^\star$
1	3	2.5	(2, 2)	3.0458	2.5154	(1.9894, 2.0094)
2	-4	1	(-1.5, -1.5)	-4.0901	1.0202	(-1.5012, -1.5128)
j	Reconstructed parameters for S_2			Reconstructed parameters for S_3		
	$\lambda_j^\star$	$\xi_j^\star$	$z_j^\star$	$\lambda_j^\star$	$\xi_j^\star$	$z_j^\star$
1	2.8525	2.4827	(2.0098, 1.9999)	3.0494	2.3827	(2.0211, 1.9951)
2	-4.1944	1.0136	(-1.5002, -1.5067)	-3.9265	1.0216	(-1.5064, -1.4779)

Table 2.4: Exact and reconstructed parameters for Example 3.

2.5.4 Example 4

Let $F(x) = \sum_{j=1}^4 \lambda_j \exp(-\xi_j \|x - z_j\|^2)$ with

$$\{\lambda_j\}_{j=1}^4 = \{2, 4, -3, 2.5\},$$
$$\{\xi_j\}_{j=1}^4 = \{2, 3, 2, 1\},$$
$$\{z_j\}_{j=1}^4 = \{(2,2), (-2,2), (-2,-2), (2,-2)\}.$$

Set $[k_m, k_M] = [1.5, 8]$ and $N_k = 15$. In Fig. 2.6, we plot the indicator functions for S_1, S_2, S_3.

The reconstructed locations of sources $\{z_j^{DSM}\}_{j=1}^4$ by the DSM are

$$S_1 : \{(2.04, 2.04), (-2.00, 2.00), (-2.00, -2.00), (1.96, -2.00)\},$$
$$S_2 : \{(2.04, 2.04), (-2.00, 2.00), (-2.00, -1.84), (1.96, -2.20)\},$$
$$S_3 : \{(2.00, 1.64), (-1.96, 2.12), (-2.08, -2.16), (2.04, -1.64)\}.$$

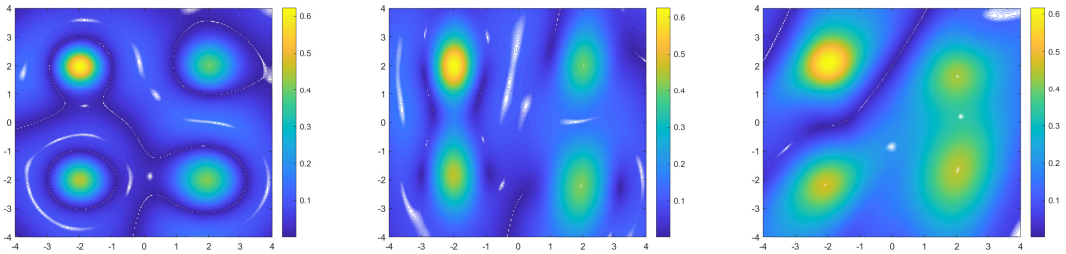

Figure 2.6: Example 4 plots of the indicators of the DSM. Left: S_1. Middle: S_2. Right: S_3.

Similar to the previous examples, the results deteriorate when data are less.

In the Bayesian inversion stage, $\beta = 0.03$ and $\sigma = 0.004$. 20000 samples are drawn and the first 5000 samples are discarded. The inversion results are shown in Table 2.5.

Given the approximate locations by the DSM, the Bayesian step not only reconstructs the intensities of the sources, but also improve the accuracy of the locations, in particular, when the data are less. In Table 2.5 for S_3, the exact location of the fourth source is $(2, -2)$. The location by the DSM is $(2.04, -1.64)$. After the Bayesian step, the location is $(1.9733, -1.7340)$. See also the reconstructions of the third sources of Example 2 in Table 2.3 and Example 3 in Table 2.4, respectively.

2.5.5 Comparison with Other Priors

We compare the DSM-Gaussian prior with two other priors. The first one is the Whittle-Matérn prior, which is a Gaussian distribution with covariance function

$$C(x,y) = \frac{2^{1-\nu}}{\Gamma(\nu)} \left(\frac{|x-y|}{l} \right)^{\nu} K_\nu \left(\frac{|x-y|}{l} \right), \tag{2.5.45}$$

where $\Gamma(\cdot)$ is the Gamma function, K_ν is the νth order second kind modified Bessel function, ν is a smoothness parameter and l is the length scale. The other one is the level set prior. Given a continuous level-set function $\varphi : V \to \mathbb{R}$ and fixed constants

j	Exact Parameters			Reconstructed parameters for S_1		
	λ_j	ξ_j	z_j	$\lambda_j^\star$	$\xi_j^\star$	$z_j^\star$
1	2	2	(2, 2)	2.2408	2.2712	(2.0392, 1.9954)
2	4	3	(-2, 2)	3.9250	2.9601	(-2.0023, 2.0165)
3	-3	2	(-2, -2)	-3.1428	2.1598	(-1.9885, -2.0034)
4	2.5	1	(2, -2)	2.5928	1.0771	(1.9531, -2.0413)
j	Reconstructed parameters for S_2			Reconstructed parameters for S_3		
	$\lambda_j^\star$	$\xi_j^\star$	$z_j^\star$	$\lambda_j^\star$	$\xi_j^\star$	$z_j^\star$
1	2.1579	2.1221	(2.0347, 1.9412)	1.9819	1.5675	(2.0824, 1.7697)
2	3.8821	2.8849	(-1.9937, 2.0028)	4.1515	2.9813	(-2.0566, 2.0335)
3	-2.8060	2.0517	(-2.0167, -1.9650)	-3.2017	1.7718	(-2.0677, -2.1082)
4	2.3755	0.9439	(1.9904, -2.1102)	2.2924	0.8748	(1.9733, -1.7340)

Table 2.5: Exact and reconstructed parameters for Example 4.

$\{l_i\}_{i=0}^n$, $-\infty = l_0 < l_1 \cdots < l_n = \infty$, we define

$$V_i = \{x \in V | l_{i-1} \leqslant \varphi(x) < l_i\}, \quad i = 1, \cdots, n,$$

such that $\cup_{i=1}^n \bar{V}_i = \bar{V}$ and $V_i \cap V_j = \varnothing$ for $i \neq j$. For given $w_1, \cdots, w_n$, the level-set map $\mathcal{G} : C(V; \mathbb{R}) \to L^2(V; \mathbb{R})$ is

$$\mathcal{G}(\varphi)(x) \to w(x) = \sum_{i=1}^n w_i \mathbb{I}_{V_i}(x),$$

where $\mathbb{I}_{V_i}$ denotes the characteristic function of V_i. For more details of the Whittle-Matérn prior and the level-set prior, we refer the readers to [34, 54] and the references therein.

As a test problem, we consider again Example 4. For the level-set prior, we define

$$\mathcal{G}(\varphi)(x) \to w(x) = w^+ \mathbb{I}_{V_+}(x) + w^0 \mathbb{I}_{V_0}(x) + w^- \mathbb{I}_{V_-}(x), \tag{2.5.46}$$

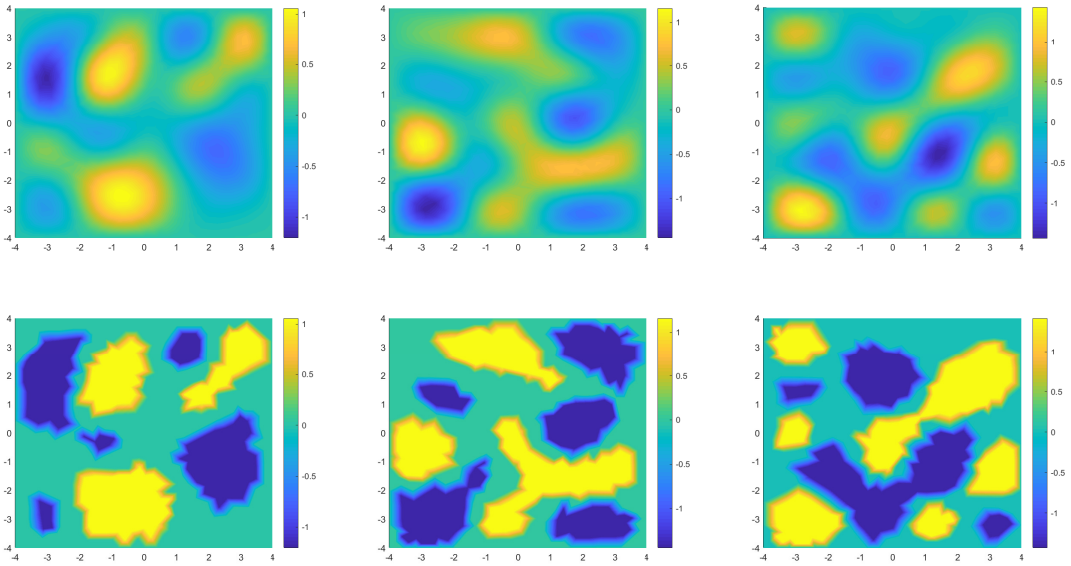

Figure 2.7: Three random draws. Top row: Whittle-Matérn prior. Bottom row: Level-set prior.

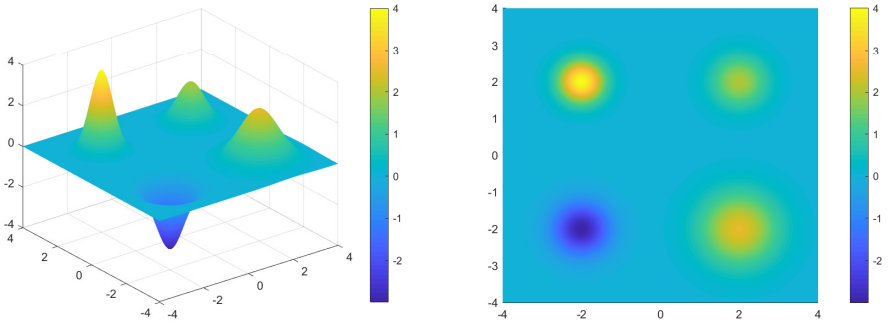

Figure 2.8: The exact source function.

where

$$\begin{cases} w^+ = \max\limits_{x \in V_+} \varphi(x), \\ w^0 = 0, \\ w^- = \min\limits_{x \in V_-} \varphi(x), \end{cases} \quad \text{and} \quad \begin{cases} V_+ = \{x \in V \mid \varphi(x) > 0.3\}, \\ V_0 = \{x \in V \mid -0.3 \leqslant \varphi(x) \leqslant 0.3\}, \\ V_- = \{x \in V \mid \varphi(x) < -0.3\}. \end{cases}$$

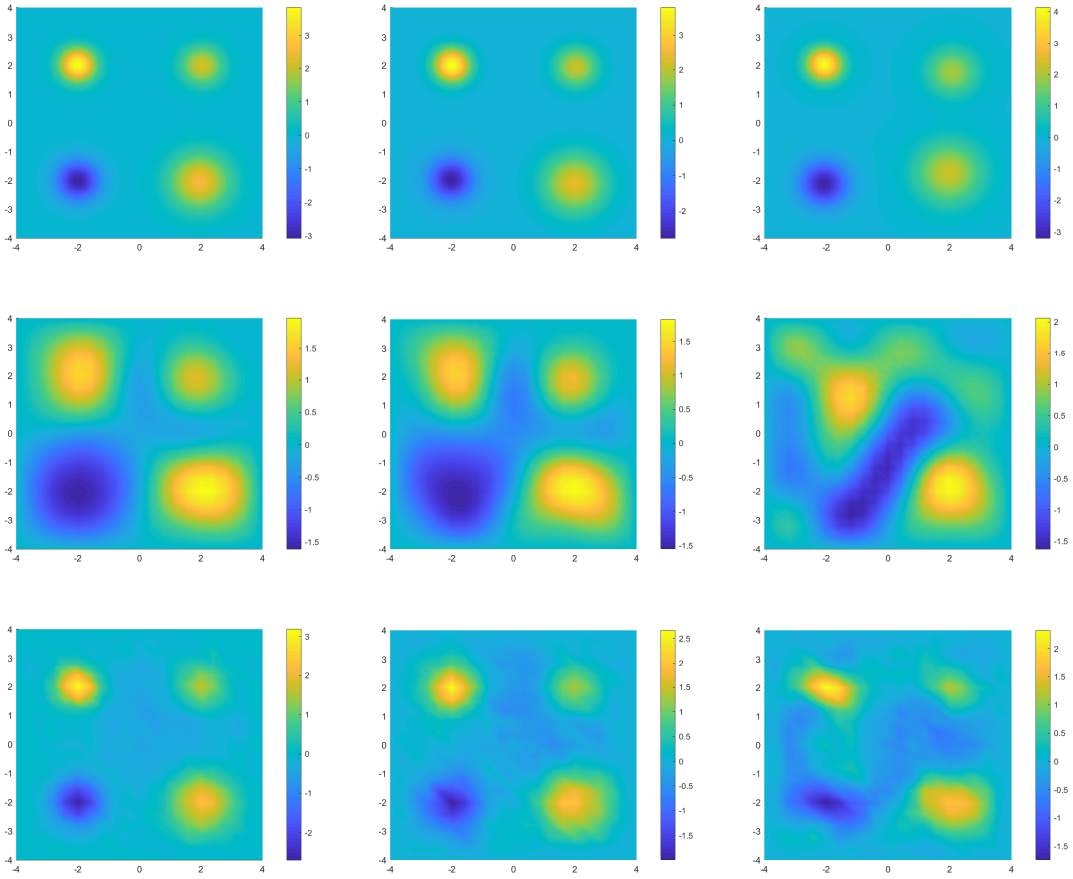

Figure 2.9: Reconstructions. Top row: DSM-Gaussian prior. Middle row: Whittle-Matérn prior. Bottom row: level-set prior. From left to right: S_1, S_2, S_3.

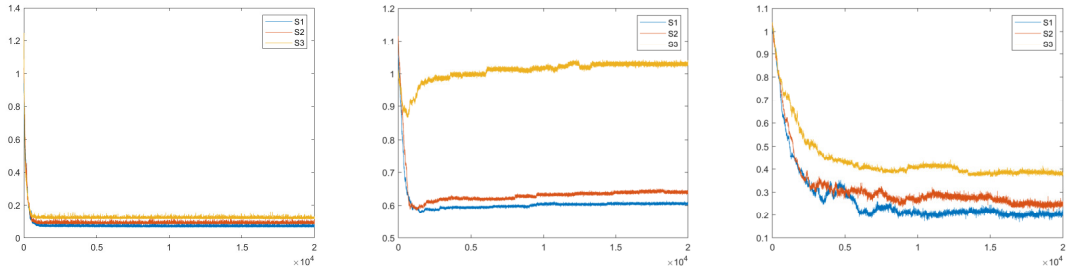

Figure 2.10: Relative errors with respect to the iterations. Left: DSM-Gaussian prior. Middle: Whittle-Matérn prior. Right: level-set prior.

For the level-set prior, one first draws φ from the Whittle-Matérn prior and computes the level-set map (2.5.46). The smoothness and length scale parameters in the Whittle-Matérn prior are $\nu = 2$ and $l = 0.1$, respectively. In Fig 2.7, we show three random draws from the Whittle-Matérn prior and the corresponding level-set prior.

We use the MCMC method discussed in Section 2.4 for all the priors. The transition kernel for the Whittle-Matérn prior is

$$\varphi_{new} = \left(1 - \beta^2\right)^{1/2} \varphi_{old} + \beta\tilde{\varphi}, \tag{2.5.47}$$

and for the level-set prior is

$$w_{new} = \left(1 - \beta^2\right)^{1/2} w_{old} + \beta\mathcal{G}(\tilde{\varphi}). \tag{2.5.48}$$

Here $\tilde{\varphi}$'s in (2.5.47) and (2.5.48) are drawn from the Whittle-Matérn prior. In Fig. 2.8, we show the exact source function. The reconstruntions are shown in Fig. 2.9. In Fig. 2.10, we show the relative errors $\|F - F_{inv}\|_{l^2}/\|F\|_{l^2}$ with respect to the iterations.

We can see that the proposed method is robust with respect to the observation aperture. As the observation aperture gets smaller, the inverse problem becomes more ill-posed. The results of the direct applications of other two priors deteriorate dramatically. When the aperture becomes quite small (S_3), it is difficult to tell the correct number of the sources from the results using the Whittle-Matérn prior (Fig. 2.9, the third column). Note that the focus of this chapter is some main characteristics of the sources (the number, locations and intensities) rather than the shape of an arbitrary source function.

2.6 Conclusions

A new quality-Bayesian approach is proposed to reconstruct the locations and intensities of the unknown acoustic sources. First, a DSM is developed to approximate the locations of the sources. Second, the Bayesian inversion is used to obtain more detailed information. The locations of the sources obtained in the first step are coded

in the priors. A Metropolis-Hastings (MH) MCMC algorithm is employed to explore the posterior density.

The DSM is fast to obtain the qualitative information of the sources, while the Bayesian method is effective for the quantitative information. The approximate locations of the sources reconstructed by the DSM are critical to the convergence of the MCMC method. The Bayesian approach constructs the intensities and also improves the location reconstructions. In particular, when the locations by the DSM for partial data is not accurate, the Bayesian inversion still can obtain reasonable results (see Example 4). The two steps are based on the same physical model and use the same measured data. The new approach inherits the merits of both the DSM and the Bayesian inversion. Numerical examples show that the proposed method is effective when only partial data are available.

In chapter 3, we will study the time harmonic inverse source problem using the combination of deterministic and statistical method.

Chapter 3

A deterministic-statistical approach to reconstruct moving sources using sparse partial data[1]

3.1 Introduction

The detection and identification of moving targets using waves have many important applications such as radar, underwater acoustics, and through the wall imaging [9, 12, 22, 76]. In this chapter, we consider the reconstruction of moving acoustic point sources, which can be mathematically formulated as a time domain inverse source problem. Several methods were proposed recently from the inverse problem community for the time-domain inverse problems of wave equations, e.g., the algebraic method, the time-reversal techniques, the sampling-type methods and the method of fundamental solutions [93, 105, 41, 37, 20]. See also [51] for a uniqueness result for the inverse moving source problem. In practice, the measured data are usually sparse, partial and compromised by noises. Classical methods such as the linear sampling

[1]This chapter has been published as an article in Inverse Problems. https://iopscience.iop.org/article/10.1088/1361-6420/abf813

method and the direct sampling method might not provide satisfactory results. In general, the performance deteriorates significantly as the data become less [89, 42].

In recent years, the Bayesian method became popular for inverse problems [63, 99]. For some recent applications of the Bayesian method for inverse problems, we refer readers to [87, 62, 114] and the references therein. Motivated by the detection of the moving object behind the wall using ultrawideband (UWB) radar [76, 107], the current chapter considers a time-domain inverse problem to determine the moving path of a radiating source with partial data. We proposed a two-step deterministic-statistical approach. In the first step, we develop an approximate direct sampling method (ADSM) to obtain the rough locations of the sources at different times. Since only partial data are available, the locations are usually not accurate compared to the case of full data. Nonetheless, the ADSM does provide useful information of the unknown sources. In the second step, a Bayesian method is used to obtain more detailed information. The priors, which are built on the information obtained in the first step, play a key role for the success of the Bayesian inversion. The idea of utilizing a combined deterministic-statistical approach was first employed to treat the inverse acoustic scattering problem to reconstruct an obstacle with limited-aperture data in [80]. Later, the approach was used to determine both the locations and strengths of static multipolar sources from partial radiated acoustic fields [81]. For recent developments on path reconstructions of moving point sources, we refer the readers to [41, 40, 20, 93, 107, 108, 109].

Inverse problems with partial measurements arise from many applications in science and engineering. Compared with the case of full measurements, it is more challenging in general. The reconstruction deteriorates when the data are less or the observation aperture becomes smaller. In this chapter, for partial data, we propose a deterministic-statistical approach to reconstruct the moving paths of acoustic sources. The contributions are as follows: 1) an approximate direct sampling method is developed to obtain rough locations of moving acoustic sources; 2) an MCMC (Markov

chain Monte Carlo) algorithm is employed to improve/construct the moving paths of the sources using the information obtained by the ADSM; and 3) the well-posedness of the posterior measure is analyzed under the Hellinger distance. Both steps, ADSM and MCMC, are based on the same physical model and use the same set of measured data. The combined approach inherits the merits of the deterministic method and Bayesian inversion as demonstrated by the numerical examples.

The rest of the chapter is organized as follows. In Section 3.2, the direct and inverse problems are introduced. An approximate direct sampling method is developed in Section 3.3. The Bayesian inversion scheme is presented in Section 3.4. Section 3.5 contains several validating numerical examples. Finally, we draw some conclusions in Section 3.6.

3.2 Direct and Inverse Source Problems

We begin with the mathematical model governing the wave source radiation. Denote by $\Omega \subset \mathbb{R}^3$ a simply-connected bounded domain. Consider the wave propagation due to a point excitation in a homogeneous and isotropic media. The speed of the wave in the background media is denoted by the constant c. Let $d_\Omega := \sup_{x,y\in\Omega} \|x-y\|$ and $T > 2d_\Omega/c$ be the terminal time for measuring the radiated data.

For a single point source, the radiated wave field u satisfies the following wave equation

$$c^{-2}\partial_{tt}u(x,t) - \Delta u(x,t) = \lambda(t)\delta(x - z(t)) \quad \text{in } \mathbb{R}^3 \times (0,T], \tag{3.2.1a}$$

with initial conditions

$$u(x,0) = \partial_t u(x,0) = 0 \quad \text{in } \mathbb{R}^3, \tag{3.2.1b}$$

where δ denotes the Dirac delta distribution, the temporal pulse (magnitude of the impulsive load) $\lambda : \mathbb{R} \to \mathbb{R}$ is Lipschitz continuous and $\lambda(t) = 0$ for $t < 0$, $z : \mathbb{R}_+ \to \Omega$ is the trajectory of the moving point source. We refer to [105] for a regularity result on the solution of problem (3.2.1) in some spatial-temporal Sobolev spaces.

Throughout the chapter, we assume that z is continuous and its velocity $v := \mathrm{d}z/\mathrm{d}t$ exists. Furthermore, we suppose that the point source moves slowly compared with the speed of the wave c, that is,

$$\|v(t)\| \ll c, \quad \forall t \in [0, T]. \tag{3.2.2}$$

This is the case for many radar applications such as through-wall imaging radars where c is the speed of electromagnetic waves and $v(t)$ is the speed of the visually obscured target, e.g., a human being inside the building [76, 107].

The direct problem can be described as follows: given $z(t)$ and $\lambda(t)$, find the radiating field u satisfying (3.2.1). It is well known that the solution to this problem is given explicitly by the Liénard–Wiechert retarded potential (see, e.g., [59]):

$$u_z(x,t) = \frac{\lambda(\tau)}{4\pi\|x - z(\tau)\| \left(1 - \frac{v(\tau)\cdot(x-z(\tau))}{c\|x-z(\tau)\|}\right)}, \quad t \in (0, T], \tag{3.2.3}$$

where the retarded time τ is the solution of the equation

$$t = \tau + c^{-1}\|x - z(\tau)\|.$$

When $z(t) \equiv z_0$ is a static point source, the solution to (3.2.1) is simply

$$u_{z_0}(x,t) = \frac{\lambda(t - c^{-1}\|x - z_0\|)}{4\pi\|x - z_0\|}. \tag{3.2.4}$$

For a fixed small enough T, since $\|v(t)\| \ll c, t \in [0, T]$, it holds that

$$|t - \tau| \ll 1 \quad \text{and} \quad \left|\frac{v(\tau)\cdot(x - z(\tau))}{c\|x - z(\tau)\|}\right| \ll 1.$$

Suppose $\Gamma \subset \mathbb{R}^3\backslash\overline{\Omega}$ is a measurement surface (see Fig 3.1 for a geometric illustration of the problem). Let $U_T := \Gamma \times [0, T]$ and define $\|u(x,t)\|^2_{U_T} := \int_0^T \int_\Gamma |u(x,t)|^2 \mathrm{d}x\mathrm{d}t$. We have that

$$\|u_z(x,t) - u_{z_0}(x,t)\|^2_{U_T} := \int_0^T \int_\Gamma |u_z(x,t) - u_{z_0}(x,t)|^2 \mathrm{d}x\mathrm{d}t \ll 1. \tag{3.2.5}$$

In this chapter, we consider the time domain inverse source problem (TISP) of recovering the trajectory $z(t)$ of a moving point source for (3.2.1) from the measurement data $u(x,t)|_{\Gamma\times(0,T]}$. In particular, we are interested in the case of partial data,

e.g., when Γ is a fraction of a sphere. The temporal pulse $\lambda(t) \in \mathcal{C}^1[0,T]$ is assumed to be a periodic function with period $p \in \mathbb{R}_+$.

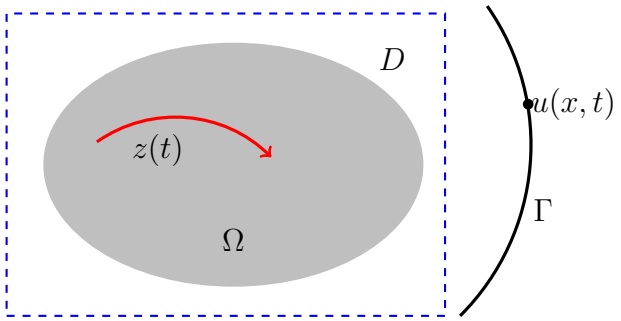

Figure 3.1: An illustration of the time-dependent inverse source problem.

3.3 Direct Sampling Method

In this section we shall develop an approximate direct sampling method (ADSM) for the inverse problem TISP to recover the path $z(t)$ from the measurement data $u(x,t)|_{\Gamma\times(0,T]}$. The sampling-type methods share the basic idea of identifying the unknown target by constructing some indicator functions over the probing/sampling region [30]. Once the indicators are evaluated, the geometrical information (e.g., location and shape) of the target could be recovered using a point-wise criterion to determine whether the sampling point lies inside or outside the target.

As one of the sampling-type methods, the direct sampling method became popular recently due to several compelling features. The direct sampling method is fast and easy to implement. Moreover, they are robust to noise-contaminated measurements in general. However, the direct sampling methods usually require a large amount of measurements and are inherently qualitative. Nonetheless, the direct sampling methods can provide useful information even for partial measurement data.

Let D be a bounded domain in $\mathbb{R}^3$ such that $\Omega \subset D$. The measurement sensors

are located on a surface $\Gamma \subset \mathbb{R}^3 \backslash \bar{D}$ (see Fig. 3.1). Define

$$\phi(x,t;y) = \frac{\lambda(t - c^{-1}\|x-y\|)}{4\pi\|x-y\|}, \quad (x,t;y) \in \Gamma \times (0,T] \times D. \tag{3.3.6}$$

Let $\{T_1, \cdots, T_J\}$ be a partition of $(0,T]$ such that $T_j = ((j-1)p, jp], j = 1, 2, \cdots, J$. Since the temporal function $\lambda(t)$ is a periodic function with period p and $\|v\| \ll c$, the displacement of the point source is small on each T_j. Thus $z(t)$ can be approximated by a stationary point $y \in \mathbb{R}^3$ on T_j.

Given the measurement data $u(x,t)$ with $x \in \Gamma$ and $t \in T_j$, $j = 1, 2, \cdots, J$, we propose the following indicator function

$$I(y;T_j) := \int_{T_j} \frac{|\langle u(x,t), \phi(x,t;y)\rangle_{L^2(\Gamma)}|}{\|u(x,t)\|_{L^2(\Gamma)}\|\phi(x,t;y)\|_{L^2(\Gamma)}}\, \mathrm{d}t, \quad y \in D, \tag{3.3.7}$$

where $\langle \cdot, \cdot \rangle_{L^2(\Gamma)}$ denotes the usual L^2 inner product. Note that, in (3.3.7), instead of the exact radiating field for a moving point source $y \in D$, we use an approximated field ϕ for a stationary point source in (3.3.6). This is why we call the following algorithm the approximated direct sampling method (ADSM). It is clear that the use of ϕ simplifies the computation of the indicators.

The indicator is a superposition of the Bessel functions and decays as the sampling point moves away from the source. The behavior of the indicator can be analyzed using the arguments in [88, 81] and thus omitted here. The numerical results in Section 3.5 show that this indicator function approaches its maximum when the sampling point y tends to the exact instantaneous location of the point source at each time steps.

Now we are ready to present the approximate direct sampling method for the TISP.

ADSM: Approximate Direct Sampling Method

Step 1: Collect the data $u(x,t)$ at the measurement points $\{x_l\} \in \Gamma$, a sequence of discrete time $\{t_j^n\} \in (0,T)$ and for each j, $\{t_j^n\} \in T_j$;

Step 2: Generate the sampling points $\mathcal{T}_h$ for D;

Step 3: Compute $I(y; T_j)$ for the sub-interval T_j at sampling point $y \in \mathcal{T}_h$;

Step 4: Locate the maximum of $I(y_j; T_j)$ for each j, take the corresponding y_j as an approximation of $z(t)$ on T_j. The sequence of locations $\{y_j\}_{j=1}^{J}$ is the reconstructed moving path.

The performance of the ADSM depends on how much data $u(x,t)$ are available. If the measured data are complete or nearly complete, for example, Γ is a sphere with D inside and $u(x,t)$ is available for $x \in \Gamma$ and $t \in (0,T]$, the algorithm can produce a good reconstruction of the trajectory of the moving point source $z(t)$. However, in practice, the measured data $u(x,t)$ are usually partial and the reconstructions can be unsatisfactory. Nonetheless, the ADSM provides useful information of the moving source. Such information can be coded in the priors for the Bayesian inversion to obtain improved reconstructions.

3.4 Bayesian Inversion

In this section, we employ the Bayesian inversion to refine the results obtained by the ADSM. The TISP is reformulated as a statistical inference problem for the source location. The approximate location obtained by the ADSM is coded in the priors for Bayesian inversion. The well-posedness of the posterior density function is analyzed using the Bayesian approximation error approach [63] and the framework in [99]. An MCMC algorithm is then used to explore the posterior density function of the source location.

3.4.1 Bayesian Framework for Inverse Problems

The inverse problem can be viewed as seeking information about the unknown q given the measurement m under the model function $\mathcal{F}$, which might be inaccurate

and contain noise ξ, i.e., given m, reconstruct q such that

$$m = \mathcal{F}(q, \xi). \tag{3.4.8}$$

For statistical inverse problems, the parameters in (3.4.8) are treated as random variables. Denote the probability density function and the probability measure of a random variable γ by π_γ and μ_γ, respectively. Note that the information about q obtained by the ADSM will be coded into the prior density $\pi(q)$[2]. The probability of m given q, which is called the likelihood function, is denoted by $\pi(m|q)$.

Bayesian inversion seeks the posterior distribution $\pi(q|m)$. Using the Bayes' theorem, the joint distribution of the associated variables can be decomposed as

$$\pi(q, m, \xi) = \pi(m, \xi|q)\pi(q) = \pi(q, \xi|m)\pi(m)$$

and the posterior distribution of q is then given by

$$\pi(q|m) = \int \pi(q, \xi|m)\mathrm{d}\xi.$$

Moreover, $\pi(q|m) \propto \pi(m|q)\pi(q)$.

In (3.4.8), $m = \{u(x,t)\} \in Y = \mathbb{R}^{N_x \times N_p}$ is the noisy measurement data collected on $\Gamma \times T_j$, $j = 1, 2, \cdots, J$, where N_x and N_p are the numbers of observation positions and times. The unknown parameter $q \in X = \mathbb{R}^3$, i.e., the position of the point source on the time period T_j, is assumed to be static due to (3.2.2). The space Y is equipped with the Frobenius norm $\|A\|_Y = \left(\sum_{i=1}^{N_p} \sum_{j=1}^{N_x} |a_{ij}|^2\right)^{1/2}$ for $A \in Y$. In this chapter, the Markov chain Monte Carlo (MCMC) method is employed to explore the posterior distribution $\pi(q|m)$ using the Bayesian approximation error approach and the CM is adopted as the point estimate for q.

3.4.2 Bayesian Approximation Error Approach

The main idea of the Bayesian approximation error (BAE) approach is to replace the accurate forward model by a less accurate but computationally feasible one [63, 71,

[2]If the arguments coincide with the probability density function, we drop the subscripts. For example, we write $\pi_q(q) = \pi(q)$, $\pi_{m|q}(m|q) = \pi(m|q)$, but retain the subscript in $\pi_e(m - \mathcal{F}(q) - \zeta)$.

62]. Let $\bar{q} = z(t)$ and $\bar{\mathcal{F}}$ be the accurate forward model given by (3.2.3). We consider the following statistical model for the TISP

$$m = \bar{\mathcal{F}}(\bar{q}) + e, \tag{3.4.9}$$

where e is the additive error. Furthermore, we assume the noise e follows a normal distribution with mean e_* and variance Σ_{ee}, i.e., $\pi_e(e) = \mathcal{N}(e_*, \Sigma_{ee})$. Here we take $e_* = 0$.

Using the statistical model (3.4.9) would require the knowledge of the exact path of the point source for $t \in (0, T]$, which is inaccessible. Fortunately, the exact path is not necessary for the BAE. One proceeds as follows. Let P be a projection operator and $q = P\bar{q}$. Instead of the accurate forward model $\bar{F}(\bar{q})$, one uses the following approximate forward operator

$$\mathcal{F}(q) = \frac{\lambda(t - c^{-1}\|x - q\|)}{4\pi\|x - q\|}, \tag{3.4.10}$$

which is computationally cheaper and more approachable. Then the statistical model can be written as

$$m = \bar{\mathcal{F}}(\bar{q}) + e = \mathcal{F}(q) + \zeta + e,$$

where $\zeta = \bar{\mathcal{F}}(\bar{q}) - \mathcal{F}(q)$ is the approximation error. Due to the fact that $\|v(t)\| \ll c$ and (3.2.5), it is sufficient to study the well-posedness for the approximate forward operator $\mathcal{F}(q)$.

Assume that e is separately independent of q and ζ. According to [71, 62], the posterior distribution satisfies

$$\pi(q|m) \propto \pi(m|q)\pi(q) = \int_Y \pi_e(m - \mathcal{F}(q) - \zeta)\pi(\zeta|q)\ \mathrm{d}\zeta\ \pi(q).$$

In the approximation error approach, $\pi(\zeta|q)$ is approximated with a normal distribution. Assume that the normal approximation of the joint distribution $\pi(\zeta, q)$ is given by

$$\pi(\zeta, q) \propto \exp\left\{ -\frac{1}{2} \begin{pmatrix} \zeta - \zeta_* \\ q - q_* \end{pmatrix}^\top \begin{pmatrix} \Sigma_{\zeta\zeta} & \Sigma_{\zeta q} \\ \Sigma_{q\zeta} & \Sigma_{qq} \end{pmatrix}^{-1} \begin{pmatrix} \zeta - \zeta_* \\ q - q_* \end{pmatrix} \right\},$$

Then we can write $\zeta|q \sim \mathcal{N}(\zeta_{*|q}, \Sigma_{\zeta|q})$, where

$$\zeta_{*|q} = \zeta_* + \Sigma_{\zeta q}\Sigma_{qq}^{-1}(q - q_*),$$
$$\Sigma_{\zeta|q} = \Sigma_{\zeta\zeta} - \Sigma_{\zeta q}\Sigma_{qq}^{-1}\Sigma_{q\zeta}.$$

Define the normal random variable w so that $w = e + \zeta|q$. It holds that

$$w|q \sim \mathcal{N}(w_{*|q}, \Sigma_{w|q}),$$

where

$$w_{*|q} = e_* + \zeta_* + \Sigma_{\zeta q}\Sigma_{qq}^{-1}(q - q_*),$$
$$\Sigma_{w|q} = \Sigma_{ee} + \Sigma_{\zeta\zeta} - \Sigma_{\zeta q}\Sigma_{qq}^{-1}\Sigma_{q\zeta}.$$

The approximate posterior distribution can be written as

$$\pi(q|m) \propto \exp\left(-\frac{1}{2}(m - \mathcal{F}(q) - w_{*|q})^\top \Sigma_{w|q}^{-1}(m - \mathcal{F}(q) - w_{*|q})\right)\pi(q),$$

Let $G(q;m) = \frac{1}{2}(m-\mathcal{F}(q)-w_{*|q})^\top\Sigma_{w|q}^{-1}(m-\mathcal{F}(q)-w_{*|q})$. Assume that μ_m is absolutely continuous with respect to μ_q, i.e., $\mu_m \ll \mu_q$. Using Bayes' formula, we have that

$$\frac{\mathrm{d}\mu_m}{\mathrm{d}\mu_q}(q) = \frac{1}{L(m)}\exp(-G(q;m)),$$

where $L(m) := \int_X \exp\left(-G(q;m)\right)\mathrm{d}\mu_q(q)$. In this chapter, the prior is chosen to be a normal distribution, i.e., $q \sim \mathcal{N}(q_*, \Sigma_{qq})$. We note that in practice other prior distributions can be used as well.

We now study the properties of the operator $\mathcal{F}$ following [99].

Lemma 3.4.1. *For every $\varepsilon > 0$, there exists $C := C(\varepsilon) \in \mathbb{R}$ such that, for all $q \in X$,*

$$\|\mathcal{F}(q)\|_Y \leqslant C.$$

Proof. Since $\lambda(t)$ is Lipschitz continuous, we have

$$|\lambda(t_1) - \lambda(t_2)| \leqslant C_1|t_1 - t_2|, \ \forall t_1, t_2 \in [0, T],$$

and hence $|\lambda(t)| \leqslant C_2$ for all t for some constant C_1, C_2. Define $d = \inf\{\|y_1 - y_2\| : y_1 \in \Gamma, y_2 \in D\}$. By (3.4.10), it holds that

$$|\mathcal{F}(q)| \leqslant \frac{|\lambda(t - c^{-1}\|x - q\|)|}{4\pi d} \leqslant \frac{C_2}{4\pi d}.$$

Therefore,

$$\|\mathcal{F}(q)\|_Y \leqslant C$$

and the proof is complete. ■

Lemma 3.4.2. *For every $r > 0$ there exists a $C := C(r) > 0$ such that, for all $q_1, q_2 \in X$ with $\max\{\|q_1\|_X, \|q_2\|_X\} < r$,*

$$\|\mathcal{F}(q_1) - \mathcal{F}(q_2)\|_Y \leqslant C\|q_1 - q_2\|_X.$$

Proof. Define $\tilde{d} = \sup\{\|y_1 - y_2\| : y_1 \in \Gamma, y_2 \in D\}$. Based on the Lipschitz continuity of $\lambda(t)$,

$$\begin{aligned}
|\mathcal{F}(q_1) - \mathcal{F}(q_2)| =& \left| \frac{\lambda(t - c^{-1}\|x - q_1\|)}{4\pi\|x - q_1\|} - \frac{\lambda(t - c^{-1}\|x - q_2\|)}{4\pi\|x - q_2\|} \right| \\
=& \left| \frac{\lambda(t - c^{-1}\|x - q_1\|)\|x - q_2\| - \lambda(t - c^{-1}\|x - q_2\|)\|x - q_1\|}{4\pi\|x - q_1\|\|x - q_2\|} \right| \\
\leqslant& \left| \frac{\lambda(t - c^{-1}\|x - q_1\|)\|x - q_2\| - \lambda(t - c^{-1}\|x - q_1\|)\|x - q_1\|}{4\pi d^2} \right| \\
&+ \left| \frac{\lambda(t - c^{-1}\|x - q_1\|)\|x - q_1\| - \lambda(t - c^{-1}\|x - q_2\|)\|x - q_1\|}{4\pi d^2} \right| \\
\leqslant& C_2 \left| \frac{\|x - q_2\| - \|x - q_1\|}{4\pi d^2} \right| + C_1 \left| \frac{\|x - q_2\| - \|x - q_1\|}{4\pi d^2} \right| \frac{1}{c}\tilde{d} \\
\leqslant& \frac{\|q_1 - q_2\|_X}{4\pi d^2} \left(C_2 + \frac{1}{c} C_1 \tilde{d} \right).
\end{aligned}$$

It yields that

$$\|\mathcal{F}(q_1) - \mathcal{F}(q_2)\|_Y \leqslant C\|q_1 - q_2\|_X.$$

■

The following theorem provides the well-posedness of the Bayesian approximation error approach. It proof is standard and we refer the readers to Section 4 of [99] for more details.

Theorem 3.4.3. *Assume that μ_q is a Gaussian measure satisfying $\mu_q(X) = 1$ and $\mu_m \ll \mu_q$. For m_1 and m_2 with $\max\{\|m_1\|_Y, \|m_2\|_Y\} \leqslant r$, there exists $M = M(r) > 0$ such that*

$$d_{\mathrm{Hell}}(\mu_{m_1}, \mu_{m_2}) \leqslant M\|m_1 - m_2\|_Y.$$

Proof. Given

$$L(m) = \int_X \exp\left(-\frac{1}{2}(m - \mathcal{F}(q) - w_{*|q})^\top \Sigma_{w|q}^{-1}(m - \mathcal{F}(q) - w_{*|q})\right) \mathrm{d}\mu_q(q),$$

it is obvious that

$$0 \leqslant L(m) \leqslant 1. \tag{3.4.11}$$

According to Lemma 5.3.1, we have that

$$\begin{aligned} L(m) &\geqslant \int_{\|q\|_X \leqslant 1} \exp\left(-\left|\Sigma_{w|q}^{-1}\right| \ \|m - w_{*|q}\|_Y^2 - \left|\Sigma_{w|q}^{-1}\right| \ \|\mathcal{F}(q)\|_Y^2\right) \mathrm{d}\mu_q(q) \\ &\geqslant \int_{\|q\|_X \leqslant 1} \exp(-M) \mathrm{d}\mu_q(q) \\ &= \exp(-M)\mu_q\{\|q\|_X \leqslant 1\} \\ &> 0, \end{aligned} \tag{3.4.12}$$

since the unit ball in X has positive measure and μ_q is a Gaussian measure.

Using Lemma 5.3.1, for μ_q, it holds that

$$\begin{aligned} |L(m_1) - L(m_2)| &\leqslant \int_X |\exp(-G(q; m_1)) - \exp(-G(q; m_2))| \, \mathrm{d}\mu_q(q). \\ &\leqslant \int_X |G(q; m_1) - G(q; m_2)| \, \mathrm{d}\mu_q(q) \\ &\leqslant \int_X \frac{\left|\Sigma_{w|q}^{-1}\right|}{2} \left| \|m_1 - \mathcal{F}(q) - w_{*|q}\|_Y^2 - \|m_2 - \mathcal{F}(q) - w_{*|q}\|_Y^2 \right| \mathrm{d}\mu_q(q) \\ &\leqslant \int_X \frac{\left|\Sigma_{w|q}^{-1}\right|}{2} \left(\left| \|m_1\|_Y^2 - \|m_2\|_Y^2 \right| + \|\mathcal{F}(q) + w_{*|q}\|_Y \ \|m_1 - m_2\|_Y \right) \mathrm{d}\mu_q(q) \\ &\leqslant \int_X \frac{\left|\Sigma_{w|q}^{-1}\right|}{2} \left((\|m_1\|_Y + \|m_2\|_Y) + \|\mathcal{F}(q) + w_{*|q}\|_Y \right) \mathrm{d}\mu_q(q) \|m_1 - m_2\|_Y \\ &\leqslant M\|m_1 - m_2\|_Y. \end{aligned} \tag{3.4.13}$$

From the definition of the Hellinger distance, we obtain that

$$\begin{aligned}
d^2_{\mathrm{Hell}}(\mu_{m_1},\mu_{m_2}) =& \frac{1}{2}\int_X \left\{ \left(\frac{\exp(-G(q;m_1))}{L(m_1)}\right)^{1/2} - \left(\frac{\exp(-G(q;m_2))}{L(m_2)}\right)^{1/2} \right\}^2 \mathrm{d}\mu_q(q) \\
=& \frac{1}{2}\int_X \left\{ \left(\frac{\exp(-G(q;m_1))}{L(m_1)}\right)^{1/2} - \left(\frac{\exp(-G(q;m_2))}{L(m_1)}\right)^{1/2} \right. \\
& \left. + \left(\frac{\exp(-G(q;m_2))}{L(m_1)}\right)^{1/2} - \left(\frac{\exp(-G(q;m_2))}{L(m_2)}\right)^{1/2} \right\}^2 \mathrm{d}\mu_q(q) \\
\leqslant & L(m_1)^{-1}\int_X \left\{ \exp\left(-\frac{1}{2}G(q;m_1)\right) - \exp\left(-\frac{1}{2}G(q;m_2)\right) \right\}^2 \mathrm{d}\mu_q(q) \\
& + \left|L(m_1)^{-1/2} - L(m_2)^{-1/2}\right|^2 \int_X \exp(-G(q;m_2))\mathrm{d}\mu_q(q).
\end{aligned} \tag{3.4.14}$$

With the Lemma 5.3.1, it holds that

$$\begin{aligned}
& \int_X \left\{ \exp\Big(-\frac{1}{2}G(q;m_1)\Big) - \exp\Big(-\frac{1}{2}G(q;m_2)\Big) \right\}^2 \mathrm{d}\mu_q(q) \\
\leqslant & \int_X \left|\frac{1}{2}G(q;m_1) - \frac{1}{2}G(q;m_2)\right|^2 \mathrm{d}\mu_q(q) \\
\leqslant & \frac{\left|\Sigma^{-2}_{w|q}\right|}{16}\int_X \left| \|m_1 - \mathcal{F}(q) - w_{*|q}\|^2_Y - \|m_2 - \mathcal{F}(q) - w_{*|q}\|^2_Y \right|^2 \mathrm{d}\mu_q(q) \\
\leqslant & M\|m_1 - m_2\|^2_Y.
\end{aligned} \tag{3.4.15}$$

Using the bounds on $L(m_1)$ and $L(m_2)$, we have that

$$\left|L(m_1)^{-1/2} - L(m_2)^{-1/2}\right|^2 \leqslant M \max\Big(L(m_1)^{-3}, L(m_2)^{-3}\Big)|L(m_1) - L(m_2)|^2. \tag{3.4.16}$$

Combining (3.4.11)-(5.3.12), we that

$$d_{\mathrm{Hell}}(\mu_{m_1},\mu_{m_2}) \leqslant M\|m_1 - m_2\|_Y.$$

■

We are now ready to present the MCMC method to reconstruct the trajectory $z(t)$ by incorporating in the priors the information obtained by the ADSM.

ADSM-MCMC:

1. Given p, J, and measured data $u(x_l, t_j^n)$ on U_T.

2. For $j = 1, \ldots, J$, do

   a. Use the ADSM to find y_j for T_j and set $q_j^{(1)} = y_j$.

   b. For $k = 1, \cdots, K-1$, do

      I. Generate

$$\tilde{q} = \beta y_j + (1-\beta) q_{j-1} + \sigma \mathcal{N}(0,1) \text{ if } j > 1 \, (\beta = 1 \text{ if } j = 1);$$

      II. Compute $\alpha(\tilde{q}, q_j^{(k)}) = \min\left(1, \dfrac{\pi(\tilde{q})}{\pi\left(q_j^{(k)}\right)}\right)$;

      III. Draw $\tilde{\alpha} \sim \mathcal{U}(0,1)$. If $\alpha > \tilde{\alpha}$, then $q_j^{(k+1)} = \tilde{q}$, otherwise $q_j^{(k+1)} = q_j^{(k)}$.

   c. Set $q_j = \frac{1}{K} \sum_{k=1}^{K} q_j^{(k)}$.

3. Output the moving path $\{q_j\}_{j=1}^{J}$.

We remark that how to use of the locations obtained by the ADSM is problem-dependent. For example, if the target moves rather slow, one can set $\beta = 0$. If the target moves fast, one can choose $\beta = 1$.

3.5 Numerical Examples

In this section, we will present several numerical examples to demonstrate the performance of the proposed method. On each T_j, we choose $\lambda(t)$ to be the Ricker wavelet, which has been widely used in geophysics (see, e.g., [107]),

$$\lambda(t) = \left(1 - 2\pi^2 f_0^2 (t - p/2)^2\right) \exp\left(-\pi^2 f_0^2 (t - p/2)^2\right), \quad t \in [0, p], \tag{3.5.17}$$

where $f_0 \in \mathbb{R}_+$ is the central frequency. The synthetic data $u(x,t)$ is generated using (3.2.3) with some noises:

$$u^\varepsilon(x,t) = u(x,t)(1+\varepsilon r),$$

where ε is the noise level and r is a random number from the uniform distribution $\mathcal{U}[-1,1]$.

For all examples, we set $c = 330$, the terminal time $T = 4$ and $p = 0.1$. The number of equidistant time steps in one period is N_p. Since $(0,T] = \bigcup_{j=1}^{J} T_j$, where $J = T/p$, we have the time increment $\Delta t = p/N_p$ and $N_T = JN_p$. The time discretization is $t_j^n = ((j-1)N_p + n)\,\Delta t,\ n = 1,2,\cdots,N_p,\ j = 1,\cdots,J$. Using the spherical coordinates (R,θ,η)

$$x := R(\sin\eta\cos\theta, \sin\eta\sin\theta, \cos\eta),$$

the measurement aperture Γ is a patch on the sphere with radius $R = 7$, $\theta \in (0, 2\pi]$, $\eta \in (0,\pi]$. Assume that three measurement data sets are given by

$$\{u(x,t) : (x,t) = (\theta,\eta,t) \in S_i, i = 1,2,3\},$$

where (see Fig 3.2)

$$\begin{aligned}
S_1 &= \left\{\frac{\pi}{16}l,\ l = 1,\cdots,32\right\} \times \left\{\frac{\pi}{5}s,\ s = 1,2,3,4\right\} \times \{t_j^n\},\ N_x = 128,\ N_p = 12,\\
S_2 &= \left\{\pi + \frac{\pi}{8}l,\ l = 0,1,\cdots,8\right\} \times \left\{\frac{\pi}{4}, \frac{\pi}{2}\right\} \times \{t_j^n\},\ N_x = 18,\ N_p = 10,\\
S_3 &= \left\{\pi, \frac{5\pi}{4}, \frac{3\pi}{2}\right\} \times \left\{\frac{\pi}{4}, \frac{\pi}{2}\right\} \times \{t_j^n\},\ N_x = 6,\ N_p = 7.
\end{aligned}$$

Note that the spacial coverage of S_1 is the whole sphere corresponding to the case of full aperture data. The spacial coverage is 1/4 of the sphere for S_2 and 1/8 for S_3. In fact, for S_3, there are just 6 measurement locations.

Let the central frequency $f_0 = 100$ for the temporal function $\lambda(t)$ in (3.5.17) in one period (see Fig 3.2(a)). The measurement locations are showed in Fig 3.2(b)-(d) for S_1, S_2 and S_3, respectively.

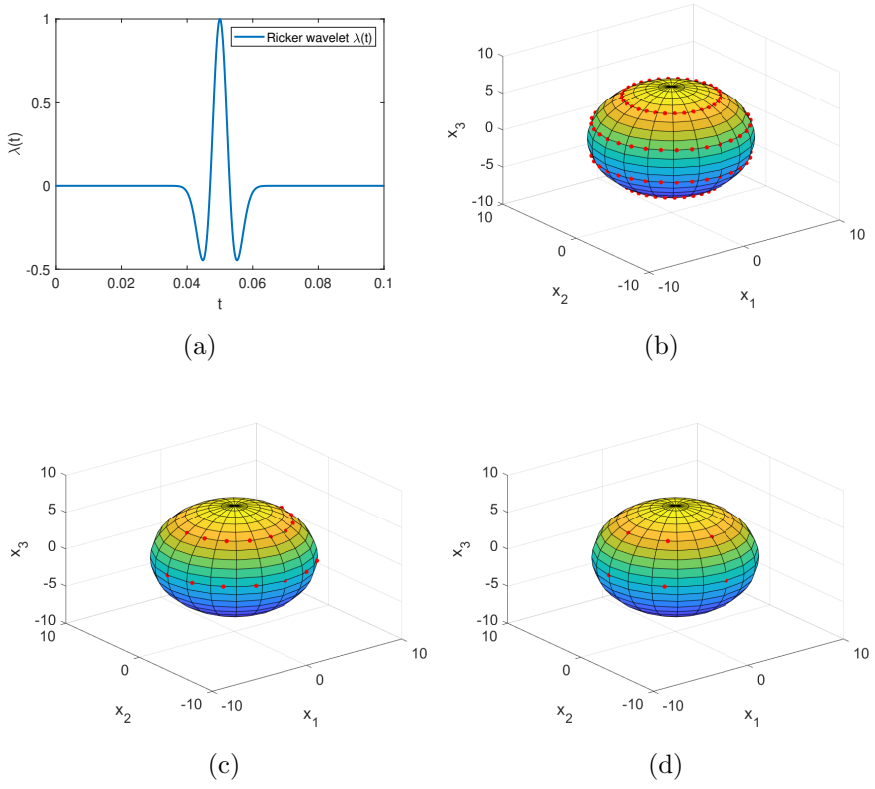

Figure 3.2: The pulse function and measurement locations. (a) the temporal function $\lambda(t)$; (b)-(d) measurement locations for S_1, S_2 and S_3.

We take $101 \times 101 \times 101$ sampling points, denoted by $\mathcal{T}_h$, uniformly distributed in the sampling domain $D = [-5, 5]^3$. For $j = 1, 2, \cdots, J$, the discrete version of the indicator function (3.3.7) can be written as

$$\boldsymbol{I}(y, T_j) := \frac{\sum_{n=1}^{N_p} \sum_{l=1}^{N_x} |u(x_l, t_j^n)\phi(x_l, t_j^n; y)|}{\sum_{n=1}^{N_p} \left(\sum_{l=1}^{N_x} u^2(x_l, t_j^n) \right)^{1/2} \sum_{n=1}^{N_p} \left(\sum_{l=1}^{N_x} \phi^2(x_l, t_j^n; y) \right)^{1/2}}, \qquad y \in \mathcal{T}_h.$$

The ADSM reconstructs the locations of the source as the global maximum points y_j of the discrete indicator function $\boldsymbol{I}(y, T_j)$ for $y \in \mathcal{T}_h$. The sequence $\{y_j\}_{j=1}^J$ is the reconstructed path $z(t)$ by the ADSM. For partial data, the reconstructed path by the ADSM can be unsatisfactory. The result becomes worse for less measurement

data as we shall see.

Based on the information obtained by the ADSM, the Bayesian method is employed to improve the reconstructions. We set $w|q \sim \mathcal{N}(10^{-4}\mathbf{1}_{N_x\times 1}, 10^{-3}I_{N_x\times N_x})$, where $\mathbf{1}_{N_x\times 1}$ is a N_x-by-1 vector of ones and $I_{N_x\times N_x}$ is the N_x-by-N_x identity matrix. For each T_j, $K = 5000$ samples are generated in the MCMC algorithm. The conditional means (CM) are used as the locations of the target.

3.5.1 Example 1: Reconstruction of a C-shape path

The exact moving path of a point source is given by (Fig. 3.3 (d))

$$z(t) = (1.5 + 3\cos(4-t), 2 + 3\sin(2+t), 1.2 - 4\sin(t/2)), \quad t \in [0, T].$$

We take $\Sigma_{qq} = 0.2I_{3\times 3}$ as the covariance of the prior distribution. The prior mean $q_{1,*}$ for $j = 1$ is y_1 which is obtained from the ADSM at T_1. At step $j = 2, \cdots, J$, the prior mean $q_{j,*}$ is selected to be the CM of the Markov chain $\{q_{j-1}^k\}_{k=1}^K$ in the previous step, i.e. $q_{j,*} = q_{j-1}$.

The indicator functions $\boldsymbol{I}(y, T_1)$ using the measured data on S_1, S_2, S_3 are shown in Fig 3.3 (a)-(c). The reconstructed path using the ADSM and the ADSM-MCMC are presented in Fig. 3.3(e)-(h) and (i)-(l), respectively. When the observation data is sufficient (the full aperture case S_1), the ADSM yields a satisfactory reconstruction as shown in Fig. 3.3(e). It can be seen that, when the measured data decrease, the reconstructions of both the ADSM and the ADSM-MCMC deteriorate (the second row (e)-(h) and the third row (i)-(l)). Comparing (f) and (j), (g) and (k), or (h) and (l), the ADSM-MCMC significantly outperforms the ADSM, in particular, when the measurement data are less. Moreover, the Bayesian inference is robust to noises as indicated by Fig. 3.3(k) and (l). The reconstructions are quite satisfactory for noise levels $\varepsilon = 1\%$ and 10% with $(x, t) \in S_3$.

3.5.2 Example 2: Reconstruction of a bow-shape path

We consider the path given by (Fig. 3.4 (d))

$$z(t) = (3 - 1.6t, 0.2 + 2.6\sin(1.25t), -0.3 - 2.1\sin(1.75t)), \quad t \in [0, T].$$

The covariance $\Sigma_{qq} = 0.2I_{3\times 3}$ is used. Fig. 3.4 show the reconstructions. Again, Fig. 3.4 (a)-(c) shows the plots of the indicator functions using the measured data for S_1, S_2, S_3, respectively. The recovered moving paths by the ADSM are given in Fig. 3.4 (e)-(h), which suggest that the ADSM can provide useful information, but far from accurate when the measured data are partial. In the second step, the Bayesian method refines the paths based on the information obtained by the ADSM. Similar to the previous example, as the measurement data become less, the performance of the ADSM is getting worse (Fig. 3.4 (f)-(h)). The results of the ADSM-MCMC Fig. 3.4 (j)-(l) are significantly better than those produced by the ADSM.

3.5.3 Example 3: Simultaneous reconstruction of two paths

We consider the case of two moving point sources which are well-separated. Assume that the signal functions of these sources are the same and their exact moving paths are given by (Fig. 3.5 (d))

$$\begin{aligned} z_1(t) =& (2 - 2\cos(4 - 0.5t), 1 + 3\sin(2 + t), 2), \\ z_2(t) =& (-4, -3 + 1.3t, 1.5). \end{aligned}$$

Since (3.2.1a) is linear with respect to the sources, the proposed method works the same way as the case of a single point source. To be precise, the source term of (3.2.1a) is the superposition $\lambda(t)\delta(x - z_1(t)) + \lambda(t)\delta(x - z_2(t))$. Correspondingly, the exact solution to (3.2.1) is now given by

$$u(x, t; z(t)) = u_1(x, t; z_1(t)) + u_2(x, t; z_2(t)),$$

where u_1 and u_2 are given by (3.2.3) with $z(t)$ replaced by $z_1(t)$ and $z_2(t)$, respectively.

The case of multiple sources is more challenging. We have less confidence of the reconstructions of the ADSM for partial data. Thus the covariance is set to be $\Sigma_{qq} = 0.4I_{3\times 3}$. The ADSM reconstructs two local maximums in Fig. 3.5 (a)-(c), indicating the presence of two point sources. Similar to the previous two examples, when the measured data are complete or almost complete, the ADSM can provide satisfactory reconstructions. The performance is getting worse as the data become less (Fig. 3.5 (f)-(h)). The ADSM-MCMC improves the reconstructions significantly (Fig. 3.5 (j)-(l)). If one uses the same $\Sigma_{qq} = 0.2I_{3\times 3}$ as the previous two examples, more samples ($K = 80000$) are needed to obtain satisfactory results (Fig. 3.6).

3.6 Conclusions

A deterministic-statistical approach is proposed to reconstruct the moving sources using partial data. The approach contains two steps. The first step is a deterministic method to obtain some qualitative information of the unknowns. The second step is the Bayesian inversion with the prior containing the information obtained in the first step. Both steps are based on the same physical model and use the same set of measured data. Numerical results show that it is a promising technique for tracking the moving point sources using partial data.

The reconstruction by the ADSM deteriorates significantly as the data become less. However, it still contains useful information of the sources. Coded in the prior, such information is critical for the success of the MCMC. One can use the uniform prior and perform the Bayesian inverse directly. In Fig. 3.7, we show the reconstructed path of the moving source for S_3 and $\varepsilon = 1\%$ with 5000 samples which follow the uniform distribution $\mathcal{U}[-5, 5]$. It can be seen that the reconstructions in in Fig. 3.7 (c-d) are much worse than Fig. 3.3 (i) and (k).

In next chapter, we will introduce the inverse problem of reconstructing the Stekloff eigenvalues and the index of refraction of an inhomogeneous medium from

Cauchy data.

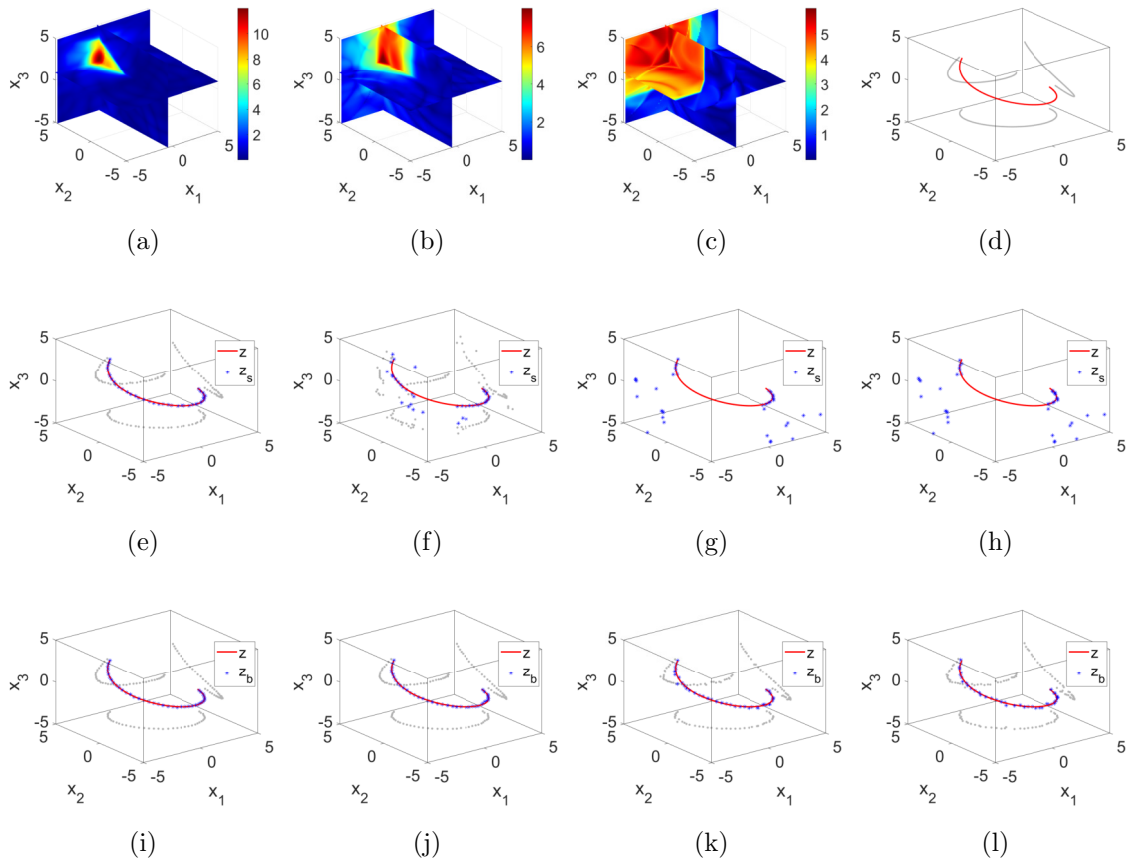

Figure 3.3: Reconstructions of a C-shape path. (a)-(c) are cross-section plots of the indicator functions $\boldsymbol{I}(y, T_1)$. (d) is the exact trajectory $z(t)$. (e)-(g) are the reconstructions by the ADSM using data on S_1, S_2, S_3 with $\varepsilon = 1\%$. (h) is the reconstruction by the ADSM using data on S_3 with $\varepsilon = 10\%$. (i)-(k) are the reconstructions by the ADSM-MCMC using data on S_1, S_2, S_3 with $\varepsilon = 1\%$. (l) is the reconstruction by the ADSM-MCMC using data on S_3 with $\varepsilon = 10\%$. z, $\mathsf{z_s}$, and $\mathsf{z_b}$ represent the exact path, the reconstruction by the ADSM, and the reconstruction by the ADSM-MCMC, respectively.

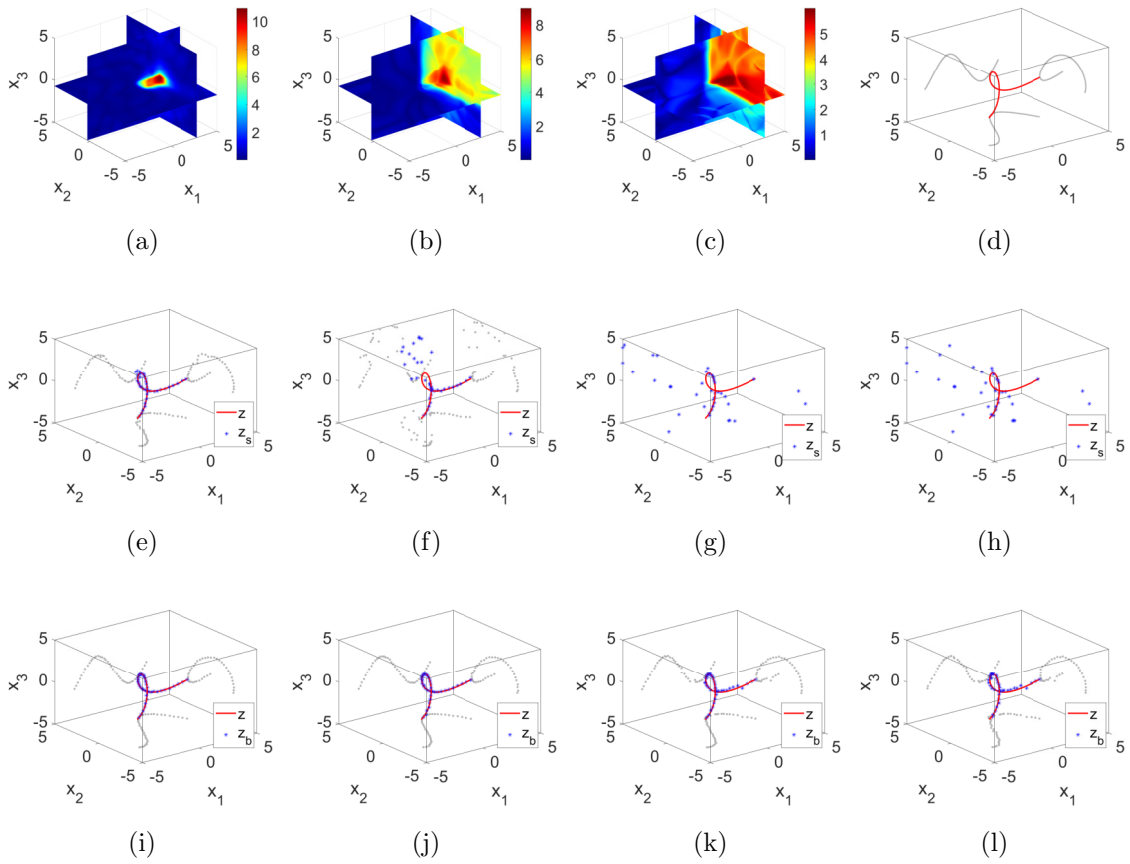

Figure 3.4: Reconstruction of a bow-shape path. (a)-(c) are the cross-section plots of the indicator functions $\boldsymbol{I}(y, T_1)$. (d) is the exact trajectory $z(t)$. (e)-(g) are the reconstructions by the ADSM using data on S_1, S_2, S_3 with $\varepsilon = 1\%$. (h) is the reconstruction by the ADSM using data on S_3 with $\varepsilon = 10\%$. (i)-(k) are the reconstructions by the ADSM-MCMC using data on S_1, S_2, S_3 with $\varepsilon = 1\%$. (l) is the reconstruction by the ADSM-MCMC using data on S_3 with $\varepsilon = 10\%$. z, $\mathsf{dz_s}$, and $\mathsf{z_b}$ represent the exact path, the reconstruction by the ADSM, and the reconstruction by the ADSM-MCMC, respectively.

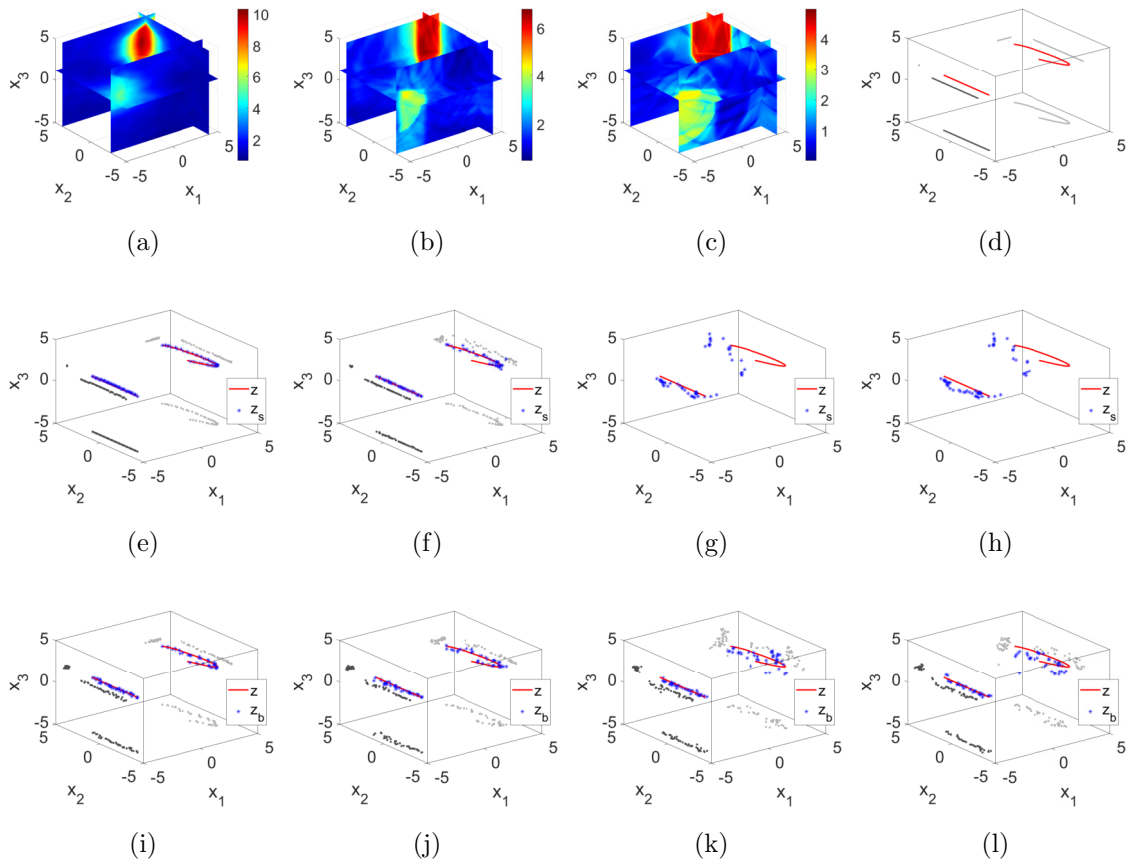

Figure 3.5: Reconstruction of two paths. (a)-(c) are the cross-section plots of the indicator functions $\boldsymbol{I}(y, T_1)$. (d) is the exact trajectory $z(t)$. (e)-(g) are the reconstructions by the ADSM using data on S_1, S_2, S_3 with $\varepsilon = 1\%$. (h) is the reconstruction by the ADSM using data on S_3 with $\varepsilon = 10\%$. For $K = 5000$ and $\Sigma_{qq} = 0.4I_{3\times 3}$, (i)-(k) are the reconstructions by the ADSM-MCMC using data on S_1, S_2, S_3 with $\varepsilon = 1\%$. (l) is the reconstruction by the ADSM-MCMC using data on S_3 with $\varepsilon = 10\%$.

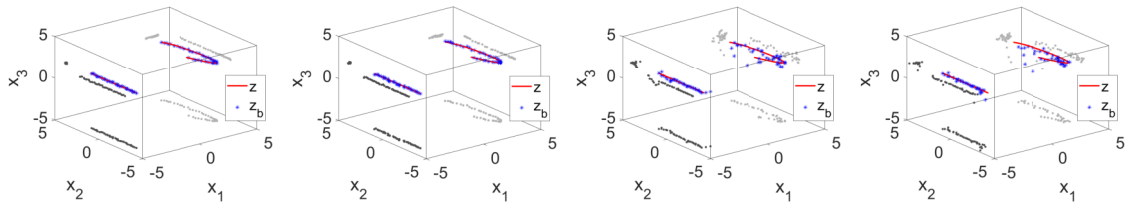

(a) (b) (c) (d)

Figure 3.6: Reconstruction of two paths for $K = 80000$ and $\Sigma_{qq} = 0.2I_{3\times3}$. (a)-(c) are the reconstructions by the ADSM-MCMC using data on S_1, S_2, S_3 with $\varepsilon = 1\%$. (d) is the reconstruction by the ADSM-MCMC using data on S_3 with $\varepsilon = 10\%$. $\mathsf{z}, \mathsf{z_s}$ and $\mathsf{z_b}$ represent the exact paths, the reconstruction by the ADSM, and the reconstruction by the ADSM-MCMC, respectively.

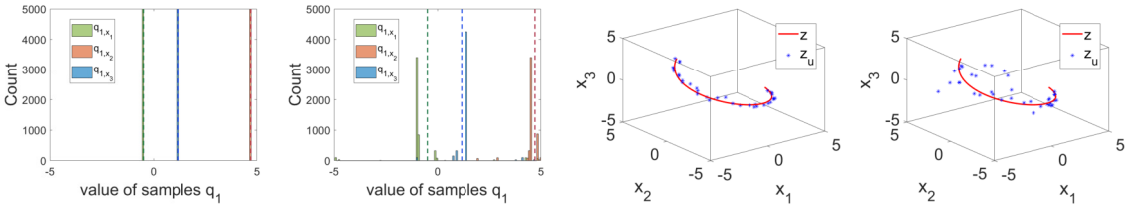

(a) (b) (c) (d)

Figure 3.7: Reconstruction of the C-shape path. (a-b) histograms of the samples $\{q_1^{(k)}\}_{k=1}^K$ with normal and uniform prior for S_1, respectively; (c-d) reconstructions by MCMC with uniform prior for S_1, S_3, $\varepsilon = 1\%$. The dashed line shows the exact value of q_1 and $\mathsf{z_u}$ is path reconstructed by the uniform prior.

Chapter 4

An inverse medium problem using Stekloff eigenvalues and a Bayesian approach[1]

4.1 Introduction

Inverse scattering problems for inhomogeneous media have many applications such as medical imaging and nondestructive testing. In this chapter, the inverse spectrum problem to reconstruct the Stekloff eigenvalues from Cauchy data is investigated using a new integral equation for the reciprocity gap method. Then these eigenvalues are used to estimate the index of refraction of the inhomogeneous medium. Due to the lack of knowledge of the relation between Stekloff eigenvalues and the index of refraction, we propose a Bayesian approach. Since the eigenvalues are complex for absorbing media and the multiplicities are not known, the recently developed spectral indicator method is employed to compute the Stekloff eigenvalues [52, 53].

The reconstruction of certain eigenvalues from the scattering data has been studied

[1]This chapter has been published as an article in Inverse Problems. https://iopscience.iop.org/article/10.1088/1361-6420/ab1be9

by many researchers. In the context of qualitative methods in inverse scattering, it has been shown that interior eigenvalues such as Dirichlet eigenvalues and transmission eigenvalues can be determined from the scattering data [14, 100, 90] (see also the special issue edited by Lechleiter and Sun [75]). Note that the inside-outside duality can also be used to compute interior eigenvalues using the scattering data [65, 73, 74, 94].

Given reconstructed eigenvalues, a legitimate question is what information about the scatterer can be obtained. For inhomogeneous non-absorbing media, transmission eigenvalues have been used to reconstruct the shape of the obstacle [101] and estimate the index of refraction [16, 100, 6, 46, 70, 11, 78]. However, the use of transmission eigenvalues has two drawbacks: 1) multi-frequency data are necessary; and 2) only real transmission eigenvalues can be determined from the scattering data so far.

Recently, it is shown that Stekloff eigenvalues associated with the scattering problem can be determined from far field data of a single frequency [18, 6]. In contrast to transmission eigenvalues, complex Stekloff eigenvalues can also be determined from far field data. Hence the use of Stekloff eigenvalues avoids the above two drawbacks and has the potential to work for a wider class of problems. In this chapter, a new integral equation for the reciprocity gap (RG) method [23, 32, 91] is introduced to determine Stekloff eigenvalues from Cauchy data. Then a Bayesian approach is proposed to estimate the index of refraction, in which the Metropolis-Hastings (M-H) algorithm is used to explore the posterior distribution. We refer the readers to [63, 99] on the Bayesian framework for inverse problems and [10, 38, 110, 47] on its applications to some inverse scattering problems.

The rest of the chapter is organized as follows. In Section 4.2, the forward scattering problem and the associated Stekloff eigenvalue problem are introduced. In Section 4.3, a new integral equation for the reciprocity gap method is proposed to reconstruct Stekloff eigenvalues using Cauchy data. In Section 4.4, a Bayesian approach and the MCMC method are proposed to estimate the index of refraction.

Numerical examples are provided in Section 4.5. Finally, in Section4.6, we make some conclusions.

4.2 Scattering Problem and Stekloff Eigenvalues

In this section, we introduce the direct scattering problem, the Stekloff eigenvalue problem, and the inverse scattering problems using Cauchy data. Then a monotonicity of the largest negative Stekloff eigenvalue is proved.

Let D be a bounded domain in $\mathbb{R}^2$ with C^2 boundary ∂D. Let k be the wavenumber and $n(x)$ be the index of refraction such that $n(x) \in L^\infty(\mathbb{R}^2)$. Assume that $n(x) = 1$ for $\mathbb{R}^2\backslash\overline{D}$ and $\Re(n(x)) > 0, \Im(n(x)) \geqslant 0$, where $\Re(\cdot)$ and $\Im(\cdot)$ denote the real and imaginary parts, respectively. The direct scattering problem is to find the total field u such that

$$\begin{cases} \Delta u + k^2 n(x) u = 0, \quad \text{in } \mathbb{R}^2\backslash\{x_0\}, \\ u = u^s + u^i, \\ \lim\limits_{r\to\infty} r^{\frac{1}{2}}(\partial u^s/\partial r - iku^s) = 0, \quad r = |x|, \end{cases} \tag{4.2.1}$$

where u^s is the scattered field and

$$u^i := \Phi(\cdot, x_0) \quad x_0 \in \mathbb{R}\backslash\overline{D}$$

is the incident field generated by a point source. Here Φ is the fundamental solution of the Helmholtz equation.

The associated Stekloff eigenvalue problem is defined as follows [18]. Find $\lambda \in \mathbb{C}$ and a non-trivial function w such that

$$\begin{cases} \Delta w + k^2 n(x) w = 0, \quad \text{in } B, \\ \partial w/\partial\nu + \lambda w = 0, \quad \text{on } \Gamma, \end{cases} \tag{4.2.2}$$

where B is a bounded domain in $\mathbb{R}^2$ and $\Gamma := \partial B$ such that $D \subset B$.

Assume that the Cauchy data u and $\partial_\nu u := \partial u/\partial\nu$ are known on Γ for the incident field $u^i := \Phi(\cdot, x_0), x_0 \in C$, where C is a simple closed curve containing B (see Figure 4.1). The inverse scattering problems considered in this chapter are:

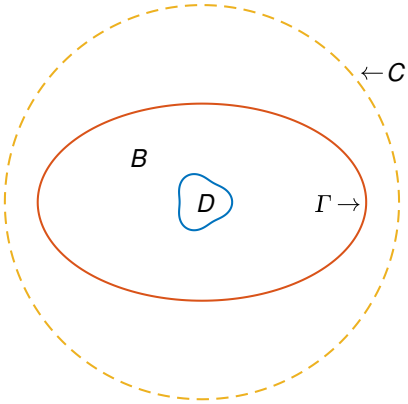

Figure 4.1: Explicative picture of the problem settings.

IP1 Reconstruct Stekloff eigenvalues from Cauchy data;

IP2 Estimate the index of refraction $n(x)$ using Stekloff eigenvalues.

When $n(x)$ is real, all Stekloff eigenvalues are real and they form an infinite discrete set [18]. We call k^2 a modified Dirichlet eigenvalue of B if there exists a nontrivial $u \in H^1(B)$ such that

$$\begin{cases} \Delta u + k^2 n u = 0, & \text{in } B, \\ u = 0, & \text{on } \Gamma. \end{cases} \tag{4.2.3}$$

Remark 4.2.0.1. Note that a standard Dirichlet eigenvalue problem is such that $n(x) \equiv 1$ in (4.2.3). For simplicity, in the rest of the chapter, we call k^2 in (4.2.3) a Dirichlet eigenvalue.

It is shown in [6] that Stekloff eigenvalues accumulate at $-\infty$ if k^2 is not a Dirichlet eigenvalue. Next, we prove a property of the largest negative Stekloff eigenvalue λ_1^- when $n(x)$ is given by

$$n(x) := n_c = \begin{cases} 1, & \text{in } B \backslash \overline{D}, \\ c, & \text{in } D. \end{cases} \tag{4.2.4}$$

Suppose n_c is perturbed by

$$\delta n_c := \begin{cases} 0, & \text{in } B \backslash \overline{D}, \\ \delta c, & \text{in } D, \end{cases}$$

where δc is also a real constant. The perturbation δn_c leads to δw and $\delta\lambda_1^-$ of the eigenpair.

The weak formulation for the Stekloff eigenvalue problem (4.2.2) is to find $(\lambda, u) \in \mathbb{C} \times H^1(B)$ such that

$$(\nabla w, \nabla v) - k^2\,(nw, v) = -\lambda\langle w, v\rangle \quad \forall\, v \in H^1(B), \tag{4.2.5}$$

where $(f,g) = \int_B f\overline{g}dx$ and $\langle f, g\rangle = \int_\Gamma f\overline{g}ds$. From (4.2.5), $\delta w \in H^1(B)$ and $\delta\lambda_1^-$ satisfies

$$\big(\nabla(w+\delta w), \nabla v\big) - k^2\big((n_c+\delta n_c)(w+\delta w), v\big) = -(\lambda_1^- + \delta\lambda_1^-)\big\langle w+\delta w, v\big\rangle \quad \forall\, v \in H^1(B).$$

Using the fact that (w, λ_1^-) is a real eigenpair, we have that

$$\begin{aligned}\big(\nabla\delta w, \nabla v\big) - k^2\big(\delta n_c(w+\delta w), v\big) - k^2\big(n_c\delta w, v\big)& \\ = -\delta\lambda_1^-\big\langle w+\delta w, v\big\rangle - \lambda_1^-\big\langle \delta w, v\big\rangle \quad \forall\, v \in H^1(B).&\end{aligned}$$

Letting $v = w$ and noting that n_c is real, we have that

$$k^2\big(\delta n_c(w+\delta w), w\big) = \delta\lambda_1^-\langle w+\delta w, w\rangle,$$

which implies

$$\begin{aligned}\delta\lambda_1^- &= \frac{k^2\big(\delta n_c(w+\delta w), w\big)}{\langle w+\delta w, w\rangle} \\ &= \frac{k^2\big(\delta n_c w, w\big) + k^2\big(\delta n_c\delta w, w\big)}{\langle w, w\rangle + \langle \delta w, w\rangle} \\ &= \frac{k^2\delta c\big(w, w\big)_D + k^2\delta c\big(\delta w, w\big)_D}{\langle w, w\rangle + \langle \delta w, w\rangle},\end{aligned} \tag{4.2.6}$$

where $(f,g)_D = \int_D f\overline{g}dx$. If $\delta c > 0$ is small enough, one has that

$$|(\delta w, w)_D| < \frac{1}{2}(w, w)_D \quad \text{and} \quad |\langle \delta w, w\rangle| < \frac{1}{2}\langle w, w\rangle. \tag{4.2.7}$$

From (4.2.6) and (4.2.7), we have

$$0 < \frac{k^2\delta c\big(w, w\big)_D}{3\langle w, w\rangle} \leqslant \delta\lambda_1^- \leqslant \frac{3k^2\delta c\big(w, w\big)_D}{\langle w, w\rangle}. \tag{4.2.8}$$

This implies that λ_1^- is monotonically increasing with respect to n_c. This breaks until k^2 becomes a (modified) Neumann eigenvalue, i.e., there exists a non-trivial u such that

$$\begin{cases} \Delta u + k^2 n_c u = 0, & \text{in } B, \\ \frac{\partial u}{\partial \nu} = 0, & \text{on } \Gamma. \end{cases} \tag{4.2.9}$$

Note that a standard Neumann eigenvalue is k^2 satisfying (4.2.9) for $n_c \equiv 1$. Again, we call k^2 for (4.2.9) a Neumann eigenvalue for simplicity. The above derivation actually proved the following theorem.

Theorem 4.2.1. *Let the index of refraction be defined in* (4.2.4) *and* $[a, b]$ *be an interval that* k^2 *is not a Neumann eigenvalue of* (4.2.9) *for any* $c \in [a, b]$. *Then the largest negative Stekloff eigenvalue* λ_1^- *is monotonically increasing on* $[a, b]$.

Assume that the largest negative Stekloff eigenvalue λ_n^- is obtained. If the shape of D is known, λ_1^- uniquely determines n_c on some suitable interval $[a, b]$ by Theorem 4.2.1. However, it is not true on $\mathbb{R}$ as it is known that different n_c's can give the same λ_1^- [18].

4.3 Reconstruction of Stekloff Eigenvalues

Now we consider **IP1** to reconstruct Stekloff eigenvalues from Cauchy data. The main ingredient is the reciprocity gap method [23, 32, 91]. Assume that u and $\partial_\nu u := \partial u/\partial \nu$ are known on Γ for each point source incident wave $u^i := \Phi(\cdot, x_0), x_0 \in C$ (see Figure 4.1). We first define an auxiliary scattering problem. Find $u_\lambda(\cdot, x_0) := u_\lambda^s(\cdot, x_0) + \Phi(\cdot, x_0)$ such that

$$\begin{cases} \Delta u_\lambda + k^2 u_\lambda = 0, & \text{in } \mathbb{R}^2 \backslash \{\overline{B} \cup \{x_0\}\}, \\ \partial_\nu u_\lambda + \lambda u_\lambda = 0, & \text{on } \Gamma, \\ \lim\limits_{r \to \infty} r^{\frac{1}{2}} (\partial u_\lambda^s / \partial r - iku_\lambda^s) = 0, & r = |x|, \end{cases} \tag{4.3.10}$$

where ν is the unit outward normal to Γ and λ is a constant such that $\Im(\lambda) \geqslant 0$. It is shown in [18] that (4.3.10) has a unique solution.

Denote by U and U_λ the sets of solutions $u(x, x_0)$ to (4.2.1) and $u_\lambda(x, x_0)$ to (4.3.10), respectively. Define the reciprocity gap functional by

$$R(v_1, v_2) = \int_\Gamma (v_1 \partial_\nu v_2 - v_2 \partial_\nu v_1) ds, \tag{4.3.11}$$

where v_1 and v_2 are solutions of the Helmholtz equation. Let $\mathbb{S} := \{d \in \mathbb{R}^2; |d| = 1\}$ and consider finding $g \in L^2(\mathbb{S})$ of the integral equation

$$R(u_\lambda(\cdot, x_0) - u(\cdot, x_0), v_g(\cdot)) = R(u_\lambda(\cdot, x_0), \Phi_z(\cdot)) \quad \forall x_0 \in C, \tag{4.3.12}$$

where $\Phi_z(\cdot) := \Phi(\cdot, z)$ for some $z \in B$ and v_g is the Herglotz wave function

$$v_g(x) := \int_{\mathbb{S}} e^{ikx\cdot d} g(d) ds(d).$$

Lemma 4.3.1. *If $\int_\Gamma u_\lambda(x, x_0) f(x) ds(x) = 0$ for all $u_\lambda \in U_\lambda$, then $f(x) = 0$ on Γ.*

Proof. Assume that $f(x)$ satisfies $\int_\Gamma u_\lambda(x, x_0) f(x) ds(x) = 0$ for all $x_0 \in C$. Let $\tilde{u}^s$ be the solution of the following problem

$$\begin{cases} \Delta \tilde{u}^s + k^2 \tilde{u}^s = 0, \quad \text{in } \mathbb{R}^2 \backslash \overline{B}, \\ \partial_\nu \tilde{u}^s + \lambda \tilde{u}^s = f, \quad \text{on } \Gamma, \\ \lim\limits_{r \to \infty} r^{\frac{1}{2}} (\partial \tilde{u}^s / \partial r - ik\tilde{u}^s) = 0, \quad r = |x|. \end{cases} \tag{4.3.13}$$

Using Green's representation theorem [30], Green's second theorem and the boundary condition $\partial_\nu u_\lambda + \lambda u_\lambda = 0$ on Γ for all $x_0 \in C$, we have that

$$\begin{aligned} \tilde{u}^s(x_0) &= \int_\Gamma \partial_\nu \Phi(x, x_0) \tilde{u}^s(x) - \Phi(x, x_0) \partial_\nu \tilde{u}^s(x) ds \\ &= \int_\Gamma \partial_\nu \Phi(x, x_0) \tilde{u}^s(x) - \Phi(x, x_0) \partial_\nu \tilde{u}^s(x) ds \\ &\qquad + \int_\Gamma \partial_\nu u_\lambda^s(x) \tilde{u}^s(x) - u_\lambda^s(x) \partial_\nu \tilde{u}^s(x) ds \\ &= -\int_\Gamma u_\lambda(x, x_0) \partial_\nu \tilde{u}^s(x) - \tilde{u}^s(x) \partial_\nu u_\lambda(x, x_0) ds \\ &= -\int_\Gamma u_\lambda(x, x_0) (\partial_\nu \tilde{u}^s(x) + \lambda \tilde{u}^s(x)) ds \\ &= -\int_\Gamma u_\lambda(x, x_0) f(x) ds \end{aligned}$$

$$= \quad 0. \tag{4.3.14}$$

The unique continuation principle implies that $\tilde{u}^s(x) = 0$ in $\mathbb{R}^2\backslash\bar{B}$. By the trace theorem, $f = 0$ on Γ. ■

Theorem 4.3.2. *If λ is not a Stekloff eigenvalue of (4.2.2), then for $u \in U$ and $u_\lambda \in U_\lambda$, the operator $\mathcal{R} : L^2(\mathbb{S}) \to L^2(C)$ defined by*

$$\mathcal{R}(g) := R\big(u_\lambda(\cdot, x_0) - u(\cdot, x_0), v_g(\cdot)\big), \quad x_0 \in C$$

is injective.

Proof. Let g satisfy $R(u_\lambda(\cdot, x_0) - u(\cdot, x_0), v_g(\cdot)) = 0$ for all $x_0 \in C$. If $g \neq 0$, let w^s solve

$$\begin{cases} \Delta w^s + k^2 n w^s = k^2(1-n)v_g, & \text{in } \mathbb{R}^2, \\ \lim\limits_{r\to\infty} r^{\frac{1}{2}}(\partial w^s/\partial\nu - ikw^s) = 0, & r = |x|. \end{cases} \tag{4.3.15}$$

Using the boundary condition $\partial_\nu u_\lambda + \lambda u_\lambda = 0$ on Γ and Green's second theorem twice, the following holds

$$\begin{aligned}
& \int_\Gamma u_\lambda\big(\partial_\nu(w^s + v_g) + \lambda(w^s + v_g)\big)ds \\
= \quad & \int_\Gamma \big[u_\lambda\partial_\nu(w^s + v_g) - (w^s + v_g)\partial_\nu u_\lambda\big]ds \\
= \quad & \int_\Gamma \big[u_\lambda\partial_\nu(w^s + v_g) - (w^s + v_g)\partial_\nu u_\lambda\big]ds - \int_\Gamma \big[u\partial_\nu(w^s + v_g) - (w^s + v_g)\partial_\nu u\big]ds \\
= \quad & \int_\Gamma \big[(u_\lambda - u)\partial_\nu(w^s + v_g) - (w^s + v_g)\partial_\nu(u_\lambda - u)\big]ds \\
= \quad & \int_\Gamma \big[(u_\lambda - u)\partial_\nu v_g - v_g\partial_\nu(u_\lambda - u)\big]ds + \int_\Gamma \big[(u_\lambda - u)\partial_\nu w^s - w^s\partial_\nu(u_\lambda - u)\big]ds \\
= \quad & \int_\Gamma \big[(u_\lambda - u)\partial_\nu v_g - v_g\partial_\nu(u_\lambda - u)\big]ds \\
= \quad & R(u_\lambda - u, v_g) \qquad (4.3.16) \\
= \quad & 0. \qquad (4.3.17)
\end{aligned}$$

From (4.3.16) and Theorem 4.3.1, we have $\partial_\nu(w^s + v_g) + \lambda(w^s + v_g) = 0$ on Γ. Together

with (4.3.15), $w^s + v_g$ satisfies

$$\begin{cases} \Delta(w^s + v_g) + k^2 n(w^s + v_g) = 0, \quad \text{in } B, \\ \partial_\nu(w^s + v_g) + \lambda(w^s + v_g) = 0 \quad \text{on } \Gamma. \end{cases} \tag{4.3.18}$$

Since λ is not a Stekloff eigenvalue, (4.3.18) only has the trivial solution $w^s + v_g = 0$ in B. From (4.3.15) and the unique continuation principle, $w^s + v_g = 0$ in $\mathbb{R}^2$, i.e., the Herglotz wave function $v_g = -w^s$ satisfies the radiating condition. This is a contradiction. ■

The following theorem is the main result on the reconstruction of Stekloff eigenvalues from Cauchy data.

Theorem 4.3.3. *1. If λ is not a Stekloff eigenvalue of (4.2.2) and $z \in B$, then there exists a sequence $\{g_n\}, g_n \in L^2(\mathbb{S})$, such that*

$$\lim_{n\to\infty} R\big(u_\lambda - u, v_{g_n}\big) = R(u_\lambda, \Phi_z), \qquad u_\lambda \in U_\lambda,\ u \in U \tag{4.3.19}$$

and v_{g_n} converges in $L^2(B)$.

2. If λ is a Stekloff eigenvalue, then for every sequence $\{g_n^z\}, g_n^z \in L^2(\mathbb{S})$ satisfying

$$\lim_{n\to\infty} R\big(u_\lambda - u, v_{g_n^z}\big) = R(u_\lambda, \Phi_z), \qquad u_\lambda \in U_\lambda,\ u \in U, \tag{4.3.20}$$

$\lim_{n\to\infty} \|v_{g_n^z}\|_{H^1(B)} = \infty$ *for almost every $z \in B$.*

Proof. 1. Let w_z be the solution of the following problem

$$\begin{cases} \Delta w_z + k^2 n w_z = 0, \quad \text{in } B, \\ \partial_\nu w_z + \lambda w_z = \partial_\nu \Phi(\cdot, z) + \lambda \Phi(\cdot, z) \quad \text{on } \Gamma. \end{cases} \tag{4.3.21}$$

From Lemma 3.1 of [18], we have

$$w_z = w_z^i + w_z^s,$$

where w_z^i satisfies the Helmholtz equation in B and $w_z^s \in H^2_{loc}(\mathbb{R}^2)$ is a radiation solution to

$$\begin{cases} \Delta w_z^s + k^2 n w_z^s = k^2(1-n) w_z^i, \quad \text{in } \mathbb{R}^2, \\ \lim_{r\to\infty} r^{\frac{1}{2}}(\partial w_z^s/\partial r - ik w_z^s) = 0, \quad r = |x|. \end{cases} \tag{4.3.22}$$

Due to the denseness property (Theorem 5.21 of [30]), there exists a sequence of Herglotz wave functions $\{v_{g_n}\}$ such that

$$v_{g_n} + w_z^s \to w_z^i + w_z^s = w_z, \qquad n \to \infty. \tag{4.3.23}$$

Next we show that $\{v_{g_n}\}$ satisfies $\lim_{n\to\infty} R\big(u_\lambda - u, v_{g_n}\big) = R(u_\lambda, \Phi_z)$. Using Green's second theorem twice, one has that

$$\begin{aligned}
&\lim_{n\to\infty} R(u_\lambda - u, v_{g_n}) - R(u_\lambda, \Phi_z) \\
=\ & \lim_{n\to\infty} \int_\Gamma \big[(u_\lambda - u)\partial_\nu v_{g_n} - v_{g_n}\partial_\nu(u_\lambda - u)\big]ds - \int_\Gamma \big[u_\lambda \partial_\nu \Phi_z - \Phi_z \partial_\nu u_\lambda\big]ds \\
=\ & \lim_{n\to\infty} \int_\Gamma \big[(u_\lambda - u)\partial_\nu (v_{g_n} + w_z^s) - (v_{g_n} + w_z^s)\partial_\nu(u_\lambda - u)\big]ds \\
& - \int_\Gamma \big[u_\lambda \partial_\nu \Phi_z - \Phi_z \partial_\nu u_\lambda\big]ds \\
=\ & \lim_{n\to\infty} \int_\Gamma \big[u_\lambda \partial_\nu (v_{g_n} + w_z^s) - (v_{g_n} + w_z^s)\partial_\nu u_\lambda\big]ds \\
& - \lim_{n\to\infty} \int_\Gamma \big[u \partial_\nu (v_{g_n} + w_z^s) - (v_{g_n} + w_z^s)\partial_\nu u\big]ds - \int_\Gamma \big[u_\lambda \partial_\nu \Phi_z - \Phi_z \partial_\nu u_\lambda\big]ds \\
=\ & \lim_{n\to\infty} \int_\Gamma \big[u_\lambda \partial_\nu (v_{g_n} + w_z^s) - (v_{g_n} + w_z^s)\partial_\nu u_\lambda\big]ds - \int_\Gamma \big[u_\lambda \partial_\nu \Phi_z - \Phi_z \partial_\nu u_\lambda\big]ds \\
=\ & \lim_{n\to\infty} \int_\Gamma \big[u_\lambda \partial_\nu (v_{g_n} + w_z^s - \Phi_z) - (v_{g_n} + w_z^s - \Phi_z)\partial_\nu u_\lambda\big]ds \\
=\ & \lim_{n\to\infty} \int_\Gamma u_\lambda \big[\partial_\nu (v_{g_n} + w_z^s - \Phi_z) + \lambda(v_{g_n} + w_z^s - \Phi_z)\big]ds \\
=\ & 0,
\end{aligned} \tag{4.3.24}$$

where the last step is due to (4.3.21) and (4.3.23).

2. Assume on the contrary that for $z \in B_\rho$, where $B_\rho \subset B$ is a small ball of radius ρ, $\|v_{g_n^z}\|_{H^1(B)}$ is bounded as $n \to \infty$. Then there exists a subsequence of $v_{g_n^z}$, still denoted by $v_{g_n^z}$, converging weakly to a function $v^i \in H^1(B)$. Then

$$\int_\Gamma \big[(u_\lambda - u)\partial_\nu v^i - v^i \partial_\nu (u_\lambda - u)\big]ds - \int_\Gamma \big[u_\lambda \partial \Phi_z - \Phi_z \partial_\nu u_\lambda\big]ds = 0. \tag{4.3.25}$$

Let $w^s \in H^2_{loc}(\mathbb{R}^2)$ be a radiating solution to

$$\begin{cases} \Delta w^s + k^2 n w^s = k^2(1-n)v^i, & \text{in } \mathbb{R}^2, \\ \lim\limits_{r\to\infty} r^{\frac{1}{2}}(\partial w^s/\partial r - ikw^s) = 0, & r = |x|. \end{cases} \tag{4.3.26}$$

From the Green's second theorem and (4.3.25), $w := v^i + w^s$ satisfies

$$\begin{aligned}
&\int_\Gamma u_\lambda\big[\partial_\nu(w-\Phi_z)+\lambda(w-\Phi_z)\big]ds \\
=\ &\int_\Gamma \big[u_\lambda\partial_\nu w - w\partial_\nu u_\lambda\big]ds - \int_\Gamma \big[u_\lambda\partial_\nu\Phi_z - \Phi_z\partial_\nu u_\lambda\big]ds \\
=\ &\int_\Gamma \big[(u_\lambda-u)\partial_\nu w - w\partial_\nu(u_\lambda-u)\big]ds - \int_\Gamma \big[u_\lambda\partial_\nu\Phi_z - \Phi_z\partial_\nu u_\lambda\big]ds \\
=\ &\int_\Gamma \big[(u_\lambda-u)\partial_\nu w^s - w^s\partial_\nu(u_\lambda-u)\big]ds \\
&+\int_\Gamma \big[(u_\lambda-u)\partial_\nu v^i - v^i\partial_\nu(u_\lambda-u)\big]ds - \int_\Gamma \big[u_\lambda\partial_\nu\Phi_z - \Phi_z\partial_\nu u_\lambda\big]ds \\
=\ &\int_\Gamma \big[(u_\lambda-u)\partial_\nu w^s - w^s\partial_\nu(u_\lambda-u)\big]ds \\
=\ &0. \qquad (4.3.27)
\end{aligned}$$

From (4.3.27) and Theorem 4.3.1,

$$\partial_\nu(w-\Phi_z)+\lambda(w-\Phi_z)=0 \quad \text{on } \Gamma,$$

which, together with (4.3.26), implies that w satisfies

$$\begin{cases} \Delta w + k^2 n w = 0 \quad \text{in } B, \\ \partial_\nu w + \lambda w = \partial_\nu\Phi(\cdot,z) + \lambda\Phi(\cdot,z) \quad \text{on } \Gamma. \end{cases} \qquad (4.3.28)$$

From Theorem 4.3.1 and the proof of Theorem 3.3 of [18], (4.3.28) is solvable if and only if

$$\int_\Gamma \left(\frac{\partial\Phi(\cdot,z)}{\partial\nu} + \lambda\Phi(\cdot,z)\right)\omega_\lambda ds = 0 \qquad (4.3.29)$$

for each Stekloff eigenfunction $\omega_\lambda \in H^1(B)$. Since ω_λ satisfies $\partial_\nu\omega_\lambda + \lambda\omega_\lambda = 0$ on Γ, (4.3.29) becomes

$$\int_\Gamma \left(\frac{\partial\Phi(\cdot,z)}{\partial\nu}\omega_\lambda - \Phi(\cdot,z)\frac{\partial\omega_\lambda}{\partial\nu}\right)ds = 0.$$

Green's representation theorem implies that $\omega_\lambda(z) = 0$ for $z \in B_\rho$. The unique continuation principle now implies that the Stekloff eigenfunction $\omega_\lambda = 0$ in B, which is a contradiction. ■

Based on Theorem 4.3.3, the following reciprocity gap algorithm is proposed to reconstruct (several) Stekloff eigenvalues from Cauchy data.

The RG Algorithm

1. For a region of interests (e.g., an interval on $\mathbb{R}$ for real Stekloff eigenvalues or a rectangular region on $\mathbb{C}$ for complex Stekloff eigenvalues), generate a grid T.

2. For each $\lambda \in T$, solve the scattering problem (4.3.10) to compute the auxiliary Cauchy data $u_\lambda(\cdot, x_0)$ and $\partial_\nu u_\lambda(\cdot, x_0)$ on Γ.

3. Fix a point $z \in B$, use the Tikhonov regularization to compute an approximate solution $g_\lambda \in L^2(\mathbb{S})$ to the integral equation

$$R\big(u_\lambda(\cdot, x_0) - u(\cdot, x_0), v_{g_\lambda}(\cdot)\big) = R\big(u_\lambda(\cdot, x_0), \Phi(\cdot, z)\big) \quad \forall x_0 \in C, \tag{4.3.30}$$

   where $u(\cdot, x_0)$ is the solution to (4.2.1) for $\Phi(\cdot, x_0), x_0 \in C$.

4. Choose λ as a Stekloff eigenvalue of (4.2.2) if the norm of g_λ is significantly larger (see Section 4.5.1).

Remark 4.3.3.1. In theory, the constructed solutions to the reciprocity gap equation (4.3.30) may not form a divergent Herglotz wave function series. Hence the above numerical algorithm might not be able to construct all the eigenvalues.

4.4 Reconstruction of the Index of Refraction

Given the reconstructed eigenvalues, in this section, we turn to **IP2** to estimate the index of refraction. The relation between the index of refraction and Stekloff eigenvalues is complicated and, to a large extend, unknown. Even when $n(x)$ is constant, a single Stekloff eigenvalue cannot uniquely determine it. Note that Theorem 4.2.1 only holds on an appropriate interval.

To this end, we resort to the Bayesian approach, which has been popular for solving inverse problems in recent years [63, 99]. Firstly, the inverse problem is reformulated

as a statistical inference for the index of refraction using a Bayes formula. Then the Metropolis-Hastings algorithm is employed to explore the posterior distribution of $n(x)$.

4.4.1 Bayesian Formulation

IP2 can be written as the statistical inference of $n(x)$ such that

$$\boldsymbol{\lambda} = \mathcal{G}(n) + E, \tag{4.4.31}$$

where $\boldsymbol{\lambda} \in \mathbb{C}^m$ is a vector of (reconstructed) Stekloff eigenvalues, $n(x)$ is a random function, $\mathcal{G}$ is the operator mapping $n(x)$ to $\boldsymbol{\lambda}$ based on (4.2.2), and E is the random noise. The noise $E \sim \mathcal{N}(0,\, \sigma^2)$, which is modeled as additive and mutually independent of $n(x)$. In the Bayesian framework, the prior information can be coded into the prior density $\pi_{pr}(n)$. For example, if n is known to be a real constant n_0 such that $a < n_0 < b$, one may take the prior as the continuous uniform distribution, i.e., $n \sim \mathcal{U}(a, b)$.

Given Stekloff eigenvalues $\boldsymbol{\lambda}$, the goal of the Bayesian inverse problem is to seek statistical information of $n(x)$ by exploring the conditional probability distribution $\pi_{post}(n|\boldsymbol{\lambda})$, called the posterior distribution of n. The conditional mean (CM) is applied to obtain a constant estimation of $n(x)$. If $n \sim \mathcal{U}(a, b)$, by the Bayes formula, the posterior distribution satisfies

$$\pi_{post}(n|\boldsymbol{\lambda}) \propto \mathcal{N}(\boldsymbol{\lambda} - \mathcal{G}(n),\, \sigma^2) \times \mathcal{U}(a, b), \tag{4.4.32}$$

i.e.,

$$\pi_{post}(n|\boldsymbol{\lambda}) \propto \exp\Big(-\frac{1}{2\sigma^2} |\boldsymbol{\lambda} - \mathcal{G}(n)| \Big) \times I(a \leqslant n \leqslant b), \tag{4.4.33}$$

where I is the density function for $\mathcal{U}(a, b)$.

4.4.2 Markov Chain Monte Carlo Method

To explore $\pi_{post}(n|\boldsymbol{\lambda})$ given in (4.4.33), we employ the popular MCMC (Markov Chain Monte Carlo). MCMC to estimate CM is as follows: design a Markov Chain $\{X_j\}_{j=0}^{\infty}$ from required distribution and take the mean of the chain to approximate the expectation. In particular, one could estimate $\mathbb{E}\{n|\boldsymbol{\lambda}\}$ by the sample mean using Monte Carlo integration:

$$\mathbb{E}\{n|\boldsymbol{\lambda}\} \approx \frac{1}{m}\sum_{j=1}^{m} n_j, \tag{4.4.34}$$

where n_j, $j = 1, \cdots, m$, are samples from $\pi_{post}(n|\boldsymbol{\lambda})$. In this chapter, we use a delayed rejection adaptive Metropolis-Hasting algorithm [48, 44].

The M-H Algorithm

1. Choose the initial value $n_1 \in \mathbb{R}$ and set $j = 1$;

2. Draw a sample w from a proposal distribution with variance γ^2

$$q(n_j, w) \propto \exp\left(-\frac{1}{2\gamma^2}|n_j - w|^2\right),$$

   and compute

$$\alpha(n_j, w) = \min\left(1, \frac{\pi_{post}(w|\boldsymbol{\lambda})}{\pi_{post}(n_j|\boldsymbol{\lambda})}\right);$$

3. Draw $t \sim \mathcal{U}(0, 1)$;

4. If $\alpha(n_j, w) \geqslant t$, set $n_j = w$, else $n_{j+1} = n_j$.

5. When $j = K$, the maximum sample size, stop; else, $j \leftarrow j + 1$ and go to 2.

4.4.3 Spectral Indicator Method

In the above algorithm, for each sample n_j, one needs to compute Stekloff eigenvalues for (4.2.2). Note that Stekloff eigenvalues may be complex if $n(x)$ is a complex function. The reconstructed eigenvalues are usually not large in magnitude and only approximate the exact ones. Furthermore, the multiplicities are not known in general.

Thus it is ideal if one only computes Stekloff eigenvalues of (4.2.2) in a region in the complex plane close to the origin. A new spectral indicator method (SIM) is a good fit for this case [52, 53]. It computes all eigenvalues inside a given region. We refer the readers to [85] for more details.

4.5 Numerical Examples

In this section, we present some numerical examples to use the RG method to reconstruct Stekloff eigenvalues from the Cauchy data and estimate the index of refraction using the Bayesian approach. Three scatterers are considered: a disc with radius 1 centered at the origin, a square with vertices given by

$$(0,-1), \quad (1,0), \quad (0,1), \quad (-1,0), \tag{4.5.35}$$

and an L-shaped domain given by

$$(-0.9,1.1)\times(-1.1,0.9)\backslash[0.1,1,1]\times[-1.1,-0.1]. \tag{4.5.36}$$

Three different indices of refraction are chosen: i) $n(x)=5$, ii) $n(x)=4+2|x|$, and iii) $n(x)=2+4i$.

The synthetic scattering data is simulated by a finite element method with a perfectly matched layer (PML) for (4.2.1) [21]. The wavenumber is $k=1$. There are 100 source points uniformly distributed on the curve C, a circle with radius 3. We compute the Cauchy data at 100 points uniformly distributed on $\Gamma := \partial B$ (a circle with radius 2) and add 3% noise.

4.5.1 Reconstruction of Stekloff eigenvalues

Given Cauchy data, we show that several Stekloff eigenvalues close to the origin can be reconstructed effectively using the RG Algorithm presented in Section 4.3. For real $n(x)$, all the eigenvalues are real. We choose an interval $[-5,5]$ and use a uniform

grid T given by

$$T := \{\lambda_m = -5 + 0.02m, \quad m = 0, 1, \cdots, 500\}.$$

For complex $n(x)$, the Skeloff eigenvalues are complex. We choose a region $[-1, 0.5] \times [-0.5, 1]$ and

$$T := \{\lambda_{m_1,m_2} = (-1 + 0.02m_1) + i(-0.5 + 0.02m_2), \quad m_1, m_2 = 0, 1, \cdots, 75\}.$$

Using a fixed point $z = (0.2, 0.6)$ in B, for each $\lambda \in T$, a discretization of (4.3.30) leads to a linear system

$$A^\lambda g_\lambda = f^\lambda, \tag{4.5.37}$$

where A^λ is a matrix given by

$$A^\lambda_{l,j} = R\big(u_\lambda(x, x_l) - u(x, x_l), \exp(ikx \cdot d_j)\big), \quad l, j = 1, 2, \cdots, 100,$$

and f^λ is a vector given by

$$f^\lambda_l = R\big(u_\lambda(x, x_l), \Phi(x, z)\big), \quad l = 1, 2, \cdots, 100.$$

The Tikhonov regularization with the parameter $\alpha = 10^{-5}$ is used to compute an approximate solution g_λ to (4.5.37):

$$g_\lambda \approx \big((A^\lambda)^* A^\lambda + \alpha A^\lambda\big)^{-1} (A^\lambda)^* f^\lambda.$$

In the following examples, we show the plots of $|g_\lambda|$. In all the figures, the crosses are the exact Stekloff eigenvalues computed using a finite element method [104, 85].

Example 1 Real index of refraction $n(x) = 5$. The exact and reconstructed eigenvalues are shown in Table 4.1. The plots of $|g_\lambda|$ for the three domains are shown in Figure 4.2.

Example 2 Real index of refraction $n(x) = 4 + 2|x|$. The exact and reconstructed eigenvalues are shown in Table 4.2. The plots of $|g_\lambda|$ for the three domains are shown in Figure 4.3.

Example 3 Complex index of refraction $n(x) = 2 + 4i$. The exact and reconstructed eigenvalues are shown in Table 4.3. The plots of $|g_\lambda|$ for the three domains are shown in Figure 4.4.

disc	1.2937	−0.4763	−0.5839	−1.2301	
	(1.30)	(−0.48)	(−0.58)	(−1.23)	
square	0.3792	−0.5418	−0.6148		
	(0.38)	(−0.54)	(−0.62)		
L-shaped	3.0218	0.6882	−0.5266	−0.5834	−1.2188
	(3.04)	(0.70)	(−0.52)	(−0.58)	(−1.20)

Table 4.1: The exact Stekloff eigenvalues and their reconstructions (in the parentheses) for $n(x) = 5$.

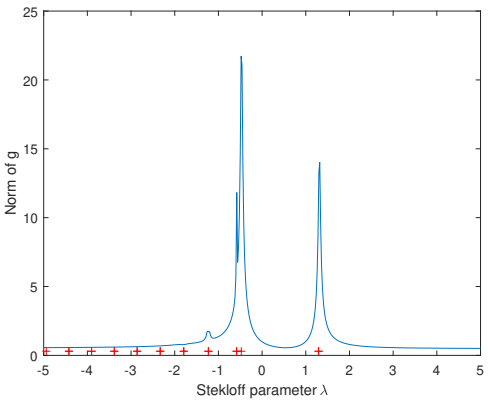

(a) **disc**

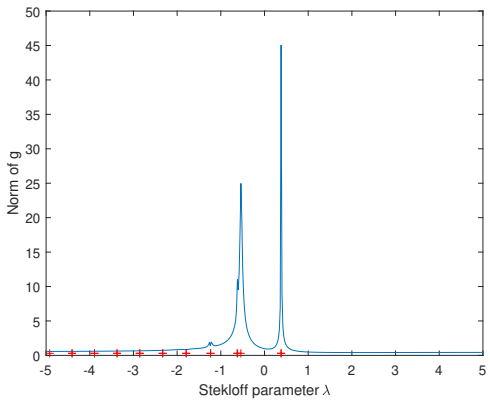

(b) **square**

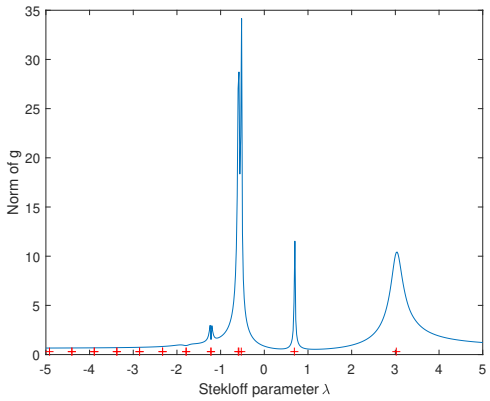

(c) **L-shaped**

Figure 4.2: The plots of $|g_\lambda|$ against λ for $n(x) = 5$.

disc	2.0856	-0.4898	-0.5714	-1.2285
	(2.10)	(-0.48)	(-0.54)	(-1.20)
square	0.4137	-0.5758	-1.2348	
	(0.42)	(-0.58)	(-1.22)	
L-shaped	0.9825	-0.4956	-0.6018	-1.2116
	(1.00)	(-0.50)	(-0.60)	(-1.20)

Table 4.2: The exact Stekloff eigenvalues and their reconstructions (in the parentheses) for $n(x) = 4 + 2|x|$.

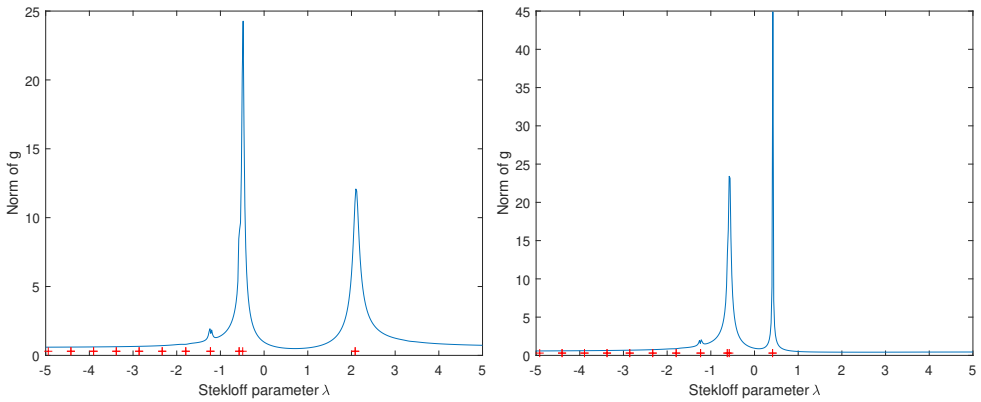

(a) **disc** (b) **square**

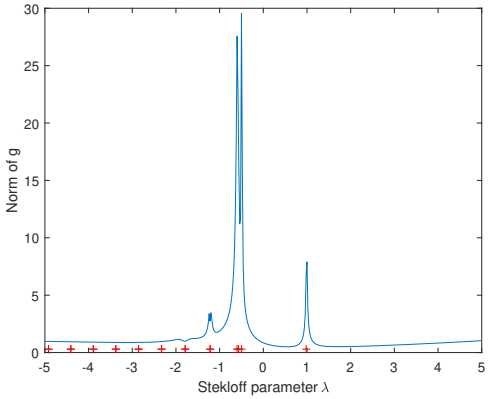

(c) **L-shaped**

Figure 4.3: The plots of $|g_\lambda|$ against λ for $n(x) = 4 + 2|x|$.

disc	$-0.0549 + 0.4854i$	$-0.0211 + 0.2652i$	$-0.6361 + 0.0390i$
	$(-0.06 + 0.46i)$	-0.02+0.26i	$(-0.64 + 0.04i)$
square	$0.1303 + 0.5812i$	$0.0779 + 0.1415i$	$-0.6338 + 0.0170i$
	$(0.12 + 0.56i)$	$(0.08 + 0.14i)$	$(-0.64 + 0.02i)$
L-shaped	$-0.0902 + 0.5468i$	$-0.1029 + 0.3600i$	$0.0364 + 0.2228i$
	$(-0.10 + 0.52i)$	$(-0.10 + 0.36i)$	$(0.04 + 0.22i)$
	$-0.6385 + 0.0764i$	$-0.6346 + 0.0412i$	
	$(-0.64 + 0.08i)$	$(-0.64 + 0.04i)$	

Table 4.3: The exact Stekloff eigenvalues and their reconstructions (in the parentheses) for $n(x) = 2 + 4i$.

4.5.2 Estimation of the index of refraction

Given the reconstructed Stekloff eigenvalues, we present some numerical examples for the estimation of the index of refraction using the Bayesian approach. The examples are rather simple. Nonetheless, the results show the potential of statistical approaches for inverse scattering problems. Since the main goal is to show the effectiveness of the Bayesian approach, we assume that the shape of the scatterer is known in the following examples.

Example 4 Real constant index of refraction $n(x) = 5$. Assume one Stekloff eigenvalue is reconstructed from Cauchy data: -0.48 for the disk, -0.54 for the square, and -0.52 for the L-shaped domain. Since n is a real constant, we take a uniform prior $\mathcal{U}(0, 8)$. The posterior density is given by

$$\pi_{post}(n|\lambda) \propto \exp\Big(-\frac{1}{2\sigma^2}\|\lambda - \mathcal{G}(n)\|^2\Big) \times I\{0 < n < 8\}. \tag{4.5.38}$$

We generate 3000 samples for each domain. The initial sample is chosen to be $n_1 = 2$. The rest samples $\{n_i\}_{i=2}^{3000}$ are drawn from the symmetric proposal distribution

$$q(n_j, n_{j-1}) \propto \exp\Big(-\frac{1}{2\gamma^2}\|n_j - n_{j-1}\|^2\Big),$$

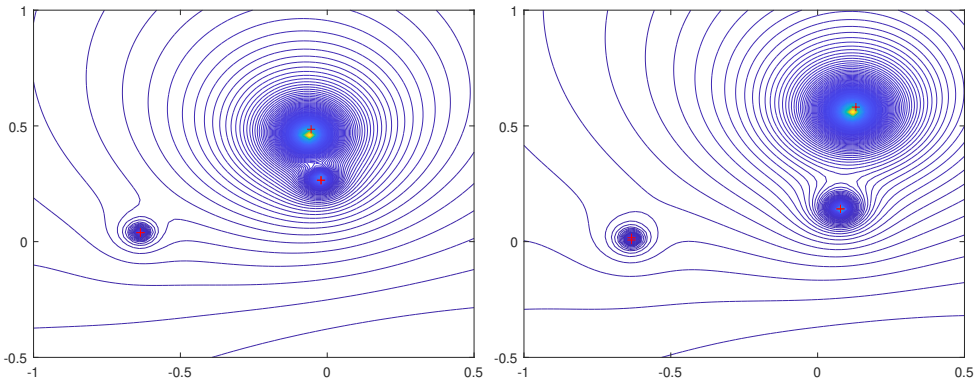

(a) **disc** (b) **square**

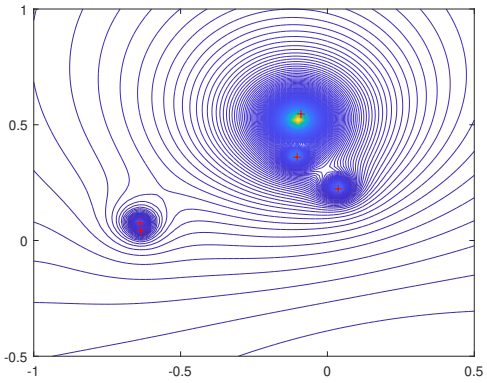

(c) **L-shaped**

Figure 4.4: The plots of $|g_\lambda|$ against λ for $n(x) = 2 + 4i$.

where $\gamma^2 = 2.4^2/2$.

Table 4.4 shows n_{CM} for the three domains. The Markov chains are shown in Figure 4.5. The samples concentrate around $n = 5$ for the unit disc and square. However, for the L-shaped domain, the samples are accumulated around two values, 5 and 7. In fact, this implies that one Stekloff eigenvalue cannot uniquely determine the constant index of refraction. If two Stekloff eigenvalues, 0.70 and -0.52, are used (see Figure 4.6), we obtain $n_{CM} = 5.0074$, which is a good approximation.

Example 5 Real index of refraction $n(x) = 4 + 2|x|$. Assume that two Stekloff eigenvalues are given and $n(x)$ is of the form $\beta^1 + \beta^2|x|$. We first obtain a constant approximation n_0 for $n(x)$ as the above example. This provides some ideas of how

σ^2	domain	n_{CM}
0.05	circle	4.9953
	square	5.0205
	L-shaped domain	6.2135 (5.0074)

Table 4.4: The posterior means for three domains ($n(x) = 5$) using one Stekloff eigenvalue. The value in the parentheses for the L-shaped domain is obtained using two Stekloff eigenvalues.

to choose the priors for β^1 and β^2. For the second step, two Stekloff eigenvalues are used. The posterior distribution is given by

$$\pi(n|\boldsymbol{\lambda}) \propto \exp\Big(-\frac{1}{2\sigma^2}\|\boldsymbol{\lambda} - \mathcal{G}(n)\|^2\Big) \times I\{3 < \beta^1 < 7\} \times I\{0 < \beta^2 < 6\}. \qquad (4.5.39)$$

Two reconstructed Stekloff eigenvalues from Table 4.2 are used for each domain: $2.10, -0.48$ for disc, $0.42, -0.58$ for the square, and $1.00, -0.50$ for the L-shaped domain. Table 4.5 shows the reconstruction results.

σ^2	domain	mean of n_0	$\beta^1_{CM} + \beta^2_{CM}\|x\|$
0.05	circle	4.9804	$4.3916 + 1.9333\|x\|$
	square	6.7791	$3.8873 + 2.3409\|x\|$
	L-shaped	6.2197	$4.2953 + 1.7263\|x\|$

Table 4.5: The posterior mean of $n(x)$ for the three domains ($n(x) = 4 + 2|x|$).

Example 6 Complex index of refraction $n(x) = 2 + 4i$. Assume that $\Re(n) \sim \mathcal{U}(0, 8)$ and $\Im(n) \sim \mathcal{U}(0, 8)$. The same proposal distribution $q(n_j, n_{j-1})$ are used to sample both $\Re(n)$ and $\Im(n)$. We use Stekloff eigenvalues, $-0.02 + 0.26i$ for the disc, $-0.64 + 0.02i, 0.12 + 0.56i$ for the square, and $-0.1 + 0.52i, 0.04 + 0.22i$ for the L-shaped domain. Table 4.6 shows the reconstruction results and Figure 4.7 shows the Markov chains.

σ^2	domain	n_{CM}
0.05	circle	$1.8511 + 3.9849i$
	square	$2.2515 + 4.1935i$
	L-shaped	$2.1204 + 4.1978i$

Table 4.6: The posterior means of $n(x)$ for the three domains ($n(x) = 2 + 4i$).

4.6 Conclusions

In this chapter, we show that the Cauchy data of a medium scattering problem can be used to detect Stekloff eigenvalues. A Bayesian approach is proposed to estimate the index of refraction using the reconstructed Stekloff eigenvalues. Since the multiplicities of the eigenvalues are not known, a spectral indicator method is developed to overcome the difficulty in the Metropolis-Hasting (M-H) algorithm. The method is particularly useful when there is a lack of understanding of the relation between the known scattering data and the unknown quantities.

In the next chapter, we extend the study here to a more challenging inverse spectrum problem.

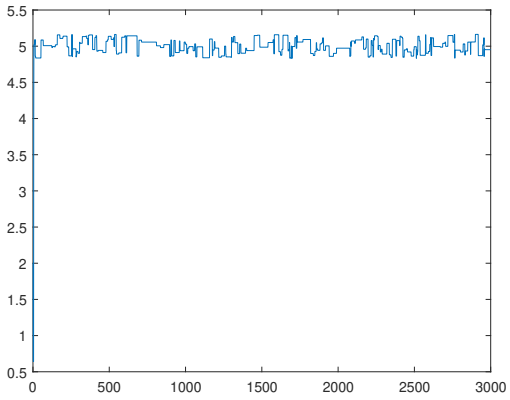

(a) **disc**

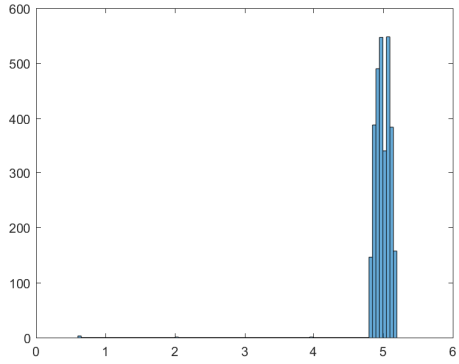

(b) **disc**

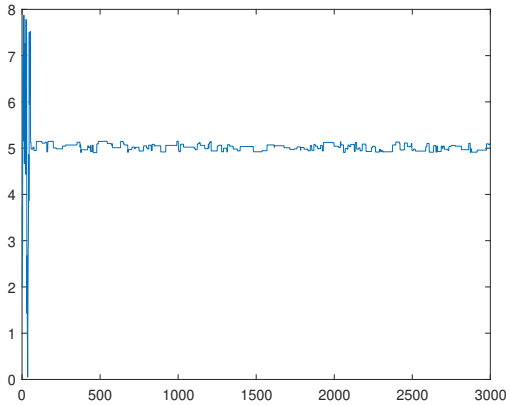

(c) **square**

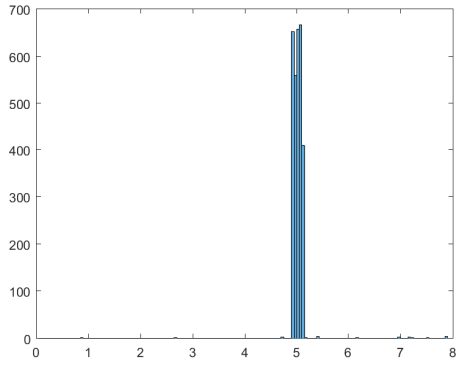

(d) **square**

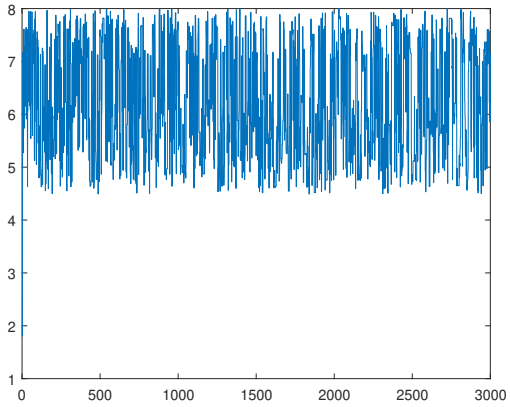

(e) **L-shaped**

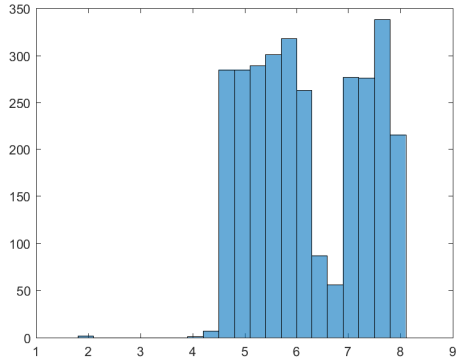

(f) **L-shaped**

Figure 4.5: Left: Trace plots and histograms of Markov chains for the three domains when $n \equiv 5$. Right: Probability histograms.

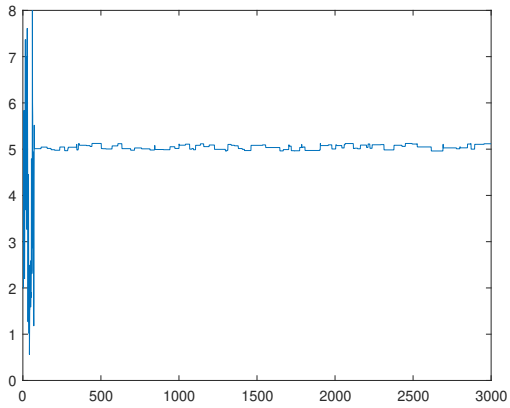

(a) **L-shaped**

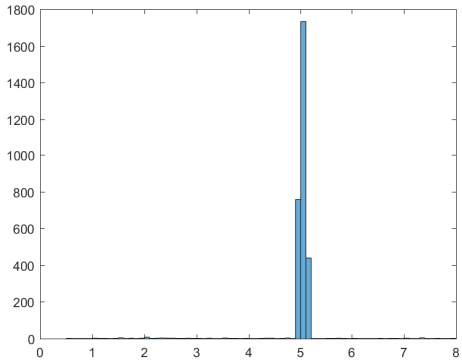

(b) **L-shaped**

Figure 4.6: Left: Trace plot of the Markov Chain for the L-shaped using two eigenvalues ($n = 5$). Right: Probability histogram.

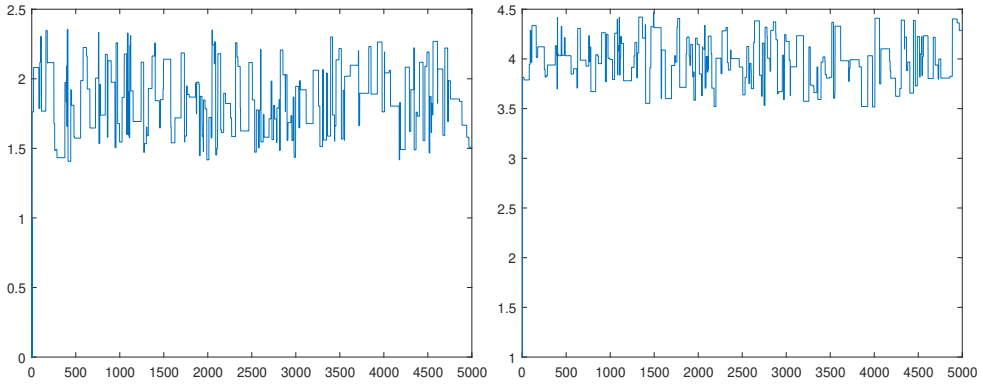

(a) **disc (real)**

(b) **disc (imag)**

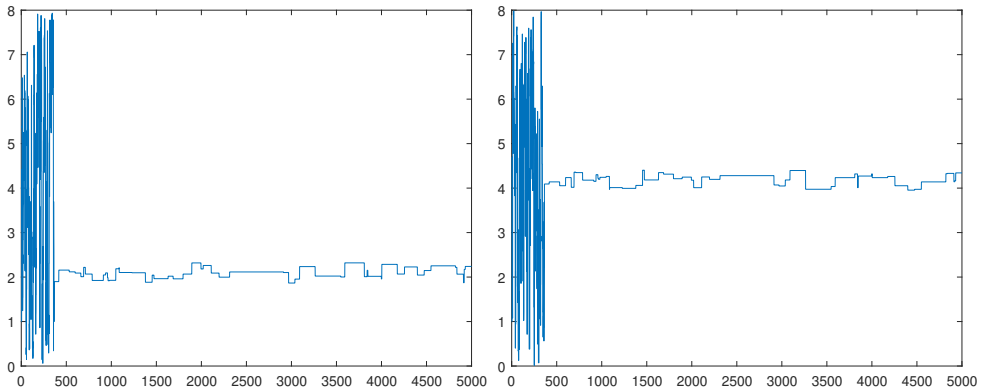

(c) **square (real)**

(d) **square (imag)**

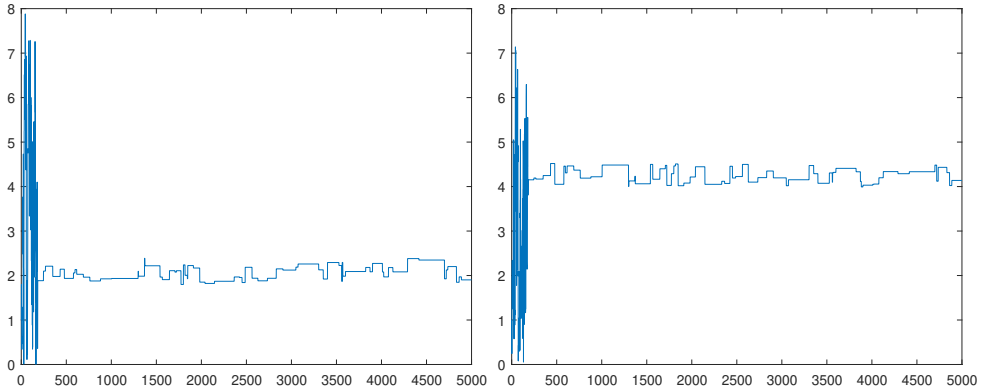

(e) **L-shaped (real)**

(f) **L-shaped (imag)**

Figure 4.7: Trace plots of Markov chains for the three domains ($n \equiv 2 + 4i$).

Chapter 5

Bayesian inversion for an inverse spectral problem of transmission eigenvalues[1]

5.1 Introduction

The transmission eigenvalue problem plays an important role in the inverse scattering theory for inhomogeneous media and received a lot of attention in the last decade. The problem is critical to the analysis of the inverse medium problem. Furthermore, it has been shown that transmission eigenvalues can be reconstructed from the scattering data and used to obtain qualitative information about the material properties. For the discreteness, existence, and the determination of transmission eigenvalues from scattering data, we refer the readers to [17, 30, 19, 15, 100, 46].

In this chapter, given a few real transmission eigenvalues, we consider the inverse spectral problem to determine the material properties of a non-absorbing medium. The problem has been treated using certain inequalities or optimization methods [28, 100]. However, due to the lack of theoretical results and non-uniqueness, these

[1]This chapter has been submitted.

methods face some difficulties. For example, the use of inequalities can only provide rough estimates of the material properties. The optimization method might not provide the correct solution when non-uniqueness of the inverse problem presents.

Bayesian inversion is an effective approach for inverse problems [63, 99]. Although sometimes computationally expensive, it is an attractive method for challenging inverse problems. In this chapter, we propose a Bayesian approach for the inverse transmission eigenvalue problem. First, using Bayes' theorem, the inverse problem is formulated as a statistical inference for the posterior density of the unknown physical properties. Then the MCMC algorithm is used to explore the posterior density. Due to the non-uniqueness nature of the problem, the local conditional means (LCM) are used to characterize the posterior density. Numerical examples validate the effectiveness of the proposed method. For applications of Bayesian approach in inverse problems, we refer the readers to, e.g., [63, 99, 62, 80]. In particular, Bayesian inversion was employed in [87] for an inverse Stekloff eigenvalue problem.

The rest of the chapter is organized as follows. In Section 5.2, we present the transmission eigenvalue problem for acoustic waves and state the inverse spectral problem of interest. Section 5.3 is devoted to the development of a Bayesian approach and the stability analysis. In Section 5.4, we first present a continuous finite element method to compute transmission eigenvalues used in the MCMC algorithm. Then we show four examples demonstrating the performance of the proposed Bayesian approach. Conclusions and future work are discussed in Section 5.5.

5.2 Inverse Transmission Eigenvalue Problem

Let $D \subset \mathbb{R}^2$ be a bounded Lipschitz domain. Let $A(x)$ be a 2×2 real matrix valued function with $C^1(D)$ entries and $n(x) \in C(D)$. Assume that $n(x) > 0$ is bounded and $A(x)$ is bounded and symmetric such that $\xi \cdot A\xi \geqslant \gamma|\xi|^2$ for all $\xi \in \mathbb{R}^2$ with $\gamma > 0$. Given an incident field u^i (e.g., plane waves), the direct scattering problem by an

inhomogeneous medium D is to find u and the scattered field u^s such that

$$\nabla \cdot A\nabla u + k^2 nu = 0, \qquad \text{in } D, \tag{5.2.1a}$$

$$\Delta u^s + k^2 u^s = 0, \qquad \text{in } \mathbb{R}^2 \backslash D, \tag{5.2.1b}$$

$$u - u^s = u^i, \qquad \text{on } \partial D, \tag{5.2.1c}$$

$$\partial_A u - \partial_\nu u^s = \partial_\nu u^i, \qquad \text{on } \partial D, \tag{5.2.1d}$$

$$\lim_{r\to\infty} r\left(\frac{\partial u^s}{\partial r} - iku^s\right) = 0, \tag{5.2.1e}$$

where k is the wave number, (5.2.1e) is the Sommerfeld radiation condition, $r = |x|$, ν is the unit outward normal to ∂D and $\partial_A u$ is the conormal derivative

$$\partial_A u(x) := \nu(x) \cdot A(x)\nabla u(x), \quad x \in \partial D.$$

It is well-known that there exists a unique solution u^s to the above scattering problem [30].

The transmission eigenvalue problem associated to (5.2.1) is as follows. Find $k^2 \in \mathbb{C}$ and non-trivial functions u, v such that

$$\nabla \cdot A\nabla u + k^2 nu = 0, \qquad \text{in } D, \tag{5.2.2a}$$

$$\Delta v + k^2 v = 0, \qquad \text{in } D, \tag{5.2.2b}$$

$$u - v = 0, \qquad \text{on } \partial D, \tag{5.2.2c}$$

$$\partial_A u - \partial_\nu v = 0, \qquad \text{on } \partial D. \tag{5.2.2d}$$

The well-posedness of the above problem has been an active research area for a decade. We summarize some existence results from [15], which are relevant to the topic discussed in the current chapter.

(a) Let $n_* = \inf_D n$ and $n^* = \sup_D n$. Assume $A = I$. If $n \geqslant n_0 > 0$ and either $n_* > 1$ or $n^* < 1$, the set of transmission eigenvalues is discrete with $+\infty$ as the only possible accumulation point. The multiplicity of the eigenvalues is finite.

(b) Let $a_* = \inf_D \inf_{|\xi|=1} \xi \cdot A\xi > 0$ and $a^* = \sup_D \sup_{|\xi|=1} \xi \cdot A\xi < \infty$. Assume that $n = 1$ and either $a_* > 1$ or $0 < a^* < 1$. Then the set of transmission eigenvalues is discrete with $+\infty$ as the only possible accumulation point.

(c) Assume that either $0 < a^* < 1$ or $a_* > 1$ and $\int_D (n-1)dx \neq 0$. Then the set of transmission eigenvalues is discrete with $+\infty$ as the only possible accumulation point.

(d) Assume that either $0 < a^* < 1$ and $0 < n^* < 1$, or $a_* > 1$ and $n_* > 1$. Then the set of transmission eigenvalues is discrete with $+\infty$ as the only possible accumulation point.

In the rest of the chapter, we assume that there exists an operator $\mathcal{G}$ such that

$$\boldsymbol{k} = \mathcal{G}(A, n), \tag{5.2.3}$$

where $\boldsymbol{k} \in \mathbb{R}^m$ is a vector consisting of m transmission eigenvalues.

Let S be the space of 2×2 symmetric matrices with real C^1 elements and $X = S \times C(D)$. Let $Y = \mathbb{R}^m$. Define two Sobolev spaces

$$\begin{aligned} V &:= \left\{(w, v) \in H^1(D) \times H^1(D) | w - v \in H_0^1(D)\right\}, \\ W &:= L^2(D) \times L^2(D). \end{aligned}$$

For $\boldsymbol{w} = (u, v) \in V$ and $\boldsymbol{\psi} = (\phi, \varphi) \in V$, we define two sesquilinear forms

$$\begin{aligned} a(\boldsymbol{w}, \boldsymbol{\psi}) &= (A\nabla u, \nabla\phi) + (n(x)u, \phi) - (\nabla v, \nabla\varphi) - (v, \varphi), \\ b(\boldsymbol{w}, \boldsymbol{\psi}) &= (n(x)u, \phi) - (v, \varphi). \end{aligned}$$

Then the transmission eigenvalue problem can be written as follows [112]. Find $k^2 \in \mathbb{C}$ and nontrivial $\boldsymbol{w}$ with $\|\boldsymbol{w}\|_W = 1$ such that

$$a(\boldsymbol{w}, \boldsymbol{\psi}) = (k^2 + 1) b(\boldsymbol{w}, \boldsymbol{\psi}) \quad \text{for all } \boldsymbol{\psi} \in V. \tag{5.2.4}$$

In this chapter, we only consider positive real transmission eigenvalue since they represent the wavenumbers that can be reconstructed from the scattering data [14,

100]. Note that $a(\cdot,\cdot)$ and $b(\cdot,\cdot)$ depend continuously on A and n and, as a consequence, k depends on A and n. We assume that the following Lipschitz continuity holds

$$\|\boldsymbol{k} - \boldsymbol{k}'\|_Y \leqslant C\|(A,n) - (A,n)'\|_X, \quad (A,n),(A,n)' \in X \tag{5.2.5}$$

for some constant C.

The interior transmission eigenvalue problem plays an essential role in the inverse scattering theory for inhomogeneous media. It received significant attention in the last decade. The study has focused on the discreteness, the existence, the determination of transmission eigenvalues from scattering data, and the relation between the transmission eigenvalues and the material properties (see, e.g., [28, 14, 17, 100, 30, 46]).

In this chapter, we are interested in the following inverse spectral problem.

ISP: Given a few real transmission eigenvalues $\boldsymbol{k} \in Y$, reconstruct A and n.

In particular, we assume that D is known as an a priori. Note that both D and the eigenvalues $\boldsymbol{k}$ can be obtained from the scattering data. For interested readers, we refer to [14, 100, 30] and the references therein.

Except a few special cases, e.g., $A = I$ and $n = n_0$ for some constant n_0 or spherically stratified media, little is known about the above inverse spectral problem. In addition, since only a few transmission eigenvalues are given, non-uniqueness can happen and it is highly challenging to develop effective deterministic methods for the **ISP**. This motivates us to develop a Bayesian approach to seek useful information about A and n.

5.3 Bayesian Inversion

In the Bayesian framework, the **ISP** is treated as a problem of statistical inference. All the parameters are modeled as random variables and the uncertainties of their values are expressed by distributions. The solution is the posterior probability distribution that provides a probabilistic description of the unknowns [63, 99].

Consider the inverse problem of (5.2.3) to reconstruct $(A, n) \in X$ from the measurement $\boldsymbol{k} \in Y$. Since the measurement $\boldsymbol{k}$ contains noise, the statistical problem can be written as

$$\boldsymbol{k} = \mathcal{G}(A, n) + E, \tag{5.3.6}$$

where $\boldsymbol{k} = (k_1, k_2, \ldots, k_m)^T$ is a vector of transmission eigenvalues, $A(x)$ and $n(x)$ are random, $\mathcal{G}$ is the operator mapping $(A(x), n(x))$ to $\boldsymbol{k}$ based on (5.2.2), and E is the additive noise, mutually independent of A and n. We assume that the noise E follows a Gaussian distribution, i.e., $E \sim \mathcal{N}(0, \Gamma_{\text{noise}})$, where $\Gamma_{\text{noise}} \in \mathbb{R}^{m\times m}$ is positive definite.

The prior density is denoted by $\pi_0(A, n)$. The conditional distribution of the measurement $\boldsymbol{k}$ given (A, n) is referred to as the likelihood, denoted by $\pi(\boldsymbol{k}|(A, n))$. From (5.3.6), $\pi(\boldsymbol{k}|(A, n)) = \mathcal{N}(\boldsymbol{k} - \mathcal{G}(A, n), \Gamma_{\text{noise}})$. The solution to the inverse problem is the posterior distribution $\pi_{\boldsymbol{k}}((A, n)|\boldsymbol{k})$. According to Bayes' rule, one has that

$$\pi_{\boldsymbol{k}}((A, n)|\boldsymbol{k}) = \frac{\pi(\boldsymbol{k}|(A, n))\pi_0(A, n)}{\int_X \pi(\boldsymbol{k}|(A, n))\pi_0(A, n)\mathrm{d}(A, n)}. \tag{5.3.7}$$

Let $P(A, n; \boldsymbol{k}) = \frac{1}{2}(\boldsymbol{k} - \mathcal{G}(A, n))^\top \Gamma_{\text{noise}}^{-1}(\boldsymbol{k} - \mathcal{G}(A, n))$. Assume that the posterior measure $\mu_{\boldsymbol{k}}$ with density $\pi_{\boldsymbol{k}}$ is absolutely continuous with respect to the prior measure μ_0 with density π_0. Using (5.3.7), we can relate $\mu_{\boldsymbol{k}}$ with μ_0 by

$$\frac{\mathrm{d}\mu_{\boldsymbol{k}}}{\mathrm{d}\mu_0} = \frac{1}{Z(\boldsymbol{k})} \exp\left(-P(A, n; \boldsymbol{k})\right), \tag{5.3.8}$$

where $Z(\boldsymbol{k}) = \int_X \exp(-P(A, n; \boldsymbol{k}))\mathrm{d}\mu_0(A, n)$ is the normalization constant. The formula (5.3.8) is understood as the Radon-Nikodym derivative of the posterior probability measure $\mu_{\boldsymbol{k}}$ with respect to the prior measure μ_0.

Now we study the stability of the Bayesian inversion scheme for the **ISP** following [99]. From (5.2.4) and the boundedness of A and n, the following lemma holds.

Lemma 5.3.1. *For every $\varepsilon > 0$, there exists $C := C(\varepsilon) \in \mathbb{R}$ such that, for all $(A, n) \in X$,*

$$\|\mathcal{G}(A, n)\|_Y \leqslant \exp(\varepsilon\|(A, n)\|_X^2 + C).$$

The assumption (5.2.5) implies that $\mathcal{G} : X \to \mathbb{R}^m$ satisfies the following property. For every $r > 0$ there exists a $C := C(r) > 0$ such that, for all $(A, n)_1, (A, n)_2 \in X$ with $\max\{\|(A, n)_1\|_X, \|(A, n)_2\|_X\} < r$,

$$\|\mathcal{G}((A, n)_1) - \mathcal{G}((A, n)_2)\|_Y \leqslant C\|(A, n)_1 - (A, n)_2\|_X.$$

Then the function $P : X \times Y \to \mathbb{R}$ has the following properties [99].

(i) For every $\varepsilon > 0$ and $r > 0$ there is an $M = M(\varepsilon, r) \in \mathbb{R}$ such that, for all $(A, n) \in X$ and $\boldsymbol{k} \in Y$ with $\|\boldsymbol{k}\|_Y < r$,

$$P(A, n; \boldsymbol{k}) \geqslant M - \varepsilon\|(A, n)\|_X.$$

(ii) For every $r > 0$ there is a $K = K(r) > 0$ such that, for all $(A, n) \in X$ and $\boldsymbol{k} \in Y$ with $\max\{\|(A, n)\|_X, \|\boldsymbol{k}\|_Y\} < r$,

$$P(A, n; \boldsymbol{k}) \leqslant K.$$

(iii) For every $r > 0$ there is an $L = L(r) > 0$ such that, for all $(A, n)_1, (A, n)_2 \in X$ and $\boldsymbol{k} \in Y$ with $\max\{\|(A, n)_1\|_X, \|(A, n)_2\|_X, \|\boldsymbol{k}\|_Y\} < r$,

$$|P((A, n)_1; \boldsymbol{k}) - P((A, n)_2; \boldsymbol{k})| \leqslant L\|(A, n)_1 - (A, n)_2\|_X.$$

(iv) For every $\varepsilon > 0$ and $r > 0$ there is a $C = C(\varepsilon, r) \in \mathbb{R}$ such that, for all $\boldsymbol{k}_1, \boldsymbol{k}_2 \in Y$ with $\max\{\|\boldsymbol{k}_1\|_Y, \|\boldsymbol{k}_2\|_Y\} < r$, and $(A, n) \in X$,

$$|P((A, n); \boldsymbol{k}_1) - P((A, n); \boldsymbol{k}_2)| \leqslant \exp(\varepsilon\|(A, n)\|_X^2 + C)\|\boldsymbol{k}_1 - \boldsymbol{k}_2\|_Y.$$

The following theorem guarantees the well-posedness of the Bayesian inverse problem (5.3.8).

Theorem 5.3.2. *Suppose X is a Banach space and μ_0 is a Borel probability measure on X with $\mu_0(X) = 1$. Then the Bayesian inverse problem* (5.3.8) *is well-posed in Hellinger metrics, i.e., for $\boldsymbol{k}_1$ and $\boldsymbol{k}_2$ with $\max\{\|\boldsymbol{k}_1\|_Y, \|\boldsymbol{k}_2\|_Y\} \leqslant r$, there exists $M = M(r) > 0$ such that*

$$d_{\text{Hell}}(\mu_{\boldsymbol{k}_1}, \mu_{\boldsymbol{k}_2}) \leqslant M\|\boldsymbol{k}_1 - \boldsymbol{k}_2\|_Y.$$

Proof. By the definition of $Z(\boldsymbol{k}) = \int_X \exp(-P(A,n;\boldsymbol{k}))\mathrm{d}\mu_0(A,n)$ and $\mu_0(X) = 1$, we have $0 < Z(\boldsymbol{k}) \leqslant 1$.

Applying the mean value theorem and using properties (i) and (iv), it holds that

$$\begin{aligned}
&|Z(\boldsymbol{k}_1) - Z(\boldsymbol{k}_2)| \\
\leqslant &\int_X \exp(-P(A,n;\boldsymbol{k}_1))\,|P(A,n;\boldsymbol{k}_1) - P(A,n;\boldsymbol{k}_2)|\,\mathrm{d}\mu_0(A,n) \\
\leqslant &\int_X \exp(\varepsilon\|(A,n)\|_X - M)\exp(\varepsilon\|(A,n)\|_X^2 + C)\mathrm{d}\mu_0(A,n)\|\boldsymbol{k}_1 - \boldsymbol{k}_2\|_Y \\
\leqslant &C\|\boldsymbol{k}_1 - \boldsymbol{k}_2\|_Y
\end{aligned} \tag{5.3.9}$$

By the definition of the Hellinger distance, we obtain that

$$\begin{aligned}
&d_{\mathrm{Hell}}^2(\mu_{\boldsymbol{k}_1}, \mu_{\boldsymbol{k}_2}) \\
=&\frac{1}{2}\int_X \left\{ \left(\frac{\exp\left(-P(A,n;\boldsymbol{k}_1)\right)}{Z(\boldsymbol{k}_1)}\right)^{1/2} - \left(\frac{\exp\left(-P(A,n;\boldsymbol{k}_2)\right)}{Z(\boldsymbol{k}_2)}\right)^{1/2} \right\}^2 \mathrm{d}\mu_0(A,n) \\
=&\frac{1}{2}\int_X \left\{ \left(\frac{\exp\left(-P(A,n;\boldsymbol{k}_1)\right)}{Z(\boldsymbol{k}_1)}\right)^{1/2} - \left(\frac{\exp\left(-P(A,n;\boldsymbol{k}_2)\right)}{Z(\boldsymbol{k}_1)}\right)^{1/2} \right. \\
&\left. + \left(\frac{\exp\left(-P(A,n;\boldsymbol{k}_2)\right)}{Z(\boldsymbol{k}_1)}\right)^{1/2} - \left(\frac{\exp\left(-P(A,n;\boldsymbol{k}_2)\right)}{Z(\boldsymbol{k}_2)}\right)^{1/2} \right\}^2 \mathrm{d}\mu_0(A,n) \\
\leqslant &Z(\boldsymbol{k}_1)^{-1}\int_X \left\{ \exp\left(-\frac{1}{2}P(A,n;\boldsymbol{k}_1)\right) - \exp\left(-\frac{1}{2}P(A,n;\boldsymbol{k}_2)\right) \right\}^2 \mathrm{d}\mu_0(A,n) \\
&+ \left|Z(\boldsymbol{k}_1)^{-1/2} - Z(\boldsymbol{k}_2)^{-1/2}\right|^2 \int_X \exp(-P(A,n;\boldsymbol{k}_2))\mathrm{d}\mu_0(A,n).
\end{aligned} \tag{5.3.10}$$

Applying again the mean value theorem and using property (iv), we have that

$$\begin{aligned}
&\int_X \left\{ \exp\Big(-\frac{1}{2}P(A,n;\boldsymbol{k}_1)\Big) - \exp\Big(-\frac{1}{2}P(A,n;\boldsymbol{k}_2)\Big) \right\}^2 \mathrm{d}\mu_0(A,n) \\
\leqslant &\int_X \left|\frac{1}{2}P(A,n;\boldsymbol{k}_1) - \frac{1}{2}P(A,n;\boldsymbol{k}_2)\right|^2 \mathrm{d}\mu_0(A,n) \\
\leqslant &\frac{1}{4}\int_X \Big|\exp(\varepsilon\|(A,n)\|_X^2 + C)\|\boldsymbol{k}_1 - \boldsymbol{k}_2\|_Y\Big|^2 \mathrm{d}\mu_0(A,n) \\
\leqslant &M\|\boldsymbol{k}_1 - \boldsymbol{k}_2\|_Y^2.
\end{aligned} \tag{5.3.11}$$

Due to the bounds on $Z(\boldsymbol{k}_1)$ and $Z(\boldsymbol{k}_2)$, it holds that

$$\left|Z(\boldsymbol{k}_1)^{-1/2} - Z(\boldsymbol{k}_2)^{-1/2}\right|^2 \leqslant M\max\Big(Z(\boldsymbol{k}_1)^{-3}, Z(\boldsymbol{k}_2)^{-3}\Big)|Z(\boldsymbol{k}_1) - Z(\boldsymbol{k}_2)|^2. \tag{5.3.12}$$

Combining (5.3.9)-(5.3.12), we obtain that

$$d_{\text{Hell}}(\mu_{\boldsymbol{k}_1}, \mu_{\boldsymbol{k}_2}) \leqslant M\|\boldsymbol{k}_1 - \boldsymbol{k}_2\|_Y.$$

■

Now we present the MCMC (Markov chain Monte Carlo) method to explore the posterior density functions of A and n given $\boldsymbol{k}$.

MCMC-ISP:

1. Given D and $\boldsymbol{k}$.
2. Draw $(A, n)_1$ from $\pi_0(A, n)$ such that A is positive definite.
3. For $j = 2, \cdots, J$, do
   a. Generate $(A, n)^*$ from $\pi_0(A, n)$ such that A^* is positive definite;
   b. Compute $\alpha((A, n)^*, (A, n)_{j-1}) = \min\left(1, \dfrac{\pi_{\boldsymbol{k}}((A, n)^*|\boldsymbol{k})}{\pi_{\boldsymbol{k}}((A, n)_{j-1}|\boldsymbol{k})}\right)$;
   c. Draw $\tilde{\alpha} \sim \mathcal{U}(0, 1)$.
   d. If $\alpha > \tilde{\alpha}$, then $(A, n)_j = (A, n)^*$, otherwise $(A, n)_j = (A, n)_{j-1}$.

As discussed above, the solution of the Bayesian inverse problem is the posterior probability densities of the unknown parameters. To characterize the posterior density functions of the inverse problem considered in this chapter, point estimators such as maximum a posteriori (MAP) and conditional mean (CM) might not carry sufficient/correct information of the unknowns due to the presence of non-unique solutions. Hence we also use the local estimators introduced in [103] when necessary. If it is found that a significant number of samples aggregate in more than one region, we shall use the local estimators instead of the global estimators. Numerical examples show that the local estimators can identify multiple solutions to the inverse spectral problems considered here.

5.4 Numerical Examples

In this section, we present some numerical examples. For the **MCMC-ISP** algorithm, one needs an effective method to compute several transmission eigenvalues of (5.2.2) given A and n. Numerical methods for the transmission eigenvalue problem have been developed by many researchers. We refer the readers to [26, 102, 4, 69, 29, 77, 113, 104, 92] and the references therein. In particular, finite element methods for (5.2.2) of anisotropic media are discussed in [60, 112, 39]. In the following, we present a continuous finite element method from [60], which is used in the simulation. Note that, from the finite element convergence theory for the transmission eigenvalue problem [104, 60, 112], the numerical method defines a discrete operator $\mathcal{G}_h$ such that

$$\boldsymbol{k}_h = \mathcal{G}_h(A, n). \tag{5.4.13}$$

The operator $\mathcal{G}_h$ approximates $\mathcal{G}$ in the sense that

$$\boldsymbol{k}_h \to \boldsymbol{k} \quad \text{as} \quad h \to 0,$$

where h is the size of the finite element mesh for D.

We first multiply (5.2.2a) by a test function ϕ and integrate by part to obtain

$$(A\nabla w, \nabla\phi) - k^2(nw, \phi) - \left\langle \frac{\partial w}{\partial \nu_A}, \phi \right\rangle = 0, \tag{5.4.14}$$

where $\langle \cdot, \cdot \rangle$ is the boundary integral on ∂D. Similarly, for (5.2.2b), we have that

$$(\nabla v, \nabla\phi) - k^2(v, \phi) - \left\langle \frac{\partial v}{\partial \nu}, \phi \right\rangle = 0. \tag{5.4.15}$$

Subtracting (5.4.15) from (5.4.14) and using (5.2.2d), it holds that

$$(A\nabla w - \nabla v, \nabla\phi) - k^2((nw - v), \phi) = 0. \tag{5.4.16}$$

Let $\mathcal{T}_h$ be a regular triangular mesh for D. Let V_h be the space of the linear Lagrange finite element, V_h^0 be the subspace of functions in V_h with vanishing degrees

of freedom on ∂D, and V_h^B be the subspace of functions in V_h with vanishing degrees of freedom in D. The boundary condition (5.2.2c) is enforced by setting

$$\begin{aligned} w_h &= w_{0,h} + w_{B,h} \text{ where } w_{0,h} \in V_h^0 \text{ and } w_{B,h} \in V_h^B, \\ v_h &= v_{0,h} + w_{B,h} \text{ where } v_{0,h} \in V_h^0. \end{aligned}$$

For $\xi_h \in V_h^0$ in (5.4.14), the weak formulation for w_h is

$$(A\nabla(w_{0,h} + w_{B,h}), \nabla\xi_h) - k^2(n(w_{0,h} + w_{B,h}), \xi_h) = 0 \quad \text{for all } \xi_h \in V_h^0. \tag{5.4.17}$$

Similarly, the weak formulation for v_h is

$$(\nabla(v_{0,h} + w_{B,h}), \nabla\eta_h) - k^2((v_{0,h} + w_{B,h}), \eta_h) = 0 \quad \text{for all } \eta_h \in V_h^0. \tag{5.4.18}$$

Setting $\phi_h \in V_h^B$ in (5.4.16), we have that

$$\begin{aligned} (A\nabla(w_{0,h} + w_{B,h}), \nabla\phi_h) - (\nabla(v_{0,h} + w_{B,h}), \nabla\phi_h\,) \\ -k^2\,(n(w_{0,h} + w_{B,h}) - (v_{0,h} + w_{B,h}), \phi_h) = 0. \end{aligned} \tag{5.4.19}$$

Let N_h, N_h^0, and N_h^B be the dimensions of V_h, V_h^0 and V_h^B, respectively. Let $\{\xi_1, \ldots, \xi_{N_h}\}$ be the finite element basis for V_h such that $\{\xi_1, \ldots, \xi_{N_h^0}\}$ is a basis for V_h^0. Let S_A be the stiffness matrix with $(S_A)_{j,\ell} = (A\nabla\xi_j, \nabla\xi_\ell)$, S be the stiffness matrix with $(S)_{j,\ell} = (\nabla\xi_j, \nabla\xi_\ell)$, M_n be the mass matrix with $(M_n)_{j,\ell} = (n\xi_j, \xi_\ell)$ and M be the mass matrix with $(M)_{j,\ell} = (\xi_j, \xi_\ell)$. The matrix form for (5.4.17), (5.4.18) and (5.4.19) is the generalized eigenvalue problem

$$\mathcal{A}\vec{x} = k^2\mathcal{B}\vec{x}, \tag{5.4.20}$$

where

$$\mathcal{A} = \begin{pmatrix} S_A^{N_h^0 \times N_h^0} & 0 & S_A^{N_h^0 \times N_h^B} \\ 0 & S^{N_h^0 \times N_h^0} & S^{N_h^0 \times N_h^B} \\ (S_A^{N_h^0 \times N_h^B})^T & (-S^{N_h^0 \times N_h^B})^T & S_A^{N_h^B \times N_h^B} - S^{N_h^B \times N_h^B} \end{pmatrix},$$

and

$$\mathcal{B} = \begin{pmatrix} M_n^{N_h^0 \times N_h^0} & 0 & M_n^{N_h^0 \times N_h^B} \\ 0 & M^{N_h^0 \times N_h^0} & M^{N_h^0 \times N_h^B} \\ (M_n^{N_h^0 \times N_h^B})^T & -(M^{N_h^0 \times N_h^B})^T & M_n^{N_h^B \times N_h^B} - M^{N_h^B \times N_h^B} \end{pmatrix}.$$

In all the numerical examples, we use Matlab "eigs" to compute several eigenvalues of (5.4.20). Note that if the transmission eigenvalues $\boldsymbol{k}$ are reconstructed using the scattering data, they are usually not large in magnitude and are only approximations of the exact ones [100]. Furthermore, the multiplicities of the eigenvalues are not known in general. Hence, given an eigenvalue k, in the Bayesian inversion stage, one only needs to know if there exists an eigenvalue k_1 of (5.4.20), which is close enough to k. In the rest of the chapter, the covariance of the noise is set to be $\Gamma_{\text{noise}} = \frac{1}{100} I$.

Example 1. Let D be a circle with radius $1/2$. We consider the isotropic medium, i.e., $A = I$ and the constant index of refraction $n(x) = n_c$. The unknown to be reconstructed is n_c. Four transmission eigenvalues are given $\boldsymbol{k} = (2.01, 2.61, 3.23, 3.80)$. These eigenvalues are computed from scattering data (see Fig. 2 in [100]). Note that the exact index of refraction is $n_c = 16$.

We first obtain some qualitative information of n_c using a deterministic method. In [28], the following Faber-Krahn type inequality is proved:

$$k_1^2(D) > \frac{\lambda_0(D)}{\sup_D n(x)}, \tag{5.4.21}$$

where $\lambda_0(D)$ is the smallest Dirichlet eigenvalue. Using the Lagrange finite element method, we find that $\lambda_0(D) \approx 23.21$ (see Chp. 3 of [104]). Consequently, the lower bound for $\sup_D n(x)$ given by (5.4.21) is roughly 5.8.

We consider the following cases:

1.1 use the first transmission eigenvalue to reconstruct n;

1.2 use the first two transmission eigenvalues to reconstruct n;

1.3 use all the four transmission eigenvalues to reconstruct n.

For all the cases, we choose a Gamma prior $n \sim \text{Gamma}(3,4) + 5.8$ incorporating the information obtained by the Faber-Krahn type inequality (5.4.21). 2000 samples are generated in the **MCMC-ISP**.

The results are shown in Fig. 5.1. For cases 1.1 and 1.2 (Fig. 5.1 (a) and (b)), the samples aggregate in two regions (around 16 and 27), which indicates the non-unique solutions. We use the local conditional means (LCM) to characterize the posterior density function. In Table 5.1, for case 1.1, two local conditional means are shown: $n^1_{LCM} = 15.90$ and $n^2_{LCM} = 27.04$. We also compute the associated transmission eigenvalue, which is close to the given one. In other words, both indices of refraction have an eigenvalue close to 2.01, which reveals the non-unique nature of the inverse problem. The scenario is the same for case 1.2.

When four transmission eigenvalues are used, the non-uniqueness disappears on the interval $[8, 30]$. As shown in Fig. 5.1(c), all the samples accumulate around 16. The conditional mean $n_{CM} = 16.23$ and the corresponding transmission eigenvalues are shown in Table 5.1. It can be seen that there exit four eigenvalues $(1.98, 2.61, 3.24, 3.78)$ for $n_{CM} = 16.23$, which are close to the given eigenvalues $\boldsymbol{k} = (2.01, 2.61, 3.23, 3.80)$.

	$n(x)$	Transmission eigenvalues			
	16	**2.01**	**2.61**	**3.23**	**3.80**
case 1.1	15.90	2.01	-	-	-
	27.04	2.01	-	-	-
case 1.2	16.05	2.00	2.63	-	-
	25.62	2.07	2.57	-	-
case 1.3	16.23	1.98	2.61	3.24	3.78

Table 5.1: Local conditional means/conditional mean and the transmission eigenvalues.

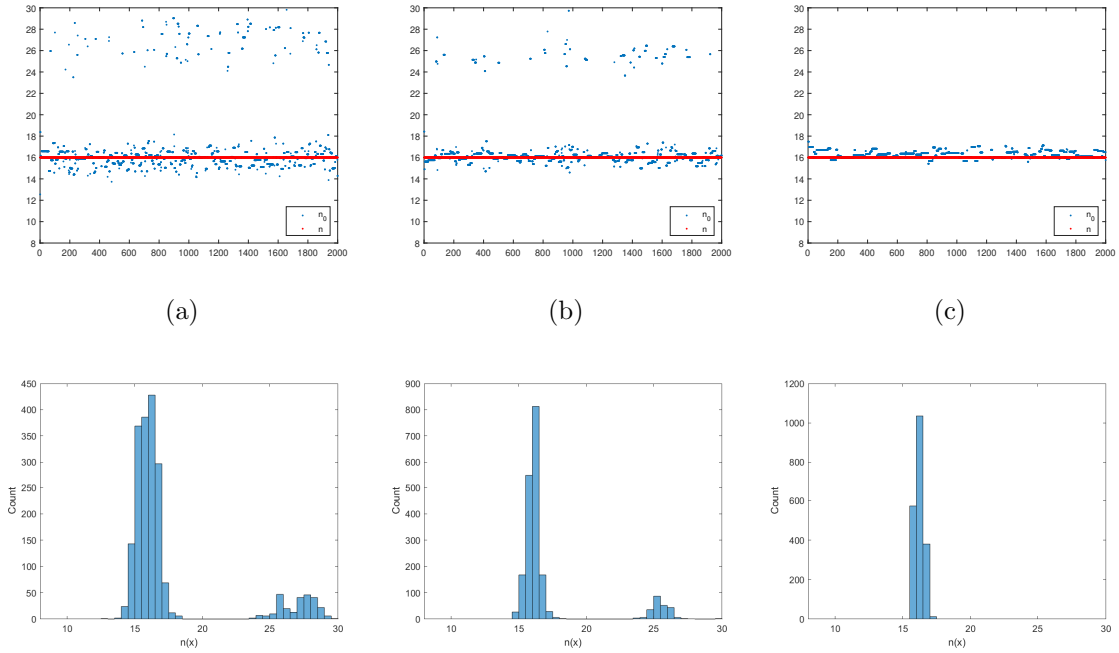

(a) (b) (c)

(d) first eig (e) first two eigs (f) four eigs

Figure 5.1: Scatter plots and histograms: (a) and (d) - $\boldsymbol{k}(1)$; (b) and (e) - $\boldsymbol{k}(1:2)$; (c) and (f) - $\boldsymbol{k}(1:4)$.

Example 2 Let D be the unit square given by $(-1/2, 1/2) \times (-1/2, 1/2)$. Again, the medium is isotropic, i.e., $A = I$. The exact index of refraction is $n(x) = 8 + x_1 - x_2$ for this example. Given the transmission eigenvalues $\boldsymbol{k} = (2.82, 3.54, 4.13)$, we consider two cases:

2.1 assuming $n = n_0$, reconstruct n_0;

2.2 assuming $n = n_0 + n_1 x_1 + n_2 x_2$, reconstruct n_0, n_1, n_2.

Applying (5.4.21) again, we obtain $\sup_D n(x) > 2.48$. 6000 samples are drawn in the MCMC stage. We first consider case 2.1 using three transmission eigenvalues. A uniform prior distribution $n_0 \sim \mathcal{U}[2.5, 14]$ is used. A large part of the samples concentrates around 8.1 (see Fig. 5.2 (a-b)). We also notice that some samples are around 12.3. Similar to Example 1, we compute the local conditional means as shown

in Table 5.2. The exact transmission eigenvalues close to $\boldsymbol{k}$ for the two LCMs are also shown in Table 5.2. The differences between the transmission eigenvalues and the given $\boldsymbol{k}$ are small.

We move on to case 2.2 by coding the reconstruction of n_0 in case 2.1 into the prior. $n(x)$ is approximated by the linear function $n = n_0 + n_1x_1 + n_2x_2$ with $\pi(n_0) = \mathcal{U}[7.5, 8.5]$ and $\pi(n_1) = \pi(n_2) = \mathcal{U}[-1.5, 1.5]$. The reconstruction is $n(x) = 8.10 - 0.01x_1 - 0x_2$. The recovery of the constant term n_0 is satisfactory. Fig. 5.2(c) shows samples of n_1, n_2. The errors of the coefficient n_1, n_2 are large. This is not surprising since x_1 and x_2 are rather small in D, which makes it difficult to recover their cofficients accurately. Indeed, as seen in Table 5.2, the exact transmission eigenvalues for the reconstructed $n(x)$ are very close to the given $\boldsymbol{k}$.

	n_0	n_1	n_2	Transmission eigenvalues		
	8	**1**	**-1**	**2.82**	**3.54**	**4.13**
case 2.1	8.11	-	-	2.81	3.54	4.13
	12.21	-	-	2.83	3.65	4.05
case 2.2	8.10	-0.01	-0.00	2.82	3.54	4.13

Table 5.2: Local conditional means/conditional mean and the transmission eigenvalues.

Example 3. Let D be an L-shape domain given by

$$(-0.5, 0.5) \times (-0.5, 0.5) \backslash [0, 0.5] \times [-0.5, 0].$$

The exact A and n are $\mathrm{diag}(\frac{1}{6}, \frac{1}{8})$ and 1, respectively. Given $\boldsymbol{k} = (4.31, 4.44, 4.95, 5.47)$, we consider the following cases:

3.1 assuming $A = \mathrm{diag}(a_0, a_1)$ and $n = n_0$, reconstruct a_0, a_1 and n_0;

3.2 assuming $A = \begin{pmatrix} a_0 & a_2 \\ a_2 & a_1 \end{pmatrix}$ and $n = n_0$, reconstruct a_0, a_1, a_2 and n_0.

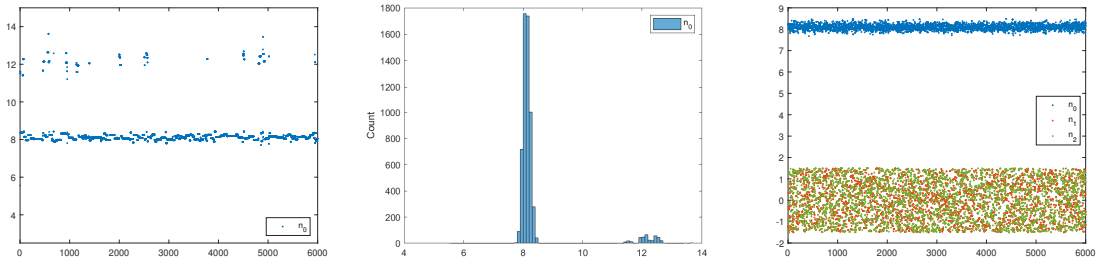

(a) (b) (c)

Figure 5.2: Scatter plot (a) and histogram (b) for case 2.1, scatter plot (c) for case 2.2.

For case 3.1, we set $a_0, a_1 \sim \mathcal{U}[0.05, 0.25]$ and $n_0 \sim \mathcal{U}[0.1, 1.6]$. The results of the **MCMC-ISP** with 6000 samples are displayed in Table 5.3. We can see that A is approximated by $\text{diag}(0.14, 0.14)$ and n_{CM} is 1.34.

Next, we consider case 3.2 using the estimators from case 3.1. As shown in Fig. 5.3(a), the diagonal elements of A are small and oscillate between 0.1 and 0.2. Hence we set $a_0, a_1 \sim \mathcal{U}[0.1, 0.2]$. Choose a_2 from $\mathcal{U}[-0.05, 0.1]$ and $n \sim \mathcal{U}[0.8, 1.6]$. Using 6000 samples to reconstruct A and n, we show the results in Table 5.3 and Fig. 5.3(b). For both cases, the reconstructions are acceptable and the eigenvalues are close to the given ones.

	$n(x)$	a_0	a_1	a_2	Transmission eigenvalues			
	1	**1/6**	**1/8**	**0**	**4.31**	**4.44**	**4.95**	**5.47**
case 3.1	1.34	0.14	0.14	-	4.53	4.53	5.00	5.56
case 3.2	1.32	0.13	0.13	0.03	4.17	4.49	4.84	5.48

Table 5.3: Conditional means and the transmission eigenvalues.

Example 4. In this example, we use the same L-shape domain D as Example

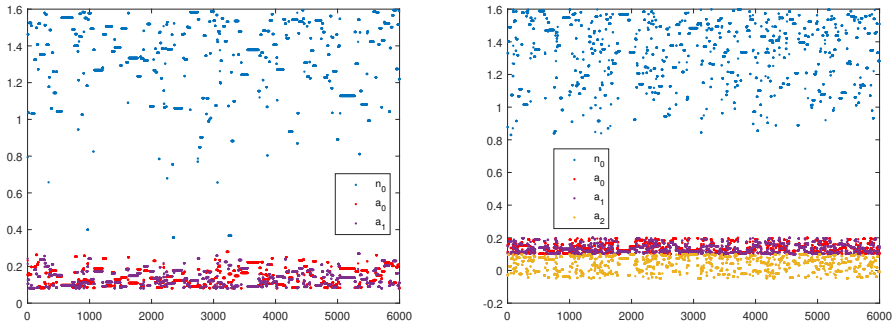

(a) (b)

Figure 5.3: Scatter plots for case 3.1 (a) and case 3.2 (b).

3 but $A = \begin{pmatrix} \frac{1}{2} & \frac{1}{7} \\ \frac{1}{7} & \frac{1}{3} \end{pmatrix}$ and $n = 2$. With $\boldsymbol{k} = (5.32, 5.73, 6.04, 6.53)$, we consider the following cases:

4.1 assuming $A = \text{diag}(a_0, a_1)$ and $n = n_0$, reconstruct a_0, a_1 and n_0;

4.2 assuming $A = \begin{pmatrix} a_0 & a_2 \\ a_2 & a_1 \end{pmatrix}$ and $n = n_0$, reconstruct a_0, a_1, a_2 and n_0.

	$n(x)$	a_0	a_1	a_2	Transmission eigenvalues			
	2	**1/2**	**1/3**	**1/7**	**5.32**	**5.73**	**6.04**	**6.53**
case 4.1	2.79	0.23	0.22	-	5.22	5.83	6.12	6.60
case 4.2	2.99	0.32	0.26	0.09	5.31	5.61	6.13	6.64

Table 5.4: Conditional means and the transmission eigenvalues.

For case 4.1, we choose the priors $a_0, a_1 \sim \mathcal{U}[0.05, 1.05]$ and $n_0 \sim \mathcal{U}[1.5, 3.5]$. The conditional means of a_0, a_1 and n are 0.23, 0.22 and 2.79, respectively. Based on the results of case 4.1, we choose $a_0 \sim \mathcal{U}[0.2, 0.6]$, $a_1 \sim \mathcal{U}[0.2, 0.4]$, $a_2 \sim \mathcal{U}[-0.05, 0.2]$ and $n \sim \mathcal{U}[1.8, 3.5]$ for case 4.2. The results are shown in Table 5.4 and Fig. 5.4.

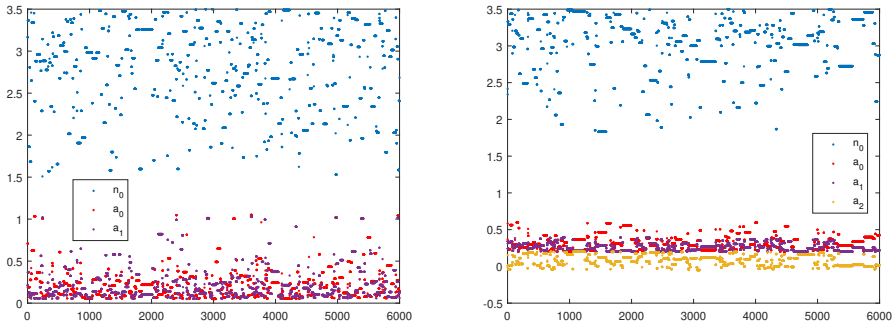

(a) (b)

Figure 5.4: Scatter plots for case 4.1 and 4.2.

The approximation of n is greater than the exact value and approximations of the entries of A are smaller than the exact ones, indicating the severe ill-posed nature of the inverse problem. Nevertheless, the computed transmission eigenvalues are close to the given $\boldsymbol{k}$ for both cases.

5.5 Conclusion

The inverse spectral problem of transmission eigenvalues is studied. Given a few transmission eigenvalues, the Bayesian approach is employed to reconstruct the material properties of the inhomogeneous medium. An MCMC algorithm is used to explore the posterior density functions of the unknowns. Due to the fact that only partial data are available (a few eigenvalues), the inverse problem is severely ill-posed and can have non-unique solutions. To characterize the density functions, we resort to the recently proposed local estimators. Numerical examples indicate that the proposed Bayesian method is effective for the inverse spectral problem considered in this chapter.

For Examples 1 and 2, the Faber-Krahn type inequality is first used to obtain some qualitative information of the index of refraction. Such information can be coded in

the priors to improve the performance of the Bayesian inversion. The results in [80, 81] also indicate that the combination of deterministic and statistical methods can successfully treat challenging inverse problems with partial data.

References

[1] B. Abdelaziz, A. El Badia and A. El Hajj. *Direct algorithm for multipolar sources reconstruction.* J. Math. Anal. Appl., 428(1), 306-336, 2015.

[2] S. Acosta, S. Chow, J. Taylor and V. Villamizar. *On the multi-frequency inverse source problem in heterogeneous media.* Inverse Problems, 28(7), 075013, 2012.

[3] A. Alzaalig, G. Hu, X. Liu and J. Sun. *Fast acoustic source imaging using multi-frequency sparse data.* Inverse Problems, 36(2), 025009, 2020.

[4] J. An and J. Shen. *A Fourier-spectral-element method for transmission eigenvalue problems.* J. Sci. Comput., 57, 670-688, 2013.

[5] T.S. Angell, D. Colton, and A. Kirsch. *The three dimensional inverse scattering problem for acoustic waves.* J. Diff.Equations, 46(1), 46-58, 1982.

[6] L. Audibert, F. Cakoni and H. Haddar. *New sets of eigenvalues in inverse scattering for inhomogeneous media and their determination from scattering data.* Inverse Problems, 33(12), 125011, 2017

[7] L. Audibert and H. Haddar. *A generalized formulation of the linear sampling method with exact characterization of targets in terms of farfield measurements.* Inverse Problems, 30(3), 035011, 2014.

[8] G. Bao, J. Lin and F. Triki. *A multi-frequency inverse source problem*, J. Differential Equations, 249(10), 3443-3465, 2010.

[9] C.E. Baum. Detection and Identification of Visually Obscured Targets, CRC Press, 1998.

[10] A. Baussard, D. Prémel and O. Venard. *A Bayesian approach for solving inverse scattering from microwave laboratory-controlled data.* Inverse Problems, 17(6), 1659-1669, 2001.

[11] O. Bondarenko, I. Harris, and A. Kleefeld. *The interior transmission eigenvalue problem for an inhomogeneous media with a conductive boundary.* Appl. Anal., 96(1), 2-22, 2017.

[12] J.L. Buchanan, R.P. Gilbert, A. Wirgin and Y.S. Xu. Marine Acoustics: Direct and Inverse Problems. SIAM, Philadelphia, PA, 2004.

[13] T. Bui-Thanh and O. Ghattas. *An analysis of infinite dimensional Bayesian inverse shape acoustic scattering and its numerical approximation.* SIAM/ASA J. Uncertain. Quantif., 2(1), 203-222, 2014.

[14] F. Cakoni, D. Colton and H. Haddar. *On the determination of Dirichlet or transmission eigenvalues from far field data.* CR Acad. Sci. Paris, 348(7-8), 379-383, 2010.

[15] F. Cakoni, D. Colton and H. Haddar. Inverse scattering theory and transmission eigenvalues. SIAM, Philadelphia, 2016.

[16] F. Cakoni, D. Colton and P. Monk. *On the use of transmission eigenvalues to estimate the index of refraction from far field data.* Inverse Problems, 23(2), 507-522, 2007.

[17] F. Cakoni, D. Colton, P. Monk and J. Sun. *The inverse electromagnetic scattering problem for anisotropic media.* Inverse Problems, 26 (7), 074004,2010.

[18] F. Cakoni, D. Colton, S. Meng and P. Monk. *Stekloff eigenvalues in inverse scattering.* SIAM J. Appl. Math. 76(4), 1737-1763, 2016.

[19] F. Cakoni and H. Haddar. *Transmission eigenvalues in inverse scattering theory. Inverse problems and applications: inside out. II.*529-580, Math. Sci. Res. Inst. Publ., 60, Cambridge Univ. Press, Cambridge, 2013.

[20] B. Chen, Y. Guo, F. Ma and Y. Sun. *Numerical schemes to reconstruct three-dimensional time-dependent point sources of acoustic waves.* Inverse Problems, 36(7), 075009, 2020.

[21] Z. Chen and X. Liu. *An adaptive perfectly matched layer technique for time-harmonic scattering problems.* SIAM J. Numer. Anal., 43(2), 645-671, 2005.

[22] M. Cheney and B. Borden. *Fundamentals of Radar Imaging.* CBMS-NSF Regional Conference Series in Applied Mathematics, 79. Society for Industrial and Applied Mathematics (SIAM), Philadelphia, PA, 2009.

[23] D. Colton and H. Haddar. *An application of the reciprocity gap functional to inverse scattering theory.* Inverse Problems, 21(1), 383-398, 2005.

[24] D. Colton, H. Haddar and M. Piana. *The linear sampling method in inverse electromagnetic scattering theory.* Inverse problems, 19(6), S105, 2003.

[25] D. Colton and A. Kirsch. *A simple method for solving inverse scattering problems in the resonance region.* Inverse problems, 12(4),383 ,1996.

[26] D. Colton, P. Monk and J. Sun. *Analytical and computational methods for transmission eigenvalues.* Inverse Problems, 26(4), 045011, 2010.

[27] D. Colton, M. Piana and R. Potthast. *A simple method using Morozov's discrepancy principle for solving inverse scattering problems.* Inverse Problems, 13(6), 1477, 1997.

[28] D. Colton, L. Päivärinta and J. Sylvester. *The interior transmission problem*, Inverse Probl. Imaging, 1 (1), 13-28, 2007.

[29] A. Cossonnière and H. Haddar. *Surface integral formulation of the interior transmission problem.* J. Integral Equations Appl., 25(3), 341-376, 2013.

[30] D. Colton and R. Kress. Inverse Acoustic and Electromagnetic Scattering Theory, 3rd ed., Springer, 2013.

[31] S.L. Cotter, G.O. Roberts, A. Stuart and D.White. *MCMC methods for functions: modifying old algorithms to make them faster.* Statist. Sci., 28(3), 424-446, 2013.

[32] M. Di Cristo and J. Sun. *An inverse scattering problem for a partially coated buried obstacle.* Inverse Problems, 22(6), 2331-2350, 2006.

[33] A.J. Devaney, E.A. Marengo and M. Li. *The inverse source problem in nonhomogeneous background media.* SIAM J. Appl. Math., 67(5), 1353-1378, 2007.

[34] M. M. Dunlop, M. A. Iglesias, and A. M. Stuart. *Hierarchical Bayesian level set inversion.* Stat. Comput., 27(6), 1555-1584, 2017.

[35] M. Eller and N.P. Valdivia. *Acoustic source identification using multiple frequency information.* Inverse Problems, 25(11), 115005, 2009.

[36] J. Elschner, G.C. Hsiao, and A. Rathsfeld. *An inverse problem for fluid-solid interaction.* Inverse Probl. Imaging, 2, 83–119, 2008.

[37] J. Garnier and M. Fink. *Super-resolution in time-reversal focusing on a moving source*, Wave Motion, 53, 80-93, 2015.

[38] L. Gharsalli, H. Ayasso, B. Duchêne and A. Mohammad-Djafari. *Inverse scattering in a Bayesian framework: application to microwave imaging for breast cancer detection.* Inverse Problems, 30(11), 114011, 2014.

[39] B. Gong, J. Sun, T. Turner and C. Zheng. *Finite element approximation of transmission eigenvalues for anisotropic media.* arXiv:2001.05340, 2020.

[40] Y. Guo, D. Hömberg, G. Hu, J. Li and H. Liu. *A time domain sampling method for inverse acoustic scattering problems.* J. Comput. Phys., 314, 647–660, 2016.

[41] Y. Guo, P. Monk and D. Colton. *Toward a time domain approach to the linear sampling method.* Inverse Problems, 29(9), 095016, 2013.

[42] Y. Guo, P. Monk and D. Colton. *The linear sampling method for sparse small aperture data.* Appl. Anal., 95 (8), 1599–1615, 2016.

[43] S. Gutman and M. Klibanov. *Iterative method for multi-dimensional inverse scattering problems at fixed frequencies.* Inverse problems, 10(3), 573, 1994.

[44] H. Haario, M. Laine, A. Mira and E. Saksman. *DRAM: Efficient adaptive MCMC.* Stat. Comput., 16, 339-354, 2006.

[45] J. Hadamard. Lectures on Cauchy's problem in linear partial differential equations. Courier Corporation, 2003.

[46] I. Harris, F. Cakoni and J. Sun. *Transmission eigenvalues and non-destructive testing of anisotropic magnetic materials with voids.* Inverse Problems, 30(3), 035016, 2014.

[47] I. Harris and S. Rome. *Near field imaging of small isotropic and extended anisotropic scatterers.* Appl. Anal., 96(10), 1713-1736, 2017.

[48] W. Hastings. *Monte Carlo sampling methods using Markov chains and their applications.* Biometrika, 57(1), 97-109, 1970.

[49] T. Hohage. *Fast numerical solution of the electromagnetic medium scattering problem and applications to the inverse problem.* J. Comp. Phys., 214, 224–238, 2006.

[50] B. Hosseini. *Well-posed Bayesian inverse problems with infinitely divisible and heavy-tailed prior measures.* SIAM/ASA J. Uncertain. Quantif., 5(1), 1024-1060, 2017.

[51] G. Hu, Y. Kian, P. Li and Y. Zhao. *Inverse moving source problems in electrodynamics.* Inverse Problems, 35(7), 075001, 2019.

[52] R. Huang, A. Struthers, J. Sun and R. Zhang. *Recursive integral method for transmission eigenvalues.* J. Comput. Phys., 327, 830-840, 2016.

[53] R. Huang, J. Sun and C. Yang. *Recursive Integral Method with Cayley Transformation.* Numer. Linear Algebra Appl., 25(6), 2018. https://doi.org/10.1002/nla.2199.

[54] M.A. Iglesias, Y. Lu, and A.M. Stuart. *A Bayesian level set method for geometric inverse problems.* Interfaces Free Bound. 18(2), 181-217, 2016.

[55] M. Ikehata. *Reconstruction of the shape of an obstacle from the scattering amplitude at a fixed frequency.* Inverse Problems, 14(4), 949-954, 1998.

[56] V. Isakov. Inverse Problems for Partial Differential Equations. 2nd Ed., Springer-Verlag, New York, 2006.

[57] K. Ito, B. Jin and J. Zou. *A direct sampling method to an inverse medium scattering problem.* Inverse Problems, 28(2), 025003, 2012.

[58] O. Ivanyshyn, and R. Kress. *Nonlinear integral equations in inverse obstacle scattering.* Mathematical methods in scattering theory and biomedical engineering, 39-50, 2006.

[59] J.D. Jackson. Classical Electrodynamics. John Wiley & Sons, 2007.

[60] X. Ji and J. Sun. *A multi-level method for transmission eigenvalues of anisotropic media.* J. Comput. Phys., 255, 422-435, 2013.

[61] B. Jin. *Conjugate gradient method for the Robin inverse problem associated with the Laplace equation.* Int J Numer Methods Eng, 71(4), 433-453, 2007.

[62] J.P. Kaipio, T. Huttunen, T. Luostari, T. Lähivaara and P. Monk. *A Bayesian approach to improving the Born approximation for inverse scattering with high-contrast materials.* Inverse Problems, 35(8), 084001, 2019.

[63] J. Kaipio and E. Somersalo. Statistical and Computational Inverse Problems. Springer, New York, 2006.

[64] J. Keller. *Inverse Problems.* Amer. Math. Monthly 83, No. 2 , 107-118, 1976

[65] A. Kirsch and A. Lechleiter. *The inside-outside duality for scattering problems by inhomogeneous media.* Inverse Problems, 29(10), 104011, 2013.

[66] A. Kirsch. *Characterization of the shape of a scattering obstacle using the spectral data of the far field operator.* Inverse Problems, 14(6), 1489, 1998.

[67] A. Kirsch. *Factorization of the far field operator for the inhomogeneous medium case and an application in inverse scattering theory.* Inverse Problems, 15(2), 413, 1999.

[68] A. Kirsch and N. Grinberg. The factorization method for inverse problems. Oxford University Press, 36, 2008.

[69] A. Kleefeld. *A numerical method to compute interior transmission eigenvalues.* Inverse Problems, 29(10), 104012, 2013.

[70] A. Kleefeld. *Numerical methods for acoustic and electromagnetic scattering: Transmission boundary-value problems, interior transmission eigenvalues, and the factorization method.* Habilitation thesis, University of Technology Cottbus, Senftenberg, Cottbus, 2015.

[71] V. Kolehmainen, T. Tarvainen, S.R. Arridge and J.P. Kaipio. *Marginalization of uninteresting distributed parameters in inverse problems-application to diffuse optical tomography.* Int. J. Uncertain. Quantif., 1(1), 1-17, 2011.

[72] S. Kusiak and J. Sylvester. *The scattering support.* Comm. Pure Applied Math., 56, 1525-1548, 2003.

[73] A. Lechleiter and S. Peters. *Determining transmission eigenvalues of anisotropic inhomogeneous media from far field data.* Commun. Math. Sci., 13(7), 1803-1827, 2015.

[74] A. Lechleiter and M. Rennoch. *Inside-outside duality and the determination of electromagnetic interior transmission eigenvalues.* SIAM J. Math. Anal., 47, 684-705, 2015.

[75] A. Lechleiter and J. Sun (ed.). Special Issue on Recent Developments in Scattering and Inverse Scattering Problems, Appl. Anal., 96(1), 1-172, 2017.

[76] J. Li, Z. Zeng, J. Sun and F. Liu. *Through-wall detection of human being's movement by UWB radar.* IEEE Geoscience and Remote Sensing Letters, 9(6), 1079–1083, 2012.

[77] T. Li, W. Huang, W. Lin, and J. Liu. *On spectral analysis and a novel algorithm for transmission eigenvalue problems.* J. Sci. Comput., 64, 83-108, 2015.

[78] T. Li, T.M. Huang, W. Lin, and J.N. Wang. *On the transmission eigenvalue problem for the acoustic equation with a negative index of refraction and a practical numerical reconstruction method.* Inverse Probl. Imaging, 12(4), 1033-1054, 2018.

[79] Z. Li, Y. Liu, J. Sun and L. Xu. *Quality-Bayesian approach to inverse acoustic source problems with partial data.* SIAM J. Sci. Comput., 43(2), A1062-A1080, 2021.

[80] Z. Li, Z. Deng and J. Sun. *Extended-sampling-Bayesian method for limited aperture inverse scattering problems.* SIAM J. Imaging Sci., 13(1), 422–444, 2020.

[81] Z. Li, Y. Liu, J. Sun and L. Xu. *Quality-Bayesian approach to inverse acoustic source problems with partial data.* SIAM J. Sci. Comput., 43(2), A1062-A1080, 2021.

[82] J. Liu, X. Liu and J. Sun. *Extended sampling method for inverse elastic scattering problems using one incident wave.* SIAM J. Imaging Sci., 12(2), 874-892, 2019.

[83] J. Liu, Y. Liu and J. Sun. *An inverse medium problem using Stekloff eigenvalues and a Bayesian approach.* Inverse Problems, 35(9), 094004, 2019.

[84] J. Liu and J. Sun. *Extended sampling method in inverse scattering.* Inverse Problems, 34(8), 085007, 2018.

[85] J. Liu, J. Sun, and T. Turner. *Spectral indicator method for a non-selfadjoint Steklov eigenvalue problem.* J. Sci. Comput., 79(3), 1814-1831, 2019.

[86] J. Liu, X. Liu and J. Sun. *Extended sampling method for inverse elastic scattering problems using one incident wave.* SIAM J. Imaging Sci., 12(2), 874-892, 2019.

[87] J. Liu, Y. Liu and J. Sun. *An inverse medium problem using Stekloff eigenvalues and a Bayesian approach.* Inverse Problems, 35(9), 094004, 2019.

[88] X. Liu. *A novel sampling method for multiple multiscale targets from scattering amplitudes at a fixed frequency.* Inverse Problems, 33(8), 085011, 2017.

[89] X. Liu and J. Sun. *Data recovery in inverse scattering: from limited-aperture to full-aperture.* J. Comput. Phys., 386, 350–364, 2019.

[90] X. Liu and J. Sun. *Reconstruction of Neumann eigenvalues and the support of a sound hard obstacle.* Inverse Problems, 30(6), 065011, 2014.

[91] P. Monk and J. Sun. *Inverse scattering using finite elements and gap reciprocity.* Inverse Probl. Imaging, 1(4), 643-660, 2007.

[92] D. Mora and I. Velásquez. *A virtual element method for the transmission eigenvalue problem.* Math. Models Methods Appl. Sci., 28(14), 2803-2831, 2018.

[93] E. Nakaguchi, H. Inui and K. Ohnaka. *An algebraic reconstruction of a moving point source for a scalar wave equation.* Inverse Problems, 28(6), 065018, 2012.

[94] S. Peters and A. Kleefeld. *Numerical computations of interior transmission eigenvalues for scattering objects with cavities.* Inverse Problems, 32(4), 045001, 2016.

[95] R. Potthast. *A study on orthogonality sampling*, Inverse Problems, 26, 074015, 2010.

[96] R. Potthast. *A survey on sampling and probe methods for inverse problems.* Inverse Problems 22(2), R1-R47, 2006.

[97] R. Potthast. *Stability estimates and reconstructions in inverse acoustic scattering using singular sources.* J. Comp. Appl. Math., 114, 247-274,2000.

[98] A. Roger. *Newton-Kantorovitch algorithm applied to an electromagnetic inverse problem.* IEEE Trans. Ant. Prop, 29(2), 232-238. 1981.

[99] A.M. Stuart. *Inverse problems: a Bayesian perspective.* Acta Numer., 19, 451-559, 2010.

[100] J. Sun. *Estimation of transmission eigenvalues and the index of refraction from Cauchy data.* Inverse Problems, 27(1), 015009, 2011.

[101] J. Sun. *An eigenvalue method using multiple frequency data for inverse scattering problems.* Inverse Problems, 28(2), 025012, 2012.

[102] J. Sun. *Iterative methods for transmission eigenvalues.* SIAM J. Numer. Anal. 49(5), 1860-1874, 2011.

[103] J. Sun. *Local estimators and Bayesian inverse problems with non-unique solutions.* arXiv:2105.09141, 2021.

[104] J. Sun and A. Zhou. Finite Element Methods for Eigenvalue Problems. CRC Press, Taylor & Francis Group, Boca Raton, London, New York, 2016.

[105] O. Takashi. *Real-time reconstruction of moving point/dipole wave sources from boundary measurements.* Inverse Probl. Sci. Eng., 28(8), 1057-1102, 2020.

[106] A. Tikhonov. *Solution of incorrectly formulated problems and the regularization method.* Soviet Math., 4, 1035-1038, 1963.

[107] K. Wang, Z. Zeng and J. Sun. *Through-wall detection of the moving paths and vital signs of human beings.* IEEE Geoscience and Remote Sensing Letters, 16(5), 717-721, 2018.

[108] X. Wang, Y. Guo, J. Li and H. Liu. *Mathematical design of a novel input/instruction device using a moving acoustic emitter.* Inverse Problems, 33(10), 105009, 2017.

[109] X. Wang, Y. Guo, J. Li and H. Liu. *Two gesture-computing approaches by using electromagnetic waves.* Inverse Probl. Imaging, 13(4), 879–901, 2019.

[110] Y. Wang, F. Ma and E. Zheng. *Bayesian method for shape reconstruction in the inverse interior scattering problem.* Math. Probl. Eng., Art., ID 935294, 2015.

[111] G.N. Watson. A Treatise on The Theory of Bessel Functions, Cambridge University Press, Cambridge, 1952.

[112] H. Xie and X. Wu. *A multilevel correction method for interior transmission eigenvalue problem.* J. Sci. Comput., 72(2), 586-604, 2017.

[113] Y. Yang, H. Bi, H. Li, and J. Han. *Mixed methods for the Helmholtz transmission eigenvalues.* SIAM J. Sci. Comput., 38(3), A1383–A1403, 2016.

[114] Z. Yang, X. Gui, J. Ming and G. Hu. *Bayesian approach to inverse time-harmonic acoustic scattering with phaseless far-field data.* Inverse Problems, 36(6), 065012, 2020.

[115] D. Zhang, Y. Guo, J. Li and H. Liu. *Locating multiple multipolar acoustic sources using the direct sampling method*, Commun. Comput. Phys., 25(5), 1328-1356, 2019.